Exploring Novel Chemotherapeutic Strategies in Breast Cancer

DISSERTATION

Presented in Partial Fulfillment of the Requirements for the Degree Doctor of Philosophy in the Graduate School of The Ohio State University

By

Lauren Elizabeth Himmel, DVM

Graduate Program in Comparative and Veterinary Medicine

The Ohio State University

2016

Dissertation Committee:

Ching-Shih Chen, Advisor

Robert Brueggemeier

Christopher Premanandan

Lisa Yee

Abstract

Breast cancer is the most common cancer in women and is the second leading cause of cancer deaths among women in the United States, according to the CDC. Despite significant improvements in survival in recent decades, largely attributable to advances in screening methods, the prognosis for patients with advanced or metastatic disease remains poor. Broadly, this thesis work explores two main topics: alternative chemotherapeutic strategies for TNBC to prevent chemotherapy-induced cognitive impairment (CICI) and therapeutic targeting of breast cancer stem cells (BCSC). CICI describes a protracted state of cognitive decline that develops in breast cancer patients following treatment with cytotoxic chemotherapy, and is an important facet of survivor care. We propose that minocycline can be used to prevent CICI without abrogating the antitumor efficacy of adjuvant chemotherapy in models of triple-negative breast cancer (TNBC). Next, we address BCSC, a subpopulation of mammary tumors which is believed to contribute to chemotherapeutic resistance, tumor recurrence, and metastasis. We have demonstrated that histone deacetylase inhibitors abrogate the BCSC phenotype in models of TNBC through a non-epigenetic effect of HDAC8 in maintaining Notch1 protein integrity. Thus, we suggest that HDAC8 may be translatable for CSC-targeted therapy in breast cancer and other malignancies. We also characterize a Her2 transgenic mouse model for the study of BCSC biology and therapeutic interventions. In these

experiments, we have found that the HDAC inhibitor AR-42 demonstrates a potent antitumor effect through dual downregulation of Neu and Notch1, and that pharmacologic HDAC8 inhibition has a unique effect in modulating BCSC through multiple nodes in the Notch1 signalome. These findings suggest that this model could be useful in studying the role of mammary stem cells in tumorigenesis.

Acknowledgments

I am deeply indebted to Ohio State and dozens of present and past faculty and staff thereof for fostering my scholarly and professional growth over the years both individually and through programmatic support. In particular, I am thankful for Drs. Ching-Shih Chen and Samuel Kulp in the College of Pharmacy for scientific mentorship and provision of resources to undertake my thesis research, Drs. Krista La Perle and Michael Oglesbee in the College of Veterinary Medicine for enthusiastically cultivating my pathology training, and Drs. Robert Brueggemeier, Christopher Premanandan, and Lisa Yee for gracious service on my advisory committee.

I would also like to recognize the funding sources which have made this work possible, including NIH 5T32OD010429-12 (Rosol/Oglesbee), NIH R01 CA112250 (Chen), The Stefanie Spielman Fund for Breast Cancer Research (Chen), The Lucius A. Wing Endowed Chair Fund (Chen), and NCI P30 CA016058 (CPMPSR).

Lastly, I am eternally grateful for the support of my husband, Mark, whose unwavering resolve, cool pragmatism, imagination, and relentless optimism keep me afloat.

Vita

1985.....Born – Royal Oak, MI

2003.....Ursuline Academy of Cincinnati

2006.....Bachelor of Science in Biology, College of Arts and Sciences, The Ohio State University, Columbus, Ohio

2011.....Doctor of Veterinary Medicine, College of Veterinary Medicine, The Ohio State University, Columbus, Ohio

2011 to 2012 .....Graduate Research Associate, Department of Veterinary Biosciences, The Ohio State University, Columbus, Ohio

2012 to 2015 .....NIH T32 Post-doctoral Fellow, Department of Veterinary Biosciences, The Ohio State University, Columbus, Ohio

2015 to present .....Graduate Research Associate, College of Pharmacy, The Ohio State University, Columbus, Ohio

Publications

1. **Himmel, Lauren**, M. O'Connor, and C. Premanandan (2014). Necrotizing hepatitis in a domestic pigeon (*Columba livia*). *Vet Pathol* 51(6): 1171-1173. DOI: 10.1177/0300985813519653.

2. **Himmel, Lauren E.**, R.B. Song, R.C. da Costa, and M.J. Oglesbee (2014). Pathology in practice: primitive neuroectodermal tumor with obstructive hydrocephalus in a 15-week-old dog. *JAVMA*. Accepted 12/2014.

3. Russell, D.S., B.A. Scansen, and **L. Himmel** (2015). Plexogenic pulmonary arteriopathy in a cat with nonrestrictive ventricular septal defect and chronic pulmonary hypertension. *Journal of Small Animal Practice* 56(8): 524-529. DOI: 10.1111/jsap.12341.

4. Chawla, P., L. Cook, **L. Himmel**, L. Zekas, and M. Oglesbee (2015). Coextensive meningioma and cholesterol granuloma in the forebrain of a cat. *JVIM* 29(6): 1638-1642. DOI: 10.1111/jvim.13601.

5. Chu, P.-C., M.-C. Yang, S.K. Kulp, S.B. Salunke, Y.-S. Shan, C.-T. Lee, M.-D. Lai, C.-S. Fang, **L.E. Himmel**, L.A. Shirley, T. Bekaii-Saab, and C.-S. Chen. Regulation of oncogenic KRAS signaling via a novel KRAS-Integrin-Linked Kinase-hnRNPA1 regulatory loop in human pancreatic cancer cells (2015). *Oncogene*. Epub ahead of print on November 30, 2015. DOI: ONC.2015.458.

6. Chao, M.-W., P.-C. Chu, H.-C. Chuang, F.-H. Shen, C.-C. Chou, E.-C. Hsu, **L.E. Himmel**, H.-L. Huang, H.-J. Tu, S.K. Kulp, C.-M. Teng, and C.-S. Chen. Non-epigenetic function of HDAC8 in regulating breast cancer stem cells by maintaining Notch1 protein stability (2016). *Oncotarget* 7(2):1796-1807. DOI: 10.18632/oncotarget.6427.

7. **Himmel, Lauren** and R. Cianciolo. Nodular typhlocolitis, heterakiasis, and mesenchymal neoplasia in a common ring-necked pheasant (*Phasianus colchicus*) with immunohistochemical characterization of visceral metastases (2016). *JVDI*. In review.

8. **Himmel, Lauren E.**, M.B. Lustberg, A.C. DeVries, M. Poi, C.-S. Chen, and S.K. Kulp. Minocycline, a putative neuroprotectant, co-administered with doxorubicin-cyclophosphamide chemotherapy in a xenograft model of triple-negative breast cancer (2016). *Exp Tox Pathol.* In revision.

Fields of Study

Major Field: Comparative and Veterinary Medicine

Table of Contents

Abstract ii

Acknowledgments iv

Vita v

Publications vi

Fields of Study vii

Table of Contents viii

List of Figures xi

List of Tables xiii

List of Abbreviations xiv

Chapter 1 : Introduction 1

Breast cancer: current epidemiology, classifications, and standards of care 1

Comparative pathology and research models 5

Chapter 2 : Minocycline, a putative neuroprotectant, co-administered with doxorubicin-cyclophosphamide chemotherapy in a xenograft model of triple-negative breast cancer 10

Abstract 10

Introduction 11

Materials and Methods 20

Results 26

Discussion 30

Limitations and Future Directions 35

Chapter 3 : Non-epigenetic effect of HDAC8 inhibition in downregulating breast cancer stem cells through Notch1 degradation and preliminary testing of the novel isoform-specific inhibitor Cpd25 45

Abstract 45

Introduction 46

Materials and Methods 57

Results 64

Discussion 69

Limitations and Future Directions 72

Chapter 4 : Characterization of breast cancer stem cells in the MMTV-Her2/neu mouse model and mechanistic insights into response to HDAC inhibitors 88

Abstract 88

Introduction 89

Materials and Methods 93

Results 101

Discussion 109

Limitations and Future Directions 112

Appendices 131

Appendix A: Western Blotting Preparations 131

Appendix B: Mouse Strains 132

Appendix C: IHC Antibodies 133

Appendix D: IHC Antibodies, Chapter 4 134

Appendix E: Cleaved Caspase 3 Quantitative Algorithm 135

Appendix F: Ki67 Quantitative Algorithm 136

Appendix G: Doublecortin Quantitative Algorithm 137

Appendix H: PCR Primers 138

References 139

List of Figures

Figure 2.1 Effects of minocycline alone and in combination with doxorubicin in MDA-MB-231 and MDA-MB-468 TNBC cells. 38

Figure 2.2 Effects of minocycline on the cytotoxicity of AC chemotherapy in MDA-MB-231 and MDA-MB-468 TNBC cells..... 39

Figure 2.3 Schematic of TNBC xenograft study. 40

Figure 2.4 Effects of minocycline on the tumor-suppressive activity of AC chemotherapy in the MDA-MB-231 TNBC xenograft model. 41

Figure 2.5 Immunohistochemistry for cleaved caspase 3 and Ki67 in formalin-fixed paraffin-embedded MDA-MB-231 xenograft tumors. 43

Figure 2.6 Neuroanatomic evaluation in MDA-MB-231 xenograft tumor-bearing mice. 44

Figure 3.1 AR-42 and cancer. 75

Figure 3.2 Evaluation of pharmacologic HDAC inhibitors in TNBC cell lines. 76

Figure 3.3 Use of the pharmacologic HDAC8-selective isoform inhibitor PCI-34051 in MDA-MB-231 cells. 77

Figure 3.4 Class I isoform and HDAC6 knockdown in TNBC. 78

Figure 3.5 Overexpression of HDAC8 in TNBC..... 79

Figure 3.6 Proteasome inhibitor and IP experiments in HDAC8 knockdown TNBC. 80

Figure 3.7 HDAC8 influences Notch1 indirectly through the E3 ligase Fbwx7. 81

Figure 3.8 Schematic of TNBC orthotopic xenograft study of HDAC8 knockdown..... 82

Figure 3.9 Percent tumor-free incidence in $HDAC8^{KD}$ *in vivo* study. 83

Figure 3.10 *In vitro* data demonstrating anti-CSC effects of the novel HDAC8 inhibitor Cpd25 in TNBC. 84

Figure 3.11 Schematic of TNBC orthotopic xenograft study of Cpd25. 85

Figure 3.12 *Ex vivo* analysis of mammosphere formation and ALDH positivity in 5 mice. 86

Figure 3.13 Toxicopathologic parameters for Cpd25 *in vivo* study..... 87

Figure 4.1 MTT assays using pharmacologic HDAC inhibitors in NT5 cells..... 116

Figure 4.2 Western blot analysis of Notch1 and other biomarkers in NT5 cells treated with pharmacologic HDAC inhibitors. 117

Figure 4.3 Mammosphere assays using pharmacologic HDAC inhibitors in NT5 cells. 118

Figure 4.4 Proteasome inhibition in NT5 cells treated with AR-42 or PCI-34051. 119

Figure 4.5 qPCR analysis of NT5 cells treated with AR-42 or PCI-34051. 120

Figure 4.6 4T1 cells treated with PCI-34051. 121

Figure 4.7 Western blot analysis of Notch1 transcription factors in NT5 cells treated with AR-42 or PCI-34051. 122

Figure 4.8 Western blot and IP analysis of HSP90 clients in NT5 cells treated with HDAC inhibitors. 123

Figure 4.9 IP analysis of Notch1 in NT5 cells treated with AR-42 or PCI-34051. 124

Figure 4.10 Western blot and qPCR analysis of Pin1 in NT5 cells treated with AR-42 or PCI-34051. 125

Figure 4.11 *In vivo* orthotopic allograft study using dietary AR-42 in an NT5 model... 126

Figure 4.12 Immunohistochemical analysis of three novel protein targets in the MMTV-Her2/neu murine model. 127

Figure 4.13 NT5-GFP transfection. 128

Figure 4.14 Schematic of NT5-GFP orthotopic allograft study using AR-42. 129

Figure 4.15 *Ex vivo* analysis by flow cytometry and mammosphere assay. 130

List of Tables

Table 2.1 Organ Weight Data 42

List of Abbreviations

7-AAD..... 7-aminoactinomycin

Ac.....Acetyl

AC.....Adriamycin (doxorubicin)-Cytoxan (cyclophosphamide)

ACSR.....Analytical cytometry shared resource

ALDH .....Aldehyde dehydrogenase

ASCO.....American Society of Clinical Oncology

BCSC .....Breast cancer stem cells

C.....Celcius

CD.....Cluster of differentiation

CDC .....Centers for Disease Control and Prevention

cDNA .....Complimentary deoxyribonucleic acid

CFA..... Colony formation assay

CICI.....Chemotherapy-induced cognitive impairment

Cl Cas3..... Cleaved caspase 3

Co-IP .....Co-immunoprecipitation

Cpd.....Compound

CSC..... Cancer stem cells

DAB .....Diaminobenzidine

DCX ..... Doublecortin

DEAB ..... Diethylaminobenzaldehyde

DMSO ..... Dimethyl sulfoxide

DMEM ..... Dulbecco's Modified Eagle Medium

DNA ..... Deoxyribonucleic acid

DNMT ..... DNA methyltransferase

EGFR ..... Epidermal growth factor receptor

EMT ..... Epithelial-mesenchymal transition

ER ..... Estrogen receptor

FACS ..... Fluorescence-activated cell sorting

FBS ..... Fetal bovine serum

GAPDH ..... Glyceraldehyde 3-Phosphase Dehydrogenase

Gent ..... Gentamicin

GFAP ..... Glial fibrillary acidic protein

GFP ..... Green fluorescent protein

GSI ..... Gamma secretase inhibitor

H&E ..... Hematoxylin and eosin

HAT ..... Histone acetyltransferase

HDAC ..... Histone deacetylase

HDACi ..... Histone deacetylase inhibitor

Her2 ..... Human epidermal growth factor receptor 2

HSP ..... Heat shock protein

Iba1 ..... Ionized Calcium-Binding Adapter Molecule 1

IC50 ..... Half-maximal inhibitory concentration

IHC ..... Immunohistochemistry

IL ..... Interleukin

IMDM ..... Iscove's Modified Dulbecco's Medium

IP ..... Immunoprecipitation

LCIS ..... Lobular carcinoma *in situ*

LTR ..... Long terminal repeat

miR ..... Micro-RNA

mL ..... Milliliter

MOI ..... Multiplicity of infection

mRNA ..... Messenger RNA

miRNA (miR) ..... micro ribonucleic acid

MMTV ..... Mouse mammary tumor virus

MTT ..... Methylthiazol tetrazolium

µL ..... Microliter

µm ..... Micrometer

µM ..... Micromolar

NC ..... Nitrocellulose

NBF ..... Neutral-buffered formalin

NOD.SCID ..... Nonobese diabetic/severe combined immunodeficiency

PARP ..... Poly adenosine diphosphate-ribose polymerase

PBS ..... Phosphate-buffered saline

PCR ..... Polymerase chain reaction

Pen-Strep ..... Penicillin-Streptomycin

Ppm ..... parts per million

PR ..... Progesterone receptor

Puro ..... Puromycin

PVDF ..... Polyvinylidene difluoride

PyMT ..... Polyoma middle T oncoprotein

qPCR ..... Quantitative PCR

rpm ..... Rotations per minute

RPMI ..... Roswell Park Memorial Institute medium

RNA ..... Ribonucleic acid

SAHA (Vorinostat, Zolinza®) ..... Suberanilohydroxamic acid

SCID ..... Severe combined immunodeficiency

SDS-PAGE ..... Sodium dodecyl sulfate polyacrylamide gel electrophoresis

shRNA ..... Short hairpin ribonucleic acid

siRNA ..... Small interfering ribonucleic acid

TBS ..... Tris-buffered saline

TMA ..... Tissue microarray

TNBC ..... Triple-negative breast cancer

TNF-α ..... Tumor necrosis factor-alpha

Ub ..... Ubiquitin

VEGF ..... Vascular endothelial growth factor

WB ..... Western blot

Chapter 1 : Introduction

Breast cancer: current epidemiology, classifications, and standards of care

Breast cancer is classified by several criteria. The most basic distinction is the anatomic distribution of the tumor pertaining to whether it originates in the duct system or the lobular/alveolar (synthetic/secretory) unit of the mammary gland. The microanatomy of the breast is also used to subclassify breast tumors according to whether they most closely resemble – at the phenotypic and molecular levels – luminal epithelium, basal/myoepithelial cells, or stem cells, which reside in the suprabasilar compartment and are believed to be responsible for repopulating both the luminal and myoepithelial components of the mammary gland. Breast tumors are classified by histologic behavior and appearance, including cell morphology and growth pattern/architecture. Behavior is described as *in situ* if it does not penetrate the basement membrane (i.e. DCIS or LCIS) or invasive. According to the World Health Organization, there are 19 distinct histologic subtypes of breast cancer, plus further morphologic variants [1, 2]. Histologic grading – known as the Elston and Ellis or Nottingham modified Bloom-Richardson grading method – accounts for percent tubule formation, mitotic index, and nuclear size/pleomorphism to calculate a composite score of 3-9 that corresponds to a grade I, II, or III tumor [3]. Around the turn of the 21st century, molecular diagnostics revolutionized

breast cancer subtyping according to further classifications with distinct treatment and prognostic profiles. There are four so-called intrinsic molecular subtypes, characterized predominantly in invasive ductal carcinomas, the most common type of breast malignancy. These are luminal A, which are hormone receptor positive, luminal B, which are somewhat less hormone receptor positive and increasingly Her2 positive, Her2, which overexpress Her2 and to a lesser extent may be hormone receptor positive, and triple-negative or TNBC, which do not express ER, PR, or Her2. Further subclassifications of the basic molecular subtypes continue to emerge based on advancing diagnostic capabilities, and new subtypes are frequently suggested. Recently, Burstein et al. proposed four TNBC subtypes with distinct molecular profiles and putative subtype-specific druggable targets which may have a bearing on treatment of TNBC patients [4].

Molecular profiling in the genomic era uses clinical companion diagnostics such as OncotypeDX, PAM50, or MammaPrint to more accurately prognosticate on an individual based on tumoral gene signatures [5, 6]. Still, these data are most meaningful when synthesized with other parameters including tumor size and nodal status for total patient evaluation [5]. Weigelt et al. take molecular diagnostics a step further, proposing re-biopsy and microarray after primary therapeutic intervention to identify emerging biomarkers which may predict drug response or resistance as a tumor evolves [5]. Some advocate a proteomic approach for identification of both tumoral and circulating plasma biomarkers associated with breast cancer that have prognostic value, including two-dimensional difference gel electrophoresis and mass spectrometry [7]. Also on the

horizon are so-called antagomiRs, a type of miRNA therapeutic that targets oncomiRs such as miR-155, which has been found to be overexpressed in different types of cancer and is thought to contribute to cancer cell growth and chemotherapy resistance [8].

The lifetime risk of breast cancer is 1 in 8 women (12.3%) in the United States, compared to a lifetime risk of 1 in 11 in the 1970s [9]. Largely due to advances in screening and detection tools such as digital mammography and tomosynthesis, overall survival has improved in recent years. Breast cancer death rates have fallen by 34% since 1990, according to a 2013 American Cancer Society report [9]. However, the overall incidence of breast cancer continues to rise. Particularly concerning is a notably higher death rate and decreased 5-year survival rate among African American women, highlighting the impact of racial disparities in healthcare access and socioeconomic status [9]. Though the genomic age ushered in a bedside assay for BRCA1/2 mutations, only 5-10% of breast cancers have a hereditary basis; for the remainder of cases, the causes are manifold, many of which likely remain yet unknown [10].

For hormone receptor positive breast cancer, the most common molecular subset of breast cancer, the American Society of Clinical Oncology recommends the use of tamoxifen followed by an aromatase inhibitor for a total of 10 years total adjuvant endocrine therapy, with slight modifications in the protocol according to pre- or post-menopausal status [11]. There is still an urgent need for chemopreventive drugs in at-risk patients without pre-existing breast cancer. The standard of care is Tamoxifen; however

the typical efficacy metric – incidence of invasive breast cancer – fails to account for other complications including fractures, thromboembolic events, endometrial cancer, and cataracts, and it does not reduce breast cancer-specific and all-cause mortality in placebo-controlled trials [12]. Her2+ breast cancer is 10-30% of all breast cancers [7, 13, 14] and is most commonly associated with gene amplification. Monoclonal antibodies against the Her2 receptor (e.g. trastuzumab) are now standard first-line of care in Her2+ disease; however, resistance to Her2-targeted therapy through compensatory pathways such as HSP90, mTOR, and IGF-1R is often quick to emerge [15].

Triple-negative breast cancer is particularly difficult to treat for comparative lack of therapeutic targets and disproportionately affects young women, women of African American or Hispanic descent, and those with a BRCA1 mutation. TNBC accounts for 15-20% of breast cancers and is usually of invasive ductal morphology [16]. Mainstays of therapy for TNBC in stage II or III include a taxane (e.g. paclitaxel, docetaxel) plus an anthracycline (e.g. doxorubicin, epirubicin) and cyclophosphamide [17]. Agents currently under investigation for TNBC include PARP inhibitors, EGFR inhibitors, and anti-angiogenic drugs [16]. However, anti-angiogenic agents such as the VEGF-A monoclonal antibody bevacizumab to standard anthracycline and/or taxane-based adjuvant chemotherapy regimens has failed to improve disease-free survival in TNBC patients and is limited by its associated toxicities such as febrile neutropenia, mucositis, and cardiovascular toxicity [17].

Comparative pathology and research models

Canine

Mammary neoplasms are the most common neoplasm in intact female dogs, of which up to 50% of cases are malignant [14, 18]. Canine mammary cancer has been championed by many as an excellent naturally-occurring model of the human disease [19]. The incidence of canine mammary cancer is similar to human breast cancer at approximately 198 cases in 100,000 in the United States. Approximately 26% of bitches who are gonadally intact or are spayed after the second estrus develop mammary cancer [19]. As in humans, the mammary gland undergoes the majority of its development in puberty, followed by terminal differentiation in pregnancy [14]. It is worth noting that the estrous cycle differs significantly between canids and humans; the discussion thereof is beyond the scope of this thesis. Cancer-associated death at 2 years following diagnosis ranges from 20-44% [14]. Broadly, canine mammary cancers are classified as simple (luminal-type) or complex (both luminal and myoepithelial). Canine mammary cancer is staged according to categories set forth in a modified WHO system [14]. Importantly, the Peña group noted in 2012 that there are unique characteristics of canine mammary cancer that warrant attention, particularly with respect to transferability of the human paradigms. These include the comparative low rate of metastasis in dogs compared to humans, the high incidence of complex and mixed mammary tumors in the dog and the failure of the Elston and Ellis method to account for them, and the commonness of nuclear pleomorphism in canine mammary cancers that may lead to overdiagnosis of malignancy [14]. Myoepithelial proliferation is common in canine mammary cancer, at approximately

20%, whereas this is rare in human cancer [19]. Biphasic tumors have been reported to be less malignant in dogs [14]. Canine myoepithelial cells are readily distinguished from luminal cells based on immunohistochemical or immunofluorescent keratin profiling [14]. In 2011, Goldschmidt et al. established eight main categories of mammary neoplasms, among which there are dozens of subsets, as well as a grading rubric for histologic criteria that is identical to the human grading scheme, including tubule formation, nuclear pleomorphism, and mitotic index [18]. Peña et al. have demonstrated that histological grade, clinical stage, age, gonadal status, and lymph node metastasis at diagnosis are associated with prognosis [14].

Recently, canine mammary cancers are beginning to be characterized at the genomic, transcriptomic, and epigenomic levels [19]. Liu et al. have demonstrated that simple carcinomas, which histologically resemble human *in situ* carcinoma, invasive ductal carcinoma, and invasive lobular carcinoma, also share molecular commonalities with human cancers including copy number abnormalities, translocation-fusion lesions, and sequence mutations [19]. Overexpression and/or amplification of several oncogenes including BRAF and MYC were identified, as well as mutation or decreased expression of tumor suppressors like PTEN, BRCA1, and NF1 [19]. In the same study, using PAM50 classification, canine simple carcinomas were found to cluster with basal-like human tumors with an 82% chance [19]. These findings are contrasted to canine complex carcinomas, which were found to arise primarily due to epigenetic rather than genetic aberrations [19]. The Liu group postulates that canine complex carcinomas arise from

mammary stem cells based on the expression of SOX2, similar epigenomic patterning between luminal and myoepithelial tumor components, and upregulation of glucose metabolic genes [19]. This warrants further investigation, but could be an attractive translational model for the study of mammary stem cells and their role in tumorigenesis. The role of Her2, ER, and PR immunohistochemical profiling in canine mammary cancer remains hotly debated. Peña et al. have recently proposed that the human IHC protocol and scoring methods for Her2 should be adopted in canine mammary cancer; however, it remains to be seen whether this has bearing on clinical outcomes. ER and PR are, on the whole, downregulated in canine malignant mammary cancers, and their analysis is not routinely performed [14]. ER and PR positivity have been reported to vary widely among both benign and malignant canine mammary tumors, and the biological threshold, or the point at which positive labeling would correlate with response to hormone therapy, has not been established in dogs [14].

Feline

Feline mammary cancer occurs commonly in female cats [20, 21] and comprises 11-17% of all tumors, excluding those of the integument [21, 22]. Feline mammary cancers are typically highly infiltrative and ER- with a propensity for recurrence and metastasis to the lymph nodes, lungs, and liver, sharing morphologic features with human ER- cancer [13, 21]. Up to 58% of feline mammary adenocarcinomas are classified, by appropriation of the human terminology, as triple-negative [23]; however no BRCA1/2 mutations were identified among this subset. To date, the Elston and Ellis histologic grading system that

is used in humans has been the single most reliable independent prognostic factor in cats [20, 23]. Other putative prognostic factors include VEGF, p53, and STAT3 expression levels [13, 22] The reported incidence of Her2 overexpression in feline mammary cancer varies widely from 5% to 92% and, when overexpressed, has been shown by ISH not to be attributable to gene amplification; thus, Her2 is not currently recognized as a prognostic factor or therapeutic target in cats [24], nor are ER and PR expression considered prognostic [22]. There remains a dire need for standard protocols and prognostic factors in feline mammary cancer [21].

Murine

WHO International Classification of Rodent Tumors: the Mouse characterizes hyperplasia, adenoma, adenocarcinoma, fibroadenoma, and malignant adenoacanthoma as the major naturally-occurring mammary tumors in mice. Murine somatic cells constitutively express telomerase [10] in contrast to humans, in which telomerase expression in somatic cells would typically be associated with acquisition of a stem-like or immortal phenotype in cancer. So-called “suprabasal small light cells” have been identified in the rodent mammary gland, similar to the so-called “basal clear cells” of humans, which have been previously identified as a putative stem cell compartment [25].

Several cell lines have been isolated from spontaneously-occurring murine tumors, panels of which are commercially available. The LA7 cell line derived from a rat mammary adenocarcinoma is phenotypically $CD133^{+}/CD49f^{+}/CD29^{+}/CD24^{-/low}$ and has been

reported to generate all three lineages of mammary gland as well as tumors from a single cell xenografted in NOD.SCID mice [25]. The 4T1 cell line is a murine model of triple-negative or basal-like breast cancer derived from a spontaneous tumor arising in a BALB/C mouse, of which some sublines readily metastasize to lungs, brain, liver, and bone in orthotopic models [10]. Owing to an easily-manipulated genome and the advent of inducible tetracycline-regulated systems and Cre-recombinase models, there has been an explosion of novel, highly specialized transgenic mouse models pertinent to the field of breast cancer, an exhaustive analysis of which is not possible in this thesis. Humanized and highly immunosuppressed inbred mice like the NOD.SCID gamma and strains built thereon have also made it possible to assess endpoints with patient-derived xenografts in a biological system more akin to *Homo sapiens* than ever before. Pertaining to this body of work, tumor-initiating or putative cancer stem cells have been identified in the MMTV-Her2/neu, MMTV-Wnt, and MMTV-PyMT models. Cell lines derived from tumors arising in the MMTV-Her2/neu mouse include N202 and NT5. An in-depth discussion of the MMTV-Her2/neu model will follow in chapter 4.

Chapter 2 : Minocycline, a putative neuroprotectant, co-administered with doxorubicin-cyclophosphamide chemotherapy in a xenograft model of triple-negative breast cancer

Abstract

Minocycline is purported to have neuroprotective properties in experimental models of some human neurologic diseases, and has therefore been identified as a putative neuroprotectant for chemotherapy-induced cognitive impairment (CICI) in breast cancer patients. However, because its mechanism of action is believed to be mediated through anti-inflammatory, anti-apoptotic, and anti-oxidant pathways, co-administration of minocycline with chemotherapeutic agents has the potential to reduce the efficacy of anticancer drugs. The objective of this study is to evaluate the effect of minocycline on the activity of the AC chemotherapeutic regimen (Adriamycin [doxorubicin], Cytoxan [cyclophosphamide]) in *in vitro* and *in vivo* models of triple-negative breast cancer (TNBC). Clonogenic and methylthiazol tetrazolium (MTT) assays were used to assess survival and viability in two TNBC cell lines treated with increasing concentrations of AC in the presence or absence of minocycline. Biomarkers of apoptosis, cell stress, and DNA damage were evaluated by western blot. The *in vivo* effects of AC and minocycline, each alone and in combination, were assessed in a xenograft model of TNBC in female athymic nude mice by weekly tumor volume measurement, body and organ weight

measurement, and histopathology. Apoptosis and proliferation were characterized by immunohistochemistry in the xenograft tumors. Brains from tumor-bearing mice were evaluated for microglial activation, glial scars, and the proportion of neural progenitor cells. Data from these *in vitro* and *in vivo* studies demonstrate that minocycline does not diminish the cytotoxic and tumor-suppressive effects of this chemotherapeutic drug combination in TNBC cells. Moreover, minocycline appeared to prevent the reduction in doublecortin-positive neural progenitor cells observed in AC-treated mice. We posit that minocycline may be useful clinically for its reported neuroprotective activity in breast cancer patients receiving AC without loss of chemotherapeutic efficacy.

Introduction

Minocycline is a semi-synthetic second-generation tetracycline derivative that, in addition to its use as a broad-spectrum antibiotic, has demonstrated antioxidant, anti-inflammatory, and anti-apoptotic effects in the nervous system which confer neuroprotection [26-29]. Increased neuron survival, preserved neuronogenesis, and reduced neuroinflammation have been reported in cell culture and rodent studies of a multitude of human neurologic disease states, including hypoglycemia, ischemia, and neurodegenerative disorders [30-34]. In the brain, minocycline exerts its effects in part through protection against cell death and decreased neuroinflammation. Protection against cell death occurs via caspase-independent factors, such as upregulation of pro-survival Bcl-2, and caspase-dependent factors, including decreased cytochrome c release from mitochondria and decreased caspase-1 and caspase-3 levels [28, 35] as well as

antioxidant activity through inhibition of cyclooxygenase-2 and inducible nitric oxide synthase and decreased p38 MAP kinase phosphorylation [28, 36]. Anti-inflammatory effects of minocycline in the central nervous system are attributed to decreased microglial activation and decreased T cell migration, which are associated with lower levels of pro-inflammatory cytokines such as IL-1β, TNF-α, IL-6, and matrix metalloproteases [28, 31]. Mounting pre-clinical data in support of the neuroprotective effects of minocycline have led to phase II clinical trials for traumatic spinal cord injuries in which minocycline has shown beneficial outcomes in motor recovery in a subset of patients with cervical injury [37]. Minocycline has also demonstrated protection against ototoxicity associated with cisplatin administration in an animal model which evaluated auditory hair cell degeneration and the auditory brainstem response [35].

Because of these purported neuroprotective properties, we have identified minocycline as a candidate therapeutic agent for the treatment of chemotherapy-induced cognitive impairment (CICI). This phenomenon, colloquially termed “chemo brain” or “chemo fog,” describes a state of prolonged cognitive dysfunction resulting from administration of a variety of common cytotoxic chemotherapeutic agents, including Adriamycin (doxorubicin) and Cytoxan (cyclophosphamide) [38], which may last years after cessation of chemotherapy [39, 40]. Cognitive decline following chemotherapy is reported in 17-78% of cancer patients [39, 41, 71]. CICI is well-documented in women receiving chemotherapy for breast cancer [45, 62, 63, 71] and has been recapitulated in numerous mouse and rat models [39, 41, 44]. Because median survival times for breast

cancer patients have improved significantly in recent decades, the patients' quality of life following chemotherapy must be carefully considered as part of survivor care [42, 43]. Our particular focus is on patients with triple-negative breast cancer (TNBC), in which tumors cells do not express estrogen receptor-alpha, progesterone receptor, or human epidermal growth factor receptor 2/neu [46, 47]. The absence of these cellular receptors leaves fewer therapeutic options, and thus these patients are more likely to receive adjuvant chemotherapeutic drug combinations like Adriamycin and Cytoxan, taxanes, and 5-fluorouracil [10, 16, 48, 49].

Of significant concern, however, is that the antioxidant and anti-apoptotic effects of minocycline could diminish the cytotoxic effects of chemotherapy on tumor cells. Such concerns have driven considerable debate about the use of supplemental antioxidants and whether they can alter the efficacy of chemo- and radiotherapy in cancer patients. Reviews of published clinical trial results reporting the concurrent use of antioxidants with chemotherapy have revealed data suggesting no decrease in therapeutic efficacy, as well as those indicating compromised tumor control, and have ultimately concluded that the safety and efficacy of these combinations remains unclear and warrants further research [50-53]. In the context of CICI specifically, preclinical data indicate that N-acetyl cysteine can mitigate chemotherapy-related cognitive deficits during AC chemotherapy in tumor-free rats, supporting a role for antioxidants in the treatment of CICI [54]. Moreover, minocycline has been reported to have antineoplastic properties in studies of ovarian carcinoma [55] and in combination with antiangiogenic agents in *de*

novo pancreatic islet cell tumorigenesis in mice [56], which could potentially lead to a summational cytotoxic effect if co-administered with chemotherapeutic agents.

The over-arching goal of this study is to describe the effect of minocycline on TNBC cells *in vitro* and *in vivo* to determine whether it alters their susceptibility to common chemotherapeutic drugs, before minocycline can be considered as a potential neuroprotective agent to be safely administered to breast cancer patients concurrently receiving chemotherapy. In this study, the effects of minocycline on the activity of the AC chemotherapeutic drug combination were assessed in *in vitro* (MDA-MB-231 and MDA-MB-468 cells) and *in vivo* (MDA-MB-231 xenograft tumors) models of TNBC. In addition, the presence of neuroanatomic lesions consistent with the proposed pathophysiology of CICI and the effects of therapeutic intervention with minocycline on specific brain regions were also evaluated. To the authors' knowledge, this is the first reported study examining the effects of combined AC and minocycline therapy in xenograft tumors and the brains of tumor-bearing mice simultaneously.

Neuroprotection by Minocycline

Minocycline is a semi-synthetic second-generation tetracycline derivative which is safe, affordable, orally bioavailable, and able to penetrate the blood-brain barrier. In addition to its antibiotic properties, minocycline has been found to have other antioxidant, anti-inflammatory, and anti-apoptotic effects in the central nervous system. Recent research into animal models of human neurologic diseases including hypoglycemia, ischemia,

autoimmune encephalomyelitis, neurodegenerative disorders like Huntington's, Parkinson's, and Alzheimer's diseases, traumatic brain injury, and diabetic metabolic disorder has demonstrated that minocycline can prevent neuron death, preserve neuronogenesis, and decrease neuroinflammation [28, 30-34, 57, 58]. The dose, route of administration, and duration of treatment with minocycline for its neuroprotective effects varies widely across the literature and there is not yet a consensus on these factors [28]. Minocycline, even in high doses, is well-tolerated in rodent species and attains adequate therapeutic concentrations in the cerebrospinal fluid [30]. Mounting pre-clinical data in support of the neuroprotective effects of minocycline have led to phase II clinical trials for traumatic spinal cord injuries in which minocycline has shown beneficial outcomes in motor recovery in a subset of patients with cervical injury [37]. Minocycline has also demonstrated protection against ototoxicity associated with Cisplatin administration in an animal model which evaluated auditory hair cell degeneration and the auditory brainstem response [35]. Thus, we propose that minocycline could be utilized in the prevention and treatment of CICI in human breast cancer patients receiving chemotherapy.

The means of neuroprotection by minocycline are manifold and continue to be intensively interrogated. In the brain, minocycline exerts its effects in part through microglia - the resident phagocytic cells of central nervous system tissues - neurons, and oligodendroglia [28]. At least two basic mechanisms have been elucidated in the literature: protection against cell death and decreased neuroinflammation. Protection against cell death occurs via anti-apoptotic factors, which are primarily centered on

mitochondria, and antioxidant activity [28, 35]. Anti-apoptotic effects are mediated through caspase-independent factors, such as upregulation of pro-survival Bcl-2, and caspase-dependent factors, including decreased cytochrome c release from mitochondria and decreased caspase-1 and caspase-3 levels [28, 35]. Anti-oxidant activities of minocycline include inhibition of cyclooxygenase-2 and inducible nitric oxide synthase (iNOS) and decreased p38 MAP kinase phosphorylation [28, 36]. Anti-inflammatory effects of minocycline in the central nervous system are attributed to decreased microglial activation and decreased T cell migration, which are associated with lower levels of pro-inflammatory cytokines such as Il-1β, TNF-α, IL-6, and matrix metalloproteases [28, 31]. These pro-inflammatory factors could reach the brain by systemic cytokinemia or by local release from microglia and other inflammatory cells migrating into the nervous system. Other minocycline-driven neuroprotective effects mediated by microglia are considered indirect. For example, microglial activation has been linked to excitotoxicity of neurons [28, 59] and suppressed neurogenesis [60], both of which could be targeted for abrogation by minocycline.

Minocycline and Neoplasia

Although minocycline has been reported to have antineoplastic properties in studies of ovarian carcinoma [55] and in combination with antiangiogenic agents in *de novo* pancreatic islet cell tumorigenesis in mice [56], our data and those of others [61] suggest that this is not the case in human mammary carcinoma. Of significant concern, however, is that the antioxidant and anti-apoptotic effects of minocycline could diminish the

cytotoxic effects of AC chemotherapy on tumor cells. Recent data suggest that antioxidants like N-acetyl cysteine can mitigate chemotherapy-related cognitive deficits during AC chemotherapy [54] without decreasing the efficacy of the chemotherapeutic agents on tumor cells [50, 51]. However, there is conflicting evidence that the effect of doxorubicin in particular may either be amplified or antagonized by co-administration of antioxidants [64, 65]. The anti-apoptotic effects of minocycline are another factor to consider in the setting of breast cancer chemotherapy. Exposure of breast cancer cells to oligonucleotides against anti-apoptotic factors like Bcl-2 and Bcl-xL have been shown to increase sensitivity to chemotherapy drugs including doxorubicin [66]; conversely, we speculate that an increased level of Bcl-2 via minocycline treatment could decrease sensitivity of tumor cells to these drugs through decreased apoptosis.

Chemotherapy-induced Cognitive Impairment

The mechanisms by which chemotherapy-associated cognitive changes occur are still being elucidated, but there is little doubt at this time that brain alterations consistent with CICI, particularly in breast cancer patients receiving chemotherapy, are real and long-lasting [67-72]. Cognitive decline following chemotherapy is reported in 17-78% of cancer patients [39, 41, 71]. Metrics of CICI are primarily documented by biobehaviorists and neuroscientists and include learning, memory, processing speed, attention, executive function, and visuospatial skills [42, 41, 71]. As our ability to investigate brain biology deepens through technologies like PET scanning, diffusion tensor imaging, functional MRI, and improved neuropsychological assessments [71, 101], much-needed longitudinal

and prospective studies evaluating cognitive function pre- and post-chemotherapy and risk factors in breast cancer patients are emerging [73-77]. Breast cancer survivors, compared to healthy females matched for age, education, and intelligence, show significantly decreased global clustering and multifocally disrupted regional networks by fMRI, as well as significantly increased self-reporting of impaired executive function and memory – differences which are not explained by psychiatric distress [78]. However, to our knowledge, a thorough neuroanatomic characterization of microscopic and ultrastructural lesions in the brain consistent with CICI has not yet been reported.

Several patient factors must be considered simultaneously with the pathogenesis of CICI which might predispose certain individuals to acquiring cognitive deficits from chemotherapeutic drugs, such as age, MDR1 gene polymorphisms, patient estrogen or testosterone level, efficacy of DNA damage repair responses, and inherent neuroplasticity, which includes neural repair mechanisms, modulation of neurotransmitter activity, and cognitive reserve [75, 78, 79]. Other patient susceptibility factors that may warrant vigilance in the detection, prevention and treatment of CICI include lower education level, lower level of physical activity, and low dietary polyphenol content [69]. In addition, fMRI has demonstrated that patients affected by CICI may develop compensatory brain activation pathways which partly or fully mask signs of cognitive deficits [71, 80]. The pathophysiology of CICI is multifactorial and incompletely understood. Animal models in mice and rats have found that many chemotherapeutic drugs including platinum-containing compounds, methotrexate, 5-fluoruracil,

doxorubicin, cyclophosphamide, and combinations thereof are capable of inducing some degree of nervous system damage in tumor-free animals [35, 41, 54, 81]. Many chemotherapeutic agents do not cross the blood-brain barrier to any appreciable extent, particularly those which are a substrate for the p glycoprotein efflux transporter such as doxorubicin and paclitaxel [41]. One hypothesis as to how those chemotherapeutic drugs bring about cognitive and behavioral changes is that they trigger a systemic increase in cytokines that do penetrate the blood-brain barrier, such as TNF-α and IL-6, which can activate brain microglia to increase iNOS and reactive oxygen and nitrogen species, thus leading to oxidative stress and mitochondrial dysfunction [42]. Positive correlations have been found between circulating inflammatory cytokines and increased metabolic rates in specific brain regions in the prefrontal and temporal cortices at the time of chemotherapy and persisting for 1 year afterwards in a study of breast cancer patients [76]. Oxidative stress in the brain is thought to decrease neurogenesis and induce apoptosis [41]. One study investigating the effect of cyclophosphamide in mice found that hippocampus-dependent learning and memory were transiently impaired due to decreased neurogenesis [82]. Progenitor cells in the adult mammalian brain are indeed a susceptible population [68, 78, 83] that could be inadvertently targeted by cytotoxic agents, leading to deleterious effects on cognition [96] due to cell death and altered dendritic spine connectivity [97]. Other factors identified as candidate mechanisms in CICI include decreased cerebral bloodflow due to chemotherapy, thus leading to decreased oxygen delivery and glucose metabolism, and possibly the psychological effects of cancer itself [41, 71, 84].

Materials and Methods

Cell lines and culture conditions

The TNBC cell lines MDA-MB-231 (HTB-26) and MDA-MB-468 (HTB-132) were obtained from American Type Culture Collection (Manassas, VA) and were cultured under sterile conditions in high-glucose Dulbecco's modified Eagle medium (DMEM, Life Technologies, Corp., Grand Island, NY) supplemented with 10% fetal bovine serum (Life Technologies) and 0.1% gentamicin and maintained in a 37°C, humidified incubator with 5% CO_2. Media was changed every 48 hours and cells were passaged upon confluence.

Drugs

For *in vitro* experiments, the following stock solutions of drugs were prepared: minocycline HCl (Sigma-Aldrich, St. Louis, MO) at 25mM in sterile water, doxorubicin HCl (Sigma-Aldrich) at 25mM in sterile water, and cyclophosphamide monohydrate (Sigma-Aldrich) at 1M in sterile dimethyl sulfoxide (DMSO). For the *in vivo* experiment, minocycline for administration *per os* was completely dissolved in water (9mg/ml), physiologically balanced (pH 7.35) to eliminate the potential for chemical pharyngitis or esophagitis, and sterilized by filtration (0.22 μm). This minocycline working solution was stored at 4°C, protected from light, and prepared fresh every 48 hours. Pharmaceutical-grade doxorubicin (Bedford Laboratories, Bedford, OH) and cyclophosphamide (Baxter Healthcare Corp., Deerfield, IL) were reconstituted and

diluted in 0.9% sodium chloride (USP, Hospira, Inc., Lake Forest, IL), and then combined for intravenous injection as a cocktail containing final concentrations of doxorubicin (A) and cyclophosphamide (C) at 1.0 and 20 mg/ml, respectively.

Cell viability

Cell viability was assessed by methylthiazol tetrazolium (MTT) assays using 3-(4,5-dimethylthiasol-2-yl)-2,5-diphenyltetrazolium bromide (Biomatik, Wilmington, DE). Cells were seeded at 3-4,000 cells per well in 96-well microtiter plates, incubated overnight, and then treated with minocycline alone or in combination with doxorubicin or AC. For assays involving minocycline co-treatment, cells were pretreated with minocycline for 24 hours, followed by 48-hour exposure to the combination of minocycline with doxorubicin or AC. After drug treatment, cells were incubated with MTT solution for 60 minutes, the formazan crystals were solubilized with DMSO, and the absorbance was measured by spectrophotometry at 570nm wavelength. The IC50 values for doxorubicin and cyclophosphamide alone were determined by MTT in both the MDA-MB-231 and MDA-MB-468 cell lines (data not shown), and used to establish dose ranges for subsequent experiments.

Cell survival

Cell survival was evaluated by colony formation assays, which were performed by culturing 800 cells in 6-well plates, exposing cells to minocycline for 24 hours, followed by the minocycline-AC combination for 24 hours, then allowing the cells to proliferate

for 12 days, with media changed every 72 hours. Colonies were fixed with 4% formaldehyde (Sigma-Aldrich) and stained with crystal violet (5mg/ml in 2% ethanol, Sigma-Aldrich), then counted.

Western blotting

Western blotting was performed by lysing cells with sodium dodecyl sulfate (SDS) lysis buffer (1% SDS, 50mmol/L Tris-HCl pH 8.0, 10mmol/L EDTA) plus protease inhibitor cocktail (Sigma-Aldrich) and PhoSTOP phosphatase inhibitor (Roche) and sonication. Protein concentrations were standardized with a Micro BCA Protein Assay kit (Pierce Chemical), and each sample was homogenized in SDS sample buffer. SDS-polyacrylamide gel electrophoresis was performed using a 12% resolving gel (Appendix A; Sambrook et al., 1989). Wet transfer to PVDF membrane (Bio-Rad) was followed by blocking with 5% non-fat milk in TBS-T (TBS, 0.1% Tween-20). Incubation with primary antibodies was performed at a 1:500 dilution overnight at 4°C. Membranes were washed with TBS-T and incubated with horseradish peroxidase-conjugated secondary antibodies at a 1:5000 dilution at room temperature for 1 hour. Signal detection was performed on x-ray film using a chemiluminescence system (Amersham). Mouse primary antibody sources are: β-actin (MP Biomedicals), Bcl-2 (Santa Cruz), caspase-3 (Imgenex), γH2AX Ser139 (Millipore). Rabbit primary antibody sources are: H2AX (Millipore), p-p38 (Cell Signaling), PARP (Cell Signaling), c-myc (Cell Signaling), p38 (Cell Signaling).

In vivo studies

Eight to 12 week old athymic nude female mice were obtained from the National Institutes of Health Animal Procurement Program and were group-housed under conditions of constant photoperiod (12 hours light: 12 hours dark) with *ad libitum* access to sterilized food and water. Genotype information is tabulated in Appendix B. All experimental procedures using mice were done in accordance with protocols approved by The Ohio State University Institutional Animal Care and Use Committee. Xenograft tumors were established by suspending MDA-MB-231 cells in Matrigel (BD Biosciences) and injecting them subcutaneously into the right flank of anesthetized mice (isoflurane; $5x10^5$ cells/0.1ml/mouse). Tumor volumes and body weights were measured once weekly. Tumor length and width were measured by SK using calipers, and volume was calculated by applying the equation for the volume of a prolate ellipsoid $[0.52\times(L\times W^2)]$. Body weights of xenografted mice were adjusted for the tumor weight, as calculated by volume. Mice with a tumor volume between 50-75mm^3 were eligible for recruitment to the study, and were randomized to four treatment groups: vehicle control, minocycline only, AC only, and AC with minocycline (n=6-7/group). All animals received pre-treatment with minocycline (90 mg/kg) or vehicle (sterile distilled water) once daily *per os* for 3 days (starting on Day -3) and continuing for an additional 21 days (Day 0 – 21). On Day 0, mice were treated with a single IV injection of either AC [doxorubicin (A) at 5 mg/kg; cyclophosphamide (C) at 100 mg/kg] or vehicle (sterile normal saline). Minocycline was administered to anesthetized animals using a sterile, flexible gavage needle. AC and vehicle were administered by tail vein injection to non-

anesthetized animals in a restrainer by a laboratory animal health technician. The AC chemotherapy modeled a common clinical regimen in which patients are treated every 21 days. Animals were euthanized on Day 21 by CO_2 asphyxiation followed by cervical dislocation. Each animal was subject to complete post-mortem examination. All tissues were preserved by immersion fixation in neutral buffered 10% formalin. Organ weights were recorded post-fixation and are represented as relative organ weight (organ weight (g)/brain weight (g) ×100).

Histopathology and immunohistochemistry

Selected tissues were subject to a standard process of histopathologic evaluation [86], and routine H&E staining was performed by the Comparative Pathology and Mouse Phenotyping Shared Resource (CPMPSR). Tissues for toxicologic evaluation included: lung, heart, liver, kidney, spleen, bone marrow, small intestine, and brain. Brains were examined in 6 standard coronal sections per mouse [87] as guided by CPMPSR technical staff. Immunohistochemistry (IHC) was performed by CPMPSR using the same blocks. Five animals per treatment group closest to the group mean tumor volume were selected for immunohistochemical analysis. Primary antibodies for brain IHC are as follows: Iba1 (Abcam, 1:800), doublecortin (Abcam, 1:500), GFAP (Dako, 1:5000). Following primary antibody incubation, specimens were incubated with biotinylated secondary antibody and DAB chromagen, then counterstained with hematoxylin. Complete primary antibody information can be found in Appendix C. One xenograft cross-section per mouse was processed for histology, and IHC was performed by CPMPSR using the same blocks.

Primary antibodies for tumor IHC are as follows: cleaved caspase 3 (Cell Signaling, 1:180), Ki67 (Abcam, 1:200). Following primary antibody incubation, specimens were incubated with biotinylated secondary antibody and DAB chromagen, then counterstained with hematoxylin. All histologic analyses were performed by LH, and the features of selected tissues were peer-reviewed by a CPMPSR comparative pathologist. These assessments were performed using coding, where the pathologists were blinded to experimental conditions.

Digital immunohistochemical quantification

Blinded quantification of immunoreactivity was performed by LH with ImageScope Image Analysis Toolbox (Leica Biosystems). Quantitative algorithm specifications are tabulated in Appendices E, F, and G. In the tumors, staining was distributed evenly throughout the tissues, so a subsampling technique was employed. Cleaved caspase 3 positivity in each tumor section was calculated by applying the positive pixel count algorithm to quantify strongly positive-stained pixels per number of total pixels in 5 high-power fields (400X magnification) per tumor section. Ki67 positivity in each tumor section was calculated by applying the nuclear algorithm to quantify the number of positively labeled nuclei per total number of nuclei in 5 high-power (400X magnification) fields per tumor section. Mean values per tumor and per treatment group were calculated. In brain sections, the relative level of doublecortin (DCX) in the hippocampus was calculated by applying the positive pixel count algorithm to quantify positive-stained pixels per number of total pixels in the dentate gyrus of each brain section. Mean values

per brain and per treatment group were calculated. For all immunohistochemical digital quantitative analysis, mockup images are represented as heat maps, in which blue pixels are registered as negative, yellow as weakly positive, orange as moderately (medium) positive, and red as strongly positive.

Data analysis

Randomization for animal studies was performed using a free, web-based random sequence generator (www.random.org). All data are represented as the group mean ± 1 standard deviation. Statistical significance in each experiment was tested by determining variance by F-test, then performing a Student's t-test with the alpha level set at 0.05 *a priori*.

Results

Minocycline cannot protect TNBC cells from the cytotoxic effect of AC *in vitro*

The effect of minocycline alone on TNBC cell viability was assessed by MTT assay in MDA-MB-231 and MDA-MB-468 cells. After 48-hour treatment, relative cell viability in either cell line was not diminished by minocycline, even at concentrations of up to 100μM (Fig. 2.1A). In MDA-MB-468 cells, however, a statistically significant increase in cell viability was observed at the highest concentrations tested (75 and 100μM; t-test, $p<0.05$, vs 0μM). The clinical relevance of the effects of these minocycline concentrations, however, is questionable as they are at least an order-of-magnitude

greater than the plasma C_{max} achieved with various clinical oral formulations of minocycline [88-92].

For initial assessment of the effects of minocycline on chemotherapy-induced cytotoxicity, TNBC cells were co-treated with minocycline and doxorubicin, an anthracycline that can induce growth arrest and apoptosis in cancer cells through disruption of DNA repair and generation of reactive oxygen species [93]. As shown in Fig. 2.1B, minocycline at concentrations of up to 40μM had no significant effect on the viability of doxorubicin-treated MDA-MB-231 or MDA-MB-468 cells. Western blot analysis, however, revealed that minocycline at 40μM decreased doxorubicin-induced cleavage of caspase-3 and PARP (Fig. 2.1C), reminiscent of its effects in cisplatin-treated HEI-OC1 auditory cells [35]. While change in Bcl-2 abundance was not detected in MDA-MB-231 cells, MDA-MB-468 cells exhibited an increase in a 30kDa Bcl-2 immunopositive band in the presence of minocycline that may represent phosphorylated Bcl-2 or another isoform of the Bcl-2 protein [94].

To evaluate the effects of minocycline on the activity of a common doxorubicin-based adjuvant therapy regimen, MDA-MB-231 and MDA-MB-468 cells were co-treated with minocycline and the AC combination. Similar to the findings above, minocycline showed no protective effect against AC-induced inhibition of cell viability or clonogenicity as determined by MTT (Fig. 2.2A) and colony formation (Fig. 2.2B) assays, respectively, but still reduced the abundance of AC-induced cleaved caspase-3, as determined by

western blot (Fig. 2.2C). However, the apparent anti-apoptotic effect of minocycline on PARP cleavage that was observed in cells treated with minocycline plus doxorubicin as a single chemotherapeutic agent was lost (Fig. 2.2C). Moreover, no changes to AC-induced p38 phosphorylation, c-myc downregulation, or H2AX phosphorylation were observed with the addition of minocycline to AC treatment (Fig. 2.2C).

Minocycline cannot protect TNBC xenograft tumors from the growth suppressive effect of AC *in vivo*

To investigate the effects of minocycline on AC activity *in vivo*, athymic nude mice bearing subcutaneous MDA-MB-231 xenograft tumors were treated with minocycline at 90mg/kg or vehicle *per os* once daily for 3 days and continuing for an additional 21 days following a single administration of AC or vehicle by IV injection (Fig. 2.3). As shown in Fig. 2.4, treatment with minocycline alone did not significantly affect tumor growth compared to the vehicle–treated control, and, more importantly, minocycline co-treatment did not alter the tumor-suppressive activity of AC treatment. Moreover, mean adjusted body weights of the drug-treated groups over this time period were not significantly different from those of the vehicle-treated control group (Fig. 2.4). Both the AC and the AC plus minocycline treatment groups experienced body weight loss which was most pronounced at day 14, but recovered by day 21, following a pattern observed for a similar AC-based chemotherapeutic regimen in mice [95]. Post-mortem toxicologic evaluation revealed a consistent, significant decrease in splenic absolute weight and relative weight normalized to body or brain weight in the combined AC plus minocycline

treatment group (Table 2.1). Histologic lesions were not appreciated by light microscopic examination of the spleen or bone marrow. No evidence of drug-related systemic toxicity was identified on histopathology at the study endpoint (data not shown).

Intratumoral biomarkers of apoptosis (cleaved caspase 3) and proliferation (Ki67) were evaluated by immunohistochemistry in tumors collected at the study endpoint. No significant differences among the treatment groups for either marker were identified by routine light microscopy, and this was corroborated by quantitative analysis. Cleaved caspase 3 immunopositivity, defined as the number of strongly positive pixels per total number of pixels, was 9.98% in the vehicle-treated group, 8.13% in the minocycline group, 11.95% in the AC group, and 7.86% in the AC plus minocycline group (Fig. 2.5A). These differences, although not statistically significant, resembled the trend in cleaved caspase 3 expression observed in our *in vitro* findings (Fig. 2.2C), hinting at a partially protective effect of minocycline against AC-driven caspase 3 activation, albeit an effect that was not reflected in diminished tumor control. Ki67 immunopositivity, defined as the number of positive nuclei per total number of nuclei, was 64.20% in the vehicle treated group, 64.85% in the minocycline group, 65.18% in the AC group, and 65.32% in the AC plus minocycline group (Fig. 2.5C).

Effect of minocycline on CNS in AC-treated, TNBC tumor-bearing mice

To evaluate the presence of neuroanatomic lesions consistent with the proposed pathophysiology of CICI, the brains of the tumor-bearing mice from the *in vivo* study

described above were examined by H&E and IHC for evidence of microglial activation (Iba1) and astroglial scars (GFAP) as potential indicators of neuroinflammation. Six standard coronal sections per mouse were evaluated with particular attention to the hippocampus, and no evidence of microglial activation or glial scars was found (Fig. 2.6A). The brains were also examined by IHC for doublecortin (DCX) reactivity, a marker of immature neural progenitor cells which would be expected to be sensitive to neurotoxicity caused by AC treatment. In particular, immunopositivity was quantified in the dentate gyri (Fig. 2.6B). Differences among treatment groups were first identified in subgranular zone cells by subjective light microscopic assessment, so digitization and quantification were performed. AC-treated mice showed a 23.8% decrease in DCX positivity compared to vehicle controls, whereas mice receiving minocycline with AC showed only an 8.4% decrease in DCX-positive cells compared to the vehicle-treated group. These changes, however, did not achieve statistical significance. Mice in the vehicle control and minocycline only groups exhibited approximately equivalent levels of DCX positivity (Fig. 2.6B).

Discussion

Together, our data demonstrate that minocycline may provide protection against AC-induced neurological effects without compromising its chemotherapeutic efficacy. Specifically, minocycline did not protect TNBC cells from the cytotoxic and tumor-suppressive effects of AC chemotherapy, nor did it appear to have any inherent anti-cancer activity in TNBC cells. In MDA-MB-231 and MDA-MB-468 cells treated with

doxorubicin or AC, an anti-apoptotic effect of minocycline was consistently apparent by western blot, as evidenced by decreased caspase-3 cleavage, thus illustrating the anti-apoptotic potential of minocycline. This effect on AC-induced caspase-3 activation was also observed by IHC, although not at a statistically significant level, in TNBC xenograft tumors from mice treated with minocycline and a single cycle of AC chemotherapy. However, assays of cell viability and clonogenic survival, as well as the evaluation of other biomarkers of apoptosis (PARP), cell stress (phospho-p38), and DNA damage (γH2AX), indicated that this decreased caspase-3 cleavage was insufficient to rescue TNBC cells from the combined cytotoxicity of AC chemotherapy. Moreover, minocycline did not alter the tumor-suppressive efficacy of AC chemotherapy in TNBC xenograft tumor-bearing mice, and it appeared to be well-tolerated over the course of 24 days of once daily oral administration. Taken together, these findings support the evaluation of minocycline in clinical trials as a neuroprotective agent for the amelioration of CICI in women receiving AC chemotherapy for breast cancer.

We cannot account for the decrease in absolute and relative splenic weight in the combined AC plus minocycline treatment group. Histologic lesions such as reduced erythropoiesis or myelopoiesis were not appreciated by light microscopic examination of the spleen or bone marrow, nor did the mice develop any clinical signs of myelosuppression. One possible explanation is reduced post-mortem splenic congestion due to anemia. Complete blood cell count or packed cell volume were not measured in these mice to corroborate possible leukopenia or anemia. These findings may support the

need for increased vigilance in the clinical setting in monitoring the hemogram and leukogram of patients on an AC plus minocycline protocol.

The presence of an increased proportion of DCX-positive cells in the hippocampi of tumor-bearing, AC-treated mice that received minocycline, relative to those that did not, suggests the possibility for increased neural plasticity vis-à-vis neural regeneration from this progenitor cell pool. Progenitor cells in the adult mammalian brain are indeed a susceptible population [68, 83] that could be inadvertently targeted by cytotoxic agents, leading to deleterious effects on cognition [96] due to cell death and altered dendritic spine connectivity [97]. In a recent study, neural stem cell transplantation was proven sufficient to reverse "chemobrain" in a mouse model of CICI [98]. Thus, we posit that preservation of neural progenitor cell populations associated with minocycline treatment could have a similarly beneficial effect; further studies are warranted to determine whether the neuroprotection provided by minocycline is functionally significant. In addition, without a time course study, it is not possible to differentiate whether our findings represent a true increase in the number of neural progenitors, or possibly arrest of pre-existing progenitors in a less differentiated state. Furthermore, if minocycline is capable of increasing a stem-like or progenitor cell pool in the brain, it would be worthy of investigation to determine whether the same phenomenon occurs in tumors, where this effect may be undesirable.

Our study found no evidence of microglial activation or astroglial scarring in the brains of tumor-bearing mice 21 days after a single dose of AC, as evaluated by Iba1 and GFAP immunostaining, respectively. Importantly, tumor-bearing mice in the vehicle-treated control group also showed no neuroanatomic abnormalities by light microscopy, suggesting that the presence of a tumor alone may be insufficient to generate histologic brain lesions compatible with CICI. It is possible that neuroanatomic changes in microglia and astroglia may not be microscopically detectable following only one cycle of AC therapy (i.e. insufficient cumulative total dose), or that the cognitive ramifications of AC are manifest in functional aberrations that may be better characterized by cytokine profiling, behavioral endpoints, or functional *in vivo* assays like fMRI in conjunction with histopathology and immunohistochemistry. To our knowledge, there has been no characterization of the histologic lesions of CICI in humans. It would be interesting to determine whether histopathologic lesions are present in human breast cancer patients with CICI symptoms before beginning chemotherapy; however, availability of tissue from such a patient population through brain biopsy or accidental death is improbable and generally unavailable, reiterating the importance of establishing and validating such an animal model. Rather, the current standard of characterizing brain lesions of CICI in humans is indirectly through fMRI, where patients pre- and post-chemotherapy are compared to healthy, age-matched controls in resting state and working memory assays. Self-reporting (questionnaire) is also used to measure anxiety, fatigue, and sleep disturbances. Using biotelemetry, Borniger et al. have shown that a single cycle of AC chemotherapy in tumor-free mice leads to reduced quality of sleep and sleep

fragmentation – one symptom of CICI [99]. It is not yet known what histologic brain lesions, if any, would be expected in mice with said behavioral disturbances, but this warrants further investigation.

CICI is a complex cognitive phenomenon that poses significant challenges for recapitulation in an animal model. For example, the cognitive decline that some breast cancer patients begin to experience even before beginning chemotherapy can be attributable, at least in part, to the psycho-emotional implications of a cancer diagnosis, including depression, fatigue, and anxiety [80, 100]. Importantly, Bruno et al. emphasize that damage to neural networks associated with chemotherapy cannot be statistically explained by psychiatric distress alone [78]. Reports using advanced imaging technologies in longitudinal and prospective studies thoroughly evaluating cognitive function pre- and post-chemotherapy and risk factors in breast cancer patients are beginning to surface [71, 73-77, 101]. We anticipate that patient selection would be of utmost importance in choosing when to prescribe minocycline as a neuroprotectant in patients receiving AC chemotherapy for breast cancer. The concept of antimicrobial stewardship must not be ignored. Patient selection criteria might include patients who are more susceptible to neurotoxicity by xenobiotics due to efflux transporter mutations, or possibly patients who begin to show pre-treatment abnormalities in brain imaging following their cancer diagnosis. We anticipate that treatment of CICI symptoms in cancer patients would also involve a multidisciplinary approach, as non-pharmacologic

interventions such as cognitive and behavioral rehabilitation therapy are also of value [102].

Survivor care is a critical aspect of holistic cancer treatment and will be increasingly important moving forward, as breast cancer patients are surviving longer than ever before [103]. Because treatment for TNBC, an aggressive form of breast cancer, is still largely dependent on cytotoxic adjuvant drugs like doxorubicin and cyclophosphamide, management of untoward side-effects such as CICI is paramount. We propose that minocycline should be considered as a potential neuroprotective agent to be administered to breast cancer patients concurrently receiving AC chemotherapy and that our data support moving such a therapeutic protocol towards clinical trials.

Limitations and Future Directions

Recapitulation of a human-like model of CICI has not been achieved in the mouse. In our studies, multiple cycles of AC were not performed, and mice did not receive a total cumulative dose of said chemotherapeutic agents due to tumor burden and removal criteria. Several other features that distinguish our mouse model from the human condition must be acknowledged. Our mice were gonadally intact and of reproductive, while some women with breast cancer may be pre-menopausal and undergo surgical oophorectomy, or be post-menopausal. Thus, these effects of gonadotropic hormones on the brain were not evaluated in our study. The immunocompromised status of the mice is another limiting factor. T-cell driven processes may contribute to CICI, and this cannot

be modeled in a non-humanized xenograft-bearing mouse. The overall tumor burden differs significantly between the mouse and human conditions as well. A woman typically undergoes surgery for her primary tumor, possibly with neoadjuvant chemotherapy administered shrink the tumor beforehand and/or adjuvant chemotherapy to treat presumed micrometastases. The overall tumor burden in the adjuvant setting is little to none. In our mice, the relative tumor burden by body weight is quite high by comparison. It is not known whether factors related to a tumor itself could be responsible, at least in part, for the phenomenon of CICI, and our study does not parse this out; however, it would be feasible to include an arm that receives the same drug combinations but is non-tumor-bearing. Some practical limitations of the *in vivo* study is small group sizes, which make it difficult to achieve statistical significance when there is a moderate degree of variation within a group.

Additionally, we acknowledge that in the *in vivo* study, histopathologic lesions that might be consistent with CICI were not observed. This could be due to the relative insensitivity of histopathology, compared to other methods, to detect early changes at the biochemical, cytokine, or ultrastructural levels. Functionally, microdissection of brain locations with high proportions of neural progenitor cells and hotspots implicated in the pathogenesis of CICI could be isolated for in-depth analysis by electron microscopy, cytokine multiplexing, and biomarker arrays. It would also be possible to perform whole-brain quantitative analysis of DCX+ neural progenitor cell populations, particularly in other locations in which they are prominent in the mouse, including the subventricular zone

and olfactory bulbs. Pairing these anatomic and biochemical descriptive studies with cognitive performance assays in the same mice would surely be of value and may guide brain microdissection. If the neuroprotective effect on neural progenitor cells in the brain is validated in future studies, this work has important potential applications for cancer survivors, particularly those that might be most susceptible to the neurotoxic effects of chemotherapy such as pediatric oncology patients.

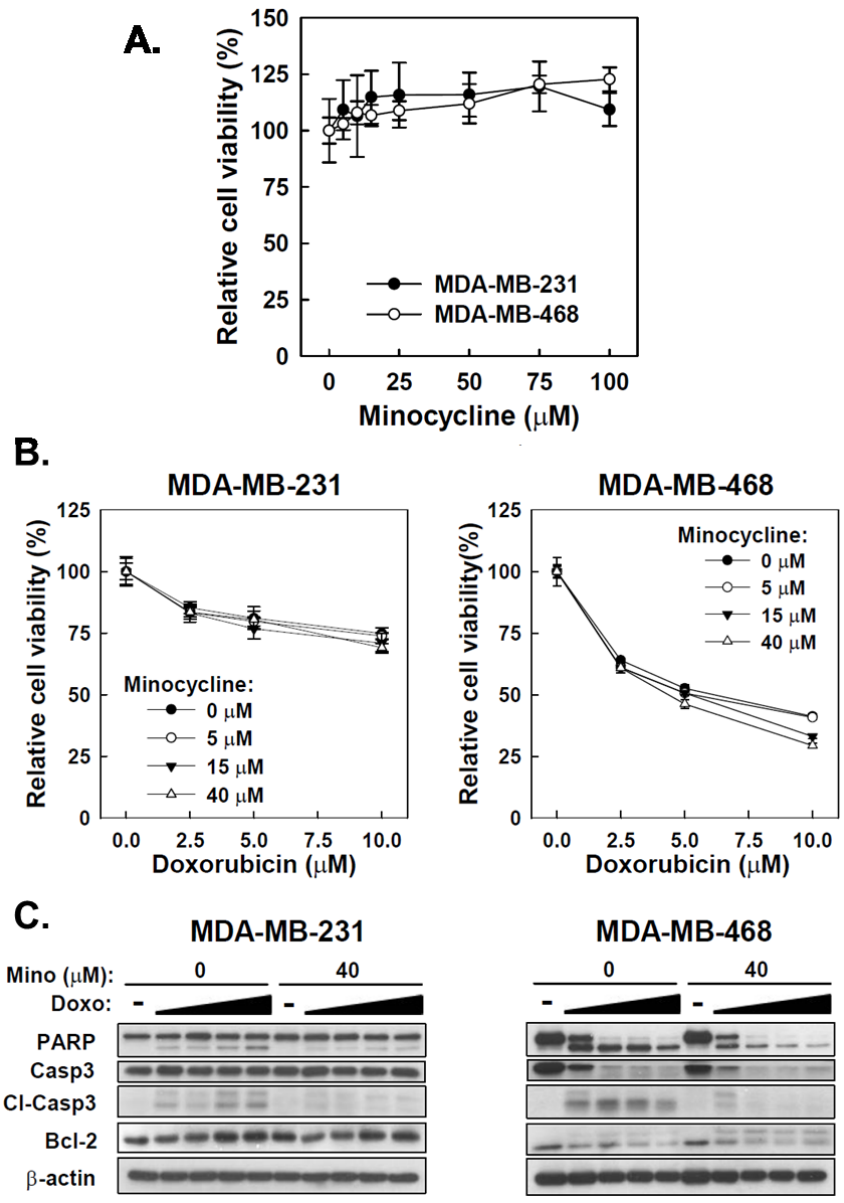

Figure 2.1 Effects of minocycline alone and in combination with doxorubicin in MDA-MB-231 and MDA-MB-468 TNBC cells.

A and B. Cell viability was assessed by MTT assay after treatment with minocycline alone (A) and in combination with doxorubicin (B). C. Evaluation of the effect of minocycline (Mino) on apoptosis-related biomarkers in doxorubicin (Doxo)-treated TNBC cells by western blot. Concentrations of doxorubicin used were 0, 1, 2.5, 5 and 10 μM. In both B and C, cells were pretreated with minocycline for 24 hours, followed by 48-hour exposure to the doxorubicin-minocycline combination.

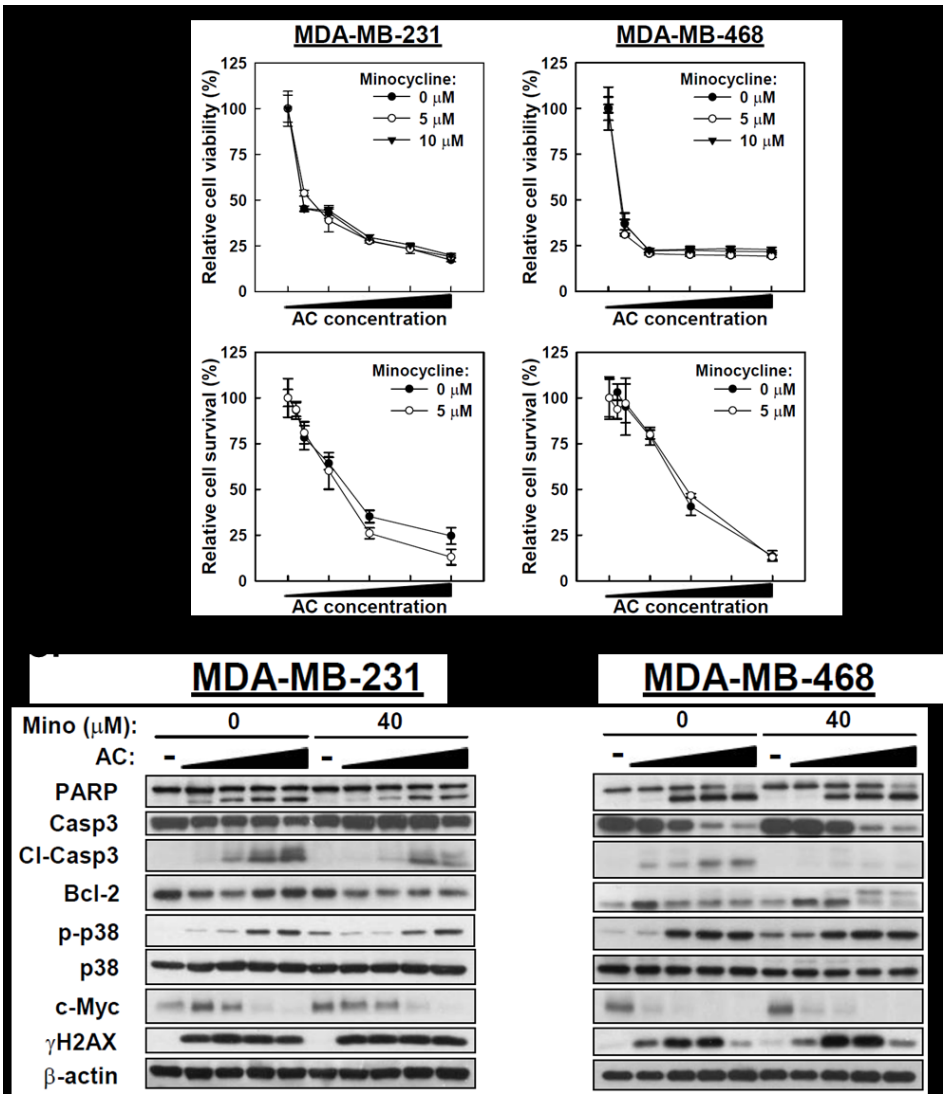

Figure 2.2 Effects of minocycline on the cytotoxicity of AC chemotherapy in MDA-MB-231 and MDA-MB-468 TNBC cells.

A. Cell viability was assessed by MTT assay after minocycline co-treatment with AC (μM/mM: 0/0, 1/2.5, 2.5/5, 5/10, 7.5/15, and 10/20). B. Cell survival was assessed by colony formation assay after minocycline co-treatment with AC (nM/μM: 0/0, 0.5/0.5, 1/1, 2.5/2.5, 5/5, 10/10). C. Evaluation of the effect of minocycline on biomarkers in AC-treated TNBC cells by western blot. Cells were treated with AC at 0/0 0.5/1, 1/2.5, 2.5/5, 5/10 μM/mM. For panels A and C, cells were pretreated with minocycline for 24 hours, followed by 48-hour exposure to the AC-minocycline combination. For B, cells were treated with minocycline for 24 hours, and then the AC-minocycline combination for 24 hours, followed by a 12-day growth period.

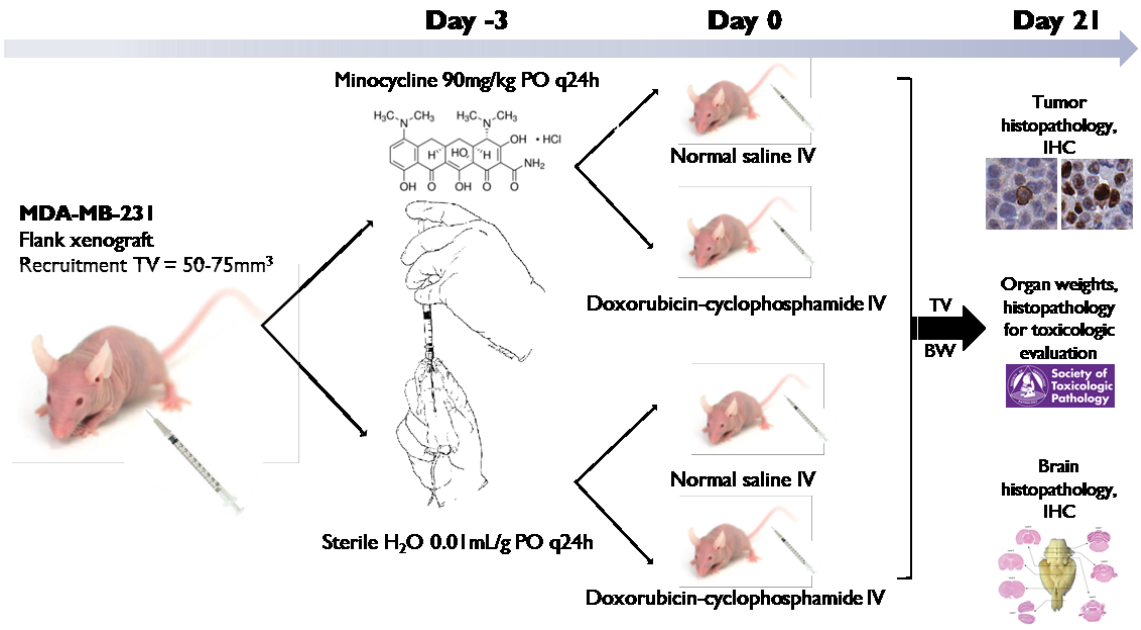

Figure 2.3 Schematic of TNBC xenograft study.

Mice were injected with $5x10^5$ MDA-MB-231 cells in the left flank. Tumor growth was monitored until recruitment volume was reached, then mice were randomized to one of four treatment groups. Minocycline pre-treatment began 72h prior to IV injection of either AC or vehicle (normal saline). Mouse body weights and tumor volumes were followed for 21d following IV injection, then post-mortem endpoints were assessed, including tumor histopathology and IHC, organ weights, and brain histopathology and IHC.

Athymic Nude Mice ©Envigo, retrieved from: http://www.envigo.com/resources/data-sheets/envigo-5193-131-leaflets-2016-nude-mouse-combination-a4-refs.pdf
Logo ©Society of Toxicologic pathology, retrieved from: http://www.toxpath.org
Oral Gavage ©University of Illinois at Chicago Biologic Resources Laboratory, retrieved from: https://www.brl.uic.edu/node/37

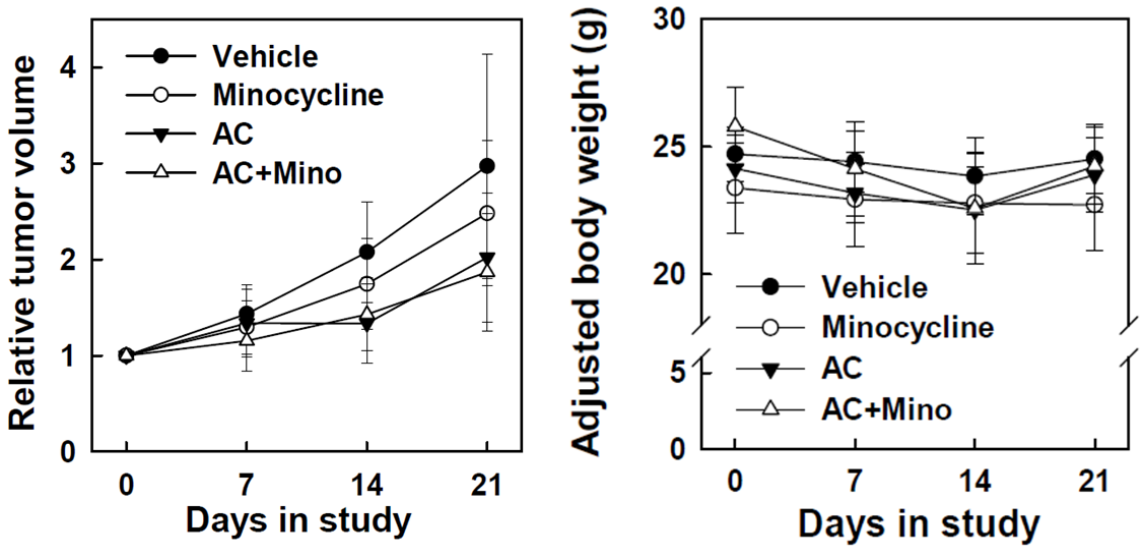

Figure 2.4 Effects of minocycline on the tumor-suppressive activity of AC chemotherapy in the MDA-MB-231 TNBC xenograft model.

Upon recruitment to the study, tumor-bearing mice were treated with minocycline (90mg/kg, *per os*, once daily) or vehicle for 24 days (Day -3 to Day 21). On Day 0, mice were treated with AC (A [doxorubicin], 5mg/kg; C [cyclophosphamide], 100mg/kg; IV) or vehicle. Relative tumor volumes and body weights in vehicle control, minocycline, AC, and AC plus minocycline treatment groups are shown.

		Vehicle	Mino	AC	AC + Mino
Liver	Absolute (mg)	1190.55 ± 79.39	1073.20 ± 172.58	1165.40 ± 135.20	1126.81 ± 119.18
	Rel BoW	4.86 ± 0.33	4.70 ± 0.52	4.82 ± 0.43	4.62 ± 0.62
	Rel BrW	239.06 ± 14.90	215.75 ± 25.13	234.66 ± 23.22	229.25 ± 24.80
Kidneys	Absolute (mg)	366.06 ± 26.54	354.53 ± 40.81	370.31 ± 63.48	494.65 ± 18.86†
	Rel BoW	1.49 ± 0.08	1.56 ± 0.12	1.53 ± 0.20	1.52 ± 0.20
	Rel BrW	73.45 ± 4.03	71.48 ± 6.69	74.57 ± 12.15	75.21 ± 7.43
Heart	Absolute (mg)	155.54 ± 21.40	147.54 ± 22.41	160.35 ± 23.68	163.80 ± 23.04
	Rel BoW	0.64 ± 0.09	0.65 ± 0.08	0.66 ± 0.09	0.67 ± 0.11
	Rel BrW	31.18 ± 3.74	29.74 ± 3.86	32.32 ± 4.60	33.33 ± 4.85
Spleen	Absolute (mg)	149.96 ± 15.97	119.04 ± 30.28*	121.15 ± 16.23	102.76 ± 20.57*
	Rel BoW	0.61 ± 0.10	0.52 ± 0.10	0.50 ± 0.10*	0.42 ± 0.10*
	Rel BrW	30.02 ± 5.33	24.16 ± 5.06*	24.50 ± 6.09	20.83 ± 4.90*

Table 2.1 Organ Weight Data.

Fixed liver, kidney, heart, and spleen weights are reported as absolute (mg), relative to body weight, and relative to brain weight in vehicle, minocycline, AC, and AC plus minocycline treatment groups.

*Statistically significant decrease relative to vehicle ($p<0.05$)

†Statistically significant increase relative to vehicle ($p<0.05$)

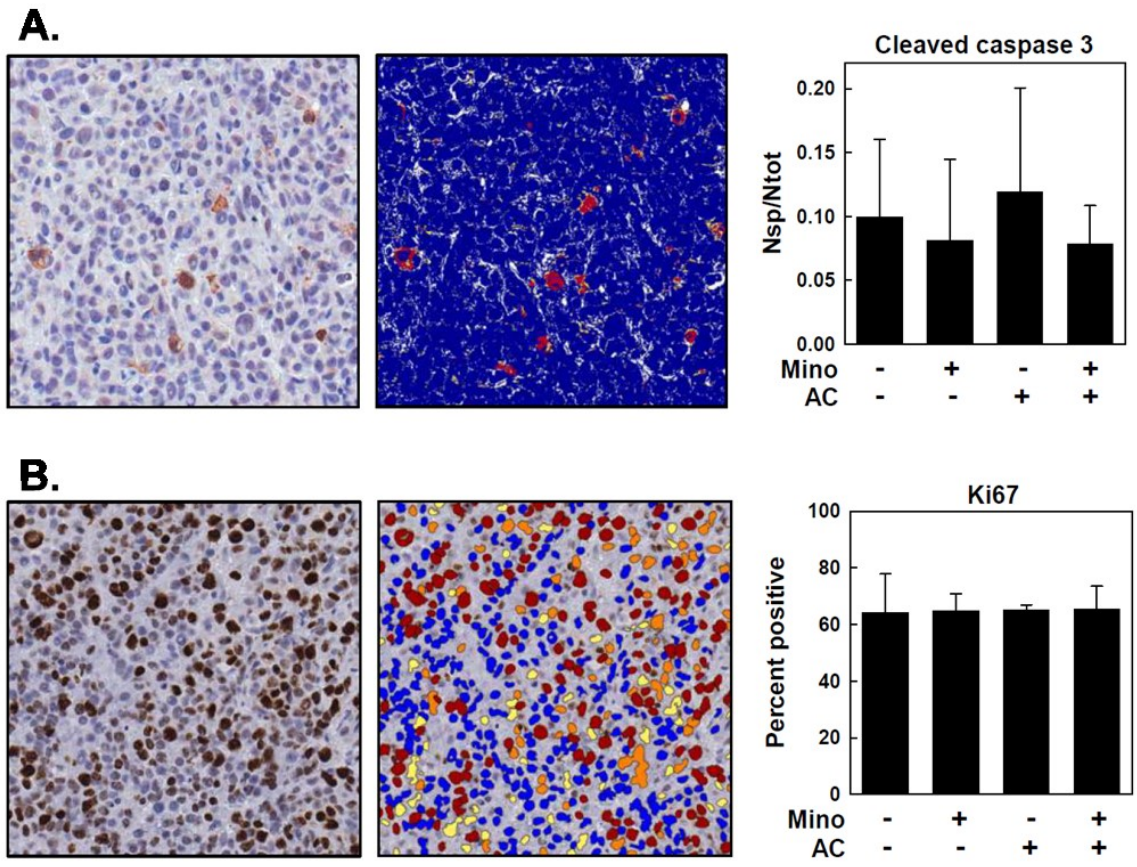

Figure 2.5 Immunohistochemistry for cleaved caspase 3 and Ki67 in formalin-fixed paraffin-embedded MDA-MB-231 xenograft tumors.

Immunohistochemistry for cleaved caspase 3 (A) and Ki67 (B). Representative immunostained sections (left panels; counterstained with hematoxylin) and corresponding mockup images for digital analysis (middle) from the vehicle treatment group are shown. Right, quantification of cleaved caspase 3 staining expressed as the number of strong positive pixels per total pixels analyzed (Nsp/Ntot) and Ki67 staining expressed as percent positive nuclei per total nuclei analyzed in tumors from the four treatment groups (n=5). Magnification, 40X.

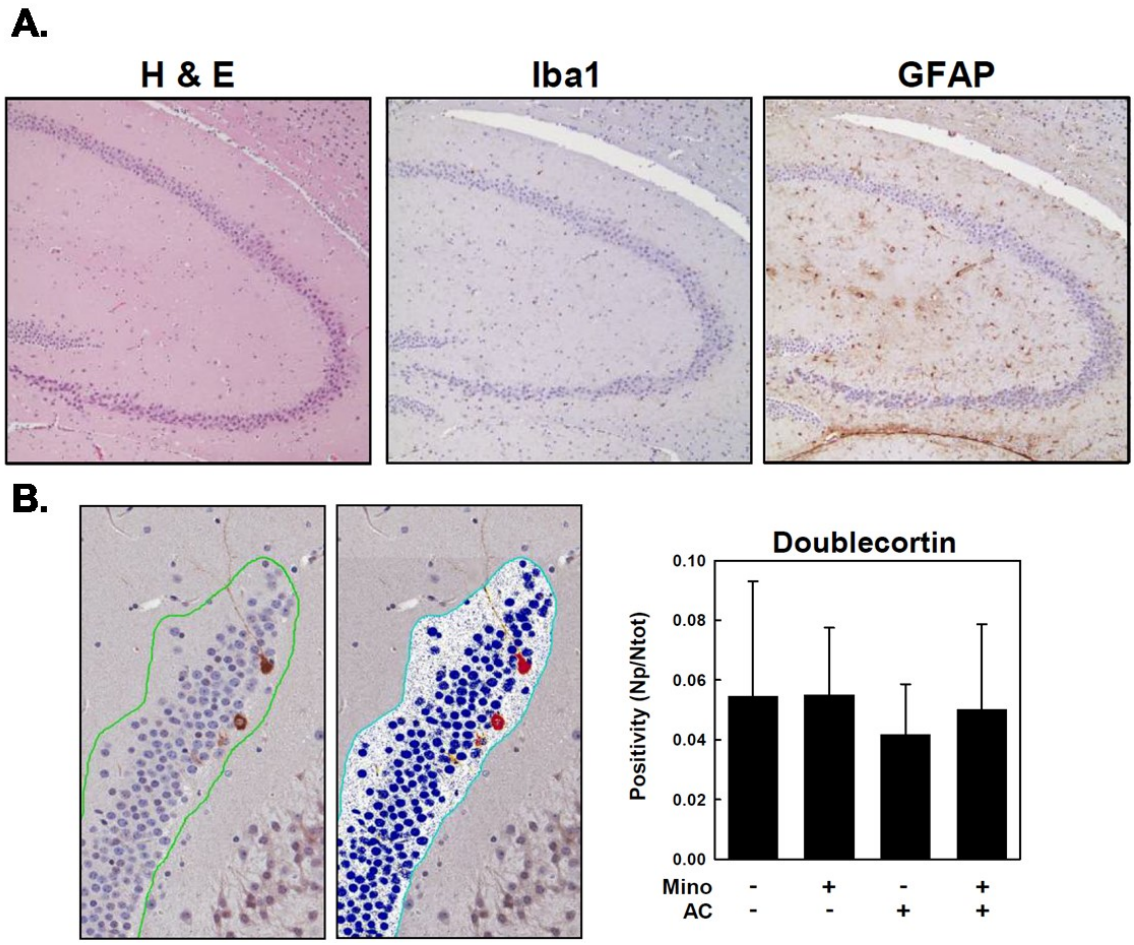

Figure 2.6 Neuroanatomic evaluation in MDA-MB-231 xenograft tumor-bearing mice.

A. Representative partial sections of hippocampus and dentate gyrus are shown for H&E, Iba1, and GFAP stains from the AC treatment group. B. Doublecortin immunohistochemistry (left) and a corresponding mockup image for digital analysis (middle) of a representative section of dentate gyrus from the vehicle treatment group. Right, quantification of doublecortin staining expressed as positivity (the number of positive pixels per total pixels analyzed) in brains from the four treatment groups (n=5). Magnification, 36X.

Chapter 3 : Non-epigenetic effect of HDAC8 inhibition in downregulating breast cancer stem cells through Notch1 degradation and preliminary testing of the novel isoform-specific inhibitor Cpd25

Abstract

In many types of cancer, a self-renewing subset of the tumor population described as cancer stem cells is linked to tumor recurrence, drug resistance, and metastasis. Here, we report a novel non-epigenetic function of HDAC8 as a Notch1 agonist and promoter of the cancer stem cell phenotype in triple-negative breast cancer via stabilization of the Notch1 protein. This mechanistic link was intimated by the observation that treatment of MDA-MB-231 and SUM-159 cells with pan-HDAC inhibitors AR-42 and vorinostat caused a dose-dependent downregulation of cancer stem cell biomarkers including Notch1, NICD, BMI-1, Zeb-1, and Nestin, as well as a decrease in mammosphere formation. By narrowing the scope from pan-HDAC inhibition to class I-selective HDAC inhibition by depsipeptide, then to individual HDAC isoform knockdown using siRNA, we found that HDAC8 alone is responsible for maintenance of Notch1 protein levels, independent of bulk histone acetylation associated with HDAC inhibitors. This finding is supported by data suggesting that the HDAC8-targeted inhibitor PCI-34051 also leads to decreased Notch1 protein expression. This suppression of Notch1 in response to HDAC8

inhibition was abrogated by the proteasome inhibitor MG132 and siRNA-induced silencing of Fbwx7, indicating that knockdown of HDAC8 ultimately leads to Notch1 polyubiquitination and proteasomal degradation. In an orthotopic xenograft study utilizing shRNA HDAC8 knockdown in MDA-MB-231 cells, the tumor incidence was markedly, stably decreased compared to the parental cell line. Overall, our work demonstrates that HDAC8 is critical to maintaining Notch1 integrity and therefore to preserving the cancer stem cell subset in triple-negative breast cancer, thus presenting a possibility for therapeutic elimination of breast cancer stem cells via targeted HDAC8 inhibition. Together, these findings suggest an important role for HDACs in the maintenance of BCSC populations and provide a therapeutic means for the strategic eradication of CSCs through HDAC8.

Introduction

Breast cancer stem cells

Mammary tumors are heterogeneous, consisting in part of a subpopulation of cancer stem cells (CSC) which, by definition, are capable of self-renewal [104-109]. These breast cancer stem cells (BCSC) are believed to contribute to chemotherapeutic resistance and possibly recurrence [106, 109-115]. CSC are also characterized by epigenetic plasticity, thus leading to tumorigenic behavior when self-renewal and differentiation pathways become dysregulated [109, 116-118]. The cancer stem cell (CSC) hypothesis holds that a proportion of cells within a given tumor are multipotent and self-renewing, giving rise to a heterogeneous tumor comprised of progenitor and lineage-committed daughter cells

[104-109, 119-124]. Thus, they are often considered responsible for cancer initiation, sustenance, and recurrence [107, 109, 113-115, 119, 126]. The origin of CSCs may be resident tissue stem cells with acquired mutations or dysregulated self-renewal pathways or possibly de-differentiation (i.e. by epithelial-mesenchymal transition (EMT)) from a differentiated cancer cell due to genetic or epigenetic instability, or possibly manipulation of the tumor microenvironment [105, 109, 119, 127, 128]. A defining characteristic of CSCs is that in xenotransplantation studies, these cells are able to self-renew and differentiate, recreating identical disease as was observed in the donor [104, 120-122]. It is reported that up to 20% of cells within a given breast tumor of human or mouse origin may bear a stem-like phenotype [105, 109, 129]; however, the composition of a tumor could vary greatly between individuals based on the prevalence of normal stem cell pools in a given tissue type, accumulation of genetic or epigenetic modifications in the cancer cells, the tumor microenvironment, and certain host factors [106, 108, 119, 127]. Stem-like cells have been characterized in the SUM-159 and MDA-MB-231 breast cancer cell lines [119, 128]. The first report of tumorigenic, cancer-initiating cells in solid cancers was published by Al-Hajj et al., who described a breast cancer stem cell (BCSC) population characterized by $CD44^{+}/CD24^{-/low}/Lin^{-}$ that had 10-50 fold increased capacity for tumor formation in NOD.SCID mice and was capable of recreating the cellular heterogeneity found in the primary tumors from which they were derived [104]. As few as 20 tumor-initiating cells are reportedly required to establish a new tumor in xenograft studies [130]. CSCs have been identified in human leukemia [122], breast cancer [104], prostate cancer [105, 124], brain tumors [105, 124], ovarian cancer [105, 124], colon

cancer [105], and some head and neck cancers [124]. Interestingly, stem cells have also been identified in mammary ductal carcinoma *in situ* (DCIS) lesions, suggesting that CSC may contribute to early tumorigenesis [119]. A study of low-grade versus high-grade DCIS tumors also found that high-grade lesions demonstrated greater mammosphere forming efficiency [131]. Comparatively, Lo et al. report anomalous expansion of a $CD49f^{+}/CD61^{+}/ESA^{+}$ CSC population in preneoplastic mammary glands of Her2/neu transgenic mice [114]. Pathways of interest include Wnt, Notch, EGF, and TGF [10, 25,128] – endow capacity for increased proliferation, stromal invasion, and resistance to anoikis – features important for normal mammary stem cells and physiologic gland function, also hijacked by CSC.

CSCs pose a significant therapeutic challenge because they are more resistant to chemotherapy [106, 109-114]. CSC are often characterized by expression of ABC drug transporters (i.e. ABCG2), the MDR1 gene, and/or high levels of the detoxifying enzyme aldehyde dehydrogenase (ALDH), thus conferring drug resistance [109, 112,113]. $CD44^{+}/CD24^{-}$ sorted CSC from primary breast tumors or breast tumor cell lines have demonstrated 10-60 fold increased resistance to chemotherapy with 5-fluorouracil, epirubicin, and cyclophosphamide compared to non-$CD44^{+}/CD24^{-}$ tumor cells [113]. Their resistance may also stem in part from the fact that they survive for prolonged periods in a nearly quiescent state [130], leading to CSC enrichment following chemotherapy [25]. Putative BCSC characterized by the same markers have been detected in patients with pleural and bone metastases, indicating that these cells may have

a propensity for metastatic behavior [106]. Similar reports have found that breast tumors containing higher proportions of stem-like cells, evidenced by $CD44^{+}/CD24^{-}$, ALDH1 enzymatic activity, and mammosphere forming capacity are associated with high histologic grade, chemotherapeutic resistance, and poorer prognosis [112]. ALDH1 has been identified as a marker of both non-malignant and CSCs [132]. When detected by IHC, high levels of ALDH1 in breast cancer patients correlate with poor clinical response to neoadjuvant chemotherapy and reduced survival [111, 113]. Strategies directed towards CSC include chemotherapy sensitization, differentiating and depleting therapy, targeting drug transporters, and inhibition of self-renewal or cell signaling pathways [109, 127]. Along these lines, pathways of particular interest include Wnt/β-catenin, Hedgehog, and Notch [107, 109, 119, 127, 128, 131, 133-137]. Our specific focus in this project is on the Notch signaling pathway, an important determinant of cell fate in breast cancer irrespective of hormonal and Her2/neu receptor status. Notch is involved in regulating cellular proliferation, differentiation, and apoptosis [107]. Inhibition of Notch signaling has been associated with reduced mammary tumorsphere formation *in vitro* [131, 137]. Furthermore, there is evidence that treatment of ER+ breast cancer with anti-estrogens or aromatase inhibitors leads to dependence on Notch signaling; thus, Notch may be a relevant target in ER+ breast cancer [107].

Histone deacetylases in cancer

Epigenetic regulation of gene expression plays a critical role in tumorigenesis [116-118, 138]. Chromatin remodeling into a more open or closed structure is largely dependent on

the activity of enzymes which post-translationally modify histone tails, including DNA methyltransferases (DNMT), histone acetyltransferases (HAT), and histone deacetylases (HDAC). These epigenetic marks constitute the histone code, which dictates in part the degree to which genes are transcribed or repressed. HDAC activity is required for cell proliferation and survival, and inhibition is associated with G1/S and G2/M cell cycle arrest [117, 118, 139-143]. Acetylation of histone tails neutralizes their positive charge, thus decreasing the strength of the interaction between DNA and the histone proteins about which it is wound and relaxing the chromatin structure [117]. Thusly, histone deacetylation by HDAC is correlated with silencing of tumor suppressor genes such as CDK inhibitors p21, p27, and p16 and dysregulated cellular proliferation, differentiation, and adhesion [117, 138, 144, 145]. HDACs are also known to directly modify the acetylation state of other non-histone proteins involved in oncogenesis such as β-catenin, c-myc, ERα, p53, HSP90, NFκB, E2F1, STAT1, STAT3, and HIF-1α [117, 138, 139, 145-148]. There are 18 human HDACs separated into four classes (I-IV), three of which depend on zinc cations for catalytic activity [117, 149]. Of these three classes, class I HDACs are ubiquitously expressed in all tissues and exert a strong catalytic effect on histone lysine residues [117, 118, 149]. Class I HDAC members include HDAC1, 2, 3, and 8, and their individual knockdown in mouse models creates embryonic lethal or postnatally-fatal phenotypes [117, 138, 150, 156]. HDAC1, 2, and 3 have been shown to be involved in cell cycle regulation and associate with transcriptional corepressor complexes [149]. As an example of how this contributes to oncogenesis, HDAC1, HDAC2, and the corepressor complex mSin3A are recruited by Snail to the E-cadherin

promoter to repress its expression [116]. Also, estrogen receptor gene transcription is regulated by multiprotein complex including HDACs, DNMTs, and Rb protein [116].

Role of HDAC8

The role of HDAC8 is not yet well-understood. HDAC8 is primarily cytoplasmic but can be found in the nucleus as well [147, 149, 150], and high levels of HDAC8 expression in childhood neuroblastoma have been found to correlate with advanced stage disease and poor survival [118, 149, 150]. Until recently, HDAC8 was not known to associate with corepressor complexes, unlike the other class I HDACs, but Kang et al. have published data which suggest that HDAC8 associates with a corepressor complex directly to repress transcription of the Bcl-2-modifying factor (*BMF*) gene and thus Bmf-mediated apoptosis [151]. It has very few identified binding partners, which include SMC3 (structural maintenance of chromosome 3), hEST1B (human ortholog of the yeast ever-shorter telomeres 1B), which it protects from ubiquitin-mediated degradation, and, very recently, retinoic acid induced 1 (RAI1), nuclear receptor co-activator 3 (NOCA3), and thyroid hormone receptor-associated protein 3 (THRAP3), among others [118, 146, 150, 152]. Other non-histone proteins that have been linked with HDAC8 include estrogen-related receptor α, cohesin, and cortactin; the enzyme has demonstrated preference for specific motifs within these proteins [152, 179, 180]. Structural analysis of HDAC8, which, in contrast to other HDACs, can be found in single polypeptides, has identified a conserved residue – Asp101 – as critical for substrate recognition and inhibitor engagement [153].

HDAC8 activity is negatively regulated by protein kinase A (PKA)-mediated phosphorylation, and phosphorylation of HDAC8 results in hyperacetylation of histones H3 and H4 [146]. Non-histone HDAC8-interacting proteins include HSP20, HSP70, and HSP90 [146, 148]. It has been reported that histones are not the primary substrates of HDAC8, but likely it has other preferred cellular substrates [152]. In terms of cancer, siRNA knockdown of HDAC8 leads to decreased cell growth in human cervical, colon, and lung cancer cells and HDAC8 expression level has been linked to degree of differentiation in childhood neuroblastoma cells [118, 146, 149, 150]. Notably, HDAC8 has also been reported to be upregulated in invasive breast tumor cells [152]. The HDAC8 selective inhibitor PCI-34051 shows a greater than 290-fold selectivity for HDAC8 compared to other HDACs, and has been a useful tool to investigate the effects of HDAC8 inhibition in cancer research [152].

Evidence supporting the use of HDACi as anti-cancer stem cell therapy

Histone deacetylases are required for normal cell cycle, proliferation, and differentiation. Aberrant HDAC activity has been shown to play a role in mechanisms regulating several features of cancer, including tumor suppressor silencing, abnormal cell cycle control and growth signaling, angiogenesis, cell adhesion, tissue evasion, and metastasis [117]. Some genes involved in the regulation of cell growth like p16, p19, p21, and p27 are known to be silenced through HDAC-mediated epigenetic mechanisms [117, 138, 139, 144-146]. HDACs have also been linked to pro-differentiation properties, both in normal and malignant cells [117, 127, 133, 138, 140, 143, 149, 150, 155, 189, 191]. Because of these

traits, HDACs have become an attractive target for cancer chemotherapy, with the aim of restoring expression of these genes by blocking histone deacetylation and maintaining open chromatin structures. HDACi exert different effects and demonstrate variable potency in cancer cells in part due to their specificity for particular HDAC isoforms.

HDACi are known to exert potent antineoplastic properties in many different tumor types through both epigenetic effects of chromatin remodeling and tumor suppressor gene re-expression, as well as via interactions with non-histone protein substrates. Inhibition of HDAC activity in tumor cells results in increased apoptosis, growth arrest, and differentiation, [117, 138, 141, 143, 157, 159-162] and has been achieved through various classes of HDAC inhibitors, or "epidrugs", including short-chain fatty acids, hydroxamic acids, cyclic tetrapeptides, aliphatic acids, and benzamides [139, 140, 147, 157, 162]. Overall, HDACi show high selectivity towards transformed cells compared to normal cells [140, 143, 154, 157]. Evidence abounds that HDAC inhibition is a useful strategy in certain cancers, and in addition to several agents in phase I, II, and III clinical trials [117, 147], there are two FDA-approved HDACi: vorinostat (Zolinza®, SAHA) and romidepsin (Istodax, depsipeptide) [143]. Because HDACs act both at the epigenetic level and directly on non-histone protein targets [153], HDACi effects include upregulation of CDK inhibitors which serve as tumor suppressor genes, including p21, p15, p19, Bop1, and Htra1, and downregulation of oncogenes, including c-myc and cyclin D1 [117, 133, 138, 139, 141, 144, 145, 147]. Other effects of HDACi arise due to HSP90 acetylation, which leads to its inactivation and increased proteasomal degradation of its client

proteins, such as ERα and Her2/neu [117, 139, 146, 147]. Experimental data have also indicated that HDACi is a useful tool in breast cancer [147,155]. Knockdown of HDAC1, 2, 3, and 6 in breast cancer leads to decreased proliferation, apoptosis, and cell cycle arrest, implicating HDAC activity as a key mediator of survival and tumorigenic capacity [118]. LAQ824, a hydroxamic acid analogue, depletes Her2 through attenuation of mRNA levels and promotion of its proteasomal degradation [139]. In nonmalignant mammary epithelium, repressive and activating histone modifications are correlated with differential gene expression during lineage determination [119]. HDACi have been shown to induce differentiation in normal rat cerebral cortical neural progenitor cells and in erythroleukemic cells [127, 133, 191]. The capacity to induce differentiation in nonmalignant embryonal cells and cancer cells has been documented [127, 140], but the pathways involved in this process are not well-characterized. According to Singh et al., proof-of-principle has been established for the notion that poorly-differentiated cancers with a high CSC content can be treated by facilitating differentiation to a more epithelial-like state [155]; however, differentiation therapy has yet to be explored in breast cancer.

In the 1970s, Leder and Leder reported that butyric acid, a naturally-occurring fatty acid and HDACi, is effective in inducing erythroid differentiation in erythroleukemic cells, determined by the percentage of benzidine-positive (hemoglobin-containing) cells following treatment [155]. In breast cancer, HDACi has been shown to induce differentiation, as evidenced by decreased ALDH and tumorsphere formation and increased CK8/18 and E-cadherin expression [154]. Li et al. observed that the gene

expression profile in residual breast tumor cells surviving after chemotherapy differs from that of the cells comprising the original tumor, particularly those genes involved in cell survival and cell cycle regulation [110]. Thus, we posit that both the CSC population within a primary tumor and those that remain following surgery or chemotherapy are clinically important and may be targeted for differentiating therapy by HDAC inhibition to prevent tumor recurrence or metastasis.

AR-42 and cancer

Early on in the field of CSC research, Pierce and colleagues recognized that malignant stem cells are an important target in cancer chemotherapy, and that to eradicate this population, exploration and development of differentiating therapies is needed [121]. HDACi are reported to possess growth-suppressive and pro-apoptotic activities at doses which are not toxic to nonmalignant cells [143, 157]. AR-42 (N-hydroxy-4-[[(2S)-3-methyl-2-phenylbutanoyl]amino]benzamide), a novel phenylbutyrate-based histone deacetylase inhibitor originated in the Chen lab, has been proven particularly efficacious at submicromolar concentrations in a variety of tumor types [141, 142, 144, 145, 154, 158-161]. The chemical structure of AR-42 (Fig. 3.1A) and its IC50 in multiple breast, prostatic, and hepatic cancer cell lines (Fig. 3.1B) are shown below. AR-42 has demonstrated anticancer efficacy in *in vitro* and *in vivo* models of hepatic cancer [160, 161], prostate cancer [141], squamous cell carcinoma [144], colonic cancer [145], lymphoma [160, 163], and vestibular meningiomas [142]. Advantageously, in mouse models AR-42 has been shown to be orally bioavailable and well-tolerated [141, 142].

AR-42 suppresses cancer cell viability at lower doses than vorinostat (SAHA), another pan-HDACi [154, 160], and does so with efficient tumor cell specificity [154] and without significant toxicity in mouse models [141, 142].

Notch1 signaling

Notch signaling has a crucial role in regulating intercellular communication during embryogenesis and normal cellular proliferation, differentiation, and apoptosis throughout life, particularly in hematopoietic cells, mammary epithelium, colorectal epithelium, and neural progenitor cells [107, 164]. The extracellular region of Notch contains many EGFR-like repeat domains which mediate its interaction with Delta-like ligands and Jagged ligands [107]. The Notch intracellular domain (NICD) is cleaved by gamma secretase, then translocates to the nucleus where it complexes with other proteins to transcriptionally induce pro-survival effects and transcription of Hes family transcriptional repressors. In the breast specifically, Notch signaling regulates alveolar development and cell fate, as well as blocks uncontrolled proliferation (Buono, 164]. There is evidence to suggest that the Notch pathway may be dysregulated in some human breast tumors [137, 165]. Coexpression of Notch1 and its ligand Jagged1 have been associated with poor overall survival in primary breast cancer [130]. Notch1 pathway activation has been shown to lead to increased mammosphere formation, whereas Notch1 blockade via co-culture with a GSI reduces tumorsphere formation [130]. In a study of low and high-grade DCIS tumors, high-grade tumors demonstrated increased mammosphere forming efficiency, which could be reduced when Notch signaling was

inhibited using DAPT (N-[N-(3,5-difluorophenacetyl)-l-alanyl]-S-phenylglycine t-butyl ester) or a Notch-neutralizing antibody. In the same study of DCIS, increased NICD staining was associated with recurrence at 5 years [131]. Similarly, in a study of mammary tumorigenesis, inhibition of Notch signaling reduced tumorsphere formation *in vitro* and induced tumor regression *in vivo* [119]. Mice injected with Notch1 knockdown cells form tumors at a reduced rate and volume [130]. Very recently, Wang et al. reported mutations in the PEST domain of Notch receptors that function as an oncogenic driver in breast cancer in approximately 13% of TNBC, providing both a potential mechanistic explanation for the Notch pathway activation often observed in breast cancer as well as a therapeutic target via GSI [166]. Some have even proposed that Notch, based on its role in angiogenesis, could be an attractive dual-inhibitor in cancer, blocking both vascularization and CSC [167]. Taken together, these data suggest that Notch is inherently involved in stemness of both normal and malignant cells. We hypothesize that Notch can be regulated by HDACi in breast cancer.

Materials and Methods

Cell culture

MDA-MB-231 breast cancer cells were purchased from American Type Culture Collection (Manassas, VA) and cultured in DMEM medium (Life Technologies; Grand Island, NY) supplemented with 10% fetal bovine serum (Life Technologies), 100 U/ml penicillin, 100 µg/ml streptomycin and 50 µg/ml gentamycin B (Life Technologies). SUM-159 cells were purchased from Asterand Biosciences (Detroit, MI) and cultured in

Ham's F-12 (Life Technologies) supplemented with 5% fetal bovine serum, 5 μg/ml insulin, 1 μg/ml hydrocortisone, 100 U/ml penicillin, 10μg/ml streptomycin and 50 μg/ml gentamycin B. All cells were cultured at 37°C in a humidified incubator containing 5% CO2, and were used in fewer than 6 months of continuous passage. AR-42 was obtained from Arno Therapeutics (Flemington, NJ). Vorinostat and romidepsin (referred to as SAHA and depsipeptide, respectively) were purchased from ChemieTek (Indianapolis, IN). PCI-34051 was purchased from Cayman Chemical (Ann Arbor, MI) and MG132 was obtained from Sigma-Aldrich (St. Louis, MO).

Western blotting

Western blotting was performed by lysing cells with sodium dodecyl sulfate (SDS) lysis buffer (1% SDS, 50mmol/L Tris-HCl pH 8.0, 10mmol/L EDTA) plus protease inhibitor cocktail (Sigma-Aldrich) and PhoSTOP phosphatase inhibitor (Roche) and sonication. Protein concentrations were standardized with a Micro BCA Protein Assay kit (Pierce Chemical), and each sample was homogenized in SDS sample buffer. SDS-PAGE gels were prepared at 1mm thickness immediately prior to sample loading and according to techniques modified from Harlow and Lane (Appendix A; Sambrook et al., 1989). The standard resolving gel percentage prepared was 10% with 8% used for proteins over 130kDa and 12% used for proteins under 20kDa. A 5% stacking gel was prepared in all cases. Samples were loaded and stacked in 1X running buffer at 130V for 15 minutes, then run at 100V for 60 minutes. Wet transfer to NC membrane was performed in 1X transfer buffer at 100V for 75-90 minutes. This was followed by blocking with 5% non-

fat milk in TBS-T (TBS, 0.1% Tween-20) for 30-60 minutes. Incubation with primary antibodies was performed at a 1:500 dilution overnight at 4°C. Membranes were washed with TBS-T and incubated with horseradish peroxidase-conjugated secondary antibodies at a 1:5000 dilution at room temperature for 60-90 minutes. Signal detection was performed on x-ray film using a chemiluminescence system (Amersham).

Mammosphere formation assay

Five hundred SUM-159 cells/well and 1,000 MDA-MB-231 cells/well were seeded onto ultra-low attachment 24-well flat bottom plates in serum-free culture medium (MammoCult™, STEMCELL Technologies; Vancouver, BC, Canada). Cells were then treated with the indicated compounds for 7 days, after which the numbers of mammospheres were counted at 100X magnification.

Knockdown and lentivirus transfection

Cells were transfected with plasmids and siRNAs using Lipofectamine 2000 (Life Technologies) according to the manufacturers' instructions. Lentivirial plasmids were cotransfected with Addgene 3rd Generation Packaging Systems (pMDLg/pRRE [#12251], pRSV-Rev [#12253] and pMD2.G [#12259]) in 293T cells following a standard calcium phosphate transfection procedure. Viral particles were used for infection of target cells and stable cells were selected by exposure to puromycin for one week. The HDAC8 expression plasmid was constructed in pLenti CMVTRE3G Puro

DEST (w811–1) vector (Addgene) by LR reaction after cloning HDAC8 cDNA into the pENTR noccDB (w48–1) entry vector (Addgene).

Immunoprecipitation

Cells were harvested, incubated in IP lysis buffer (20 mM Tris-HCl pH 7.5, 150 mM NaCl, 1% Triton X-100) for 30 min on ice, and then sonicated (3 times for 10 sec each). After centrifugation, the supernatants were collected from each sample and then pre-cleared by incubation with 10 µl protein A/G agarose beads at 4°C for 1 h with rocking. After removal of the protein A/G beads by centrifugation, protein content in each sample was measured and aliquots containing 1500 µg of protein were incubated with primary antibodies overnight at 4°C with rocking, followed by 20 µl protein A/G agarose beads for 2 h at 4°C. The immunoprecipitates were washed with IP lysis buffer, collected by centrifugation, and resuspended in 2X sample buffer for analysis by immunoblotting.

MDA-MB-231 animal study

Female NOD.SCID mice (5–6 weeks of age; Harlan, Indianapolis, IN) were group-housed under constant photoperiod (12 hours light: 12 hours dark) with *ad libitum* access to sterilized food and water. All experimental procedures were done according to protocols approved by The Ohio State University Institutional Animal Care and Use Committee. Genotype information is tabulated in Appendix B. To assess the role of HDAC8 in tumor initiation *in vivo*, HDAC8^{KD} cells (MDA-MB-231 cells stably expressing HDAC8 shRNA) were injected into the left inguinal mammary fat pads of

female NOD.SCID mice (50,000 cells/0.1 ml, in Matrigel [BD Biosciences]). An equal number of MDA-MB-231 cells expressing the pLAS Void plasmid (Void) were injected into the contralateral mammary gland to serve as negative control. Tumors were measured with calipers and the volumes were calculated using $V = 1/2$ (width^2 × length).

Cpd25

Based on the evidence for a mechanistic link among HDAC8, Notch1, and stemness suggested by our data, a novel, isoform-specific HDAC8 inhibitor invented in the Chen Laboratory, Cpd25, was subject to preliminary screening in *in vitro* and *in vivo* assays. Isoform specificity can be achieved by modification of the functional moiety of the small molecule HDAC inhibitor that interacts with the zinc-binding active site of the HDAC enzyme in a manner that is unique to that isoform. Cpd25 was tested in MDA-MB-231 cells using MTT assay, mammosphere assay, and western blot to demonstrate its potency, efficacy in reducing mammosphere formation, and downregulation of Notch1 protein. MDA-MB-231 cells cultured in high-glucose DMEM supplemented with 10% FBS and 1% pen-strep were in stable passage. MTT assay was performed as described previously using Cpd25 concentrations up to 40μM. Mammosphere assays were plated at 5,000 cells per well, and the treatment concentrations were 0, 0.25, 0.5, and 1μM. Western blot assays were plated at 5x105 cells per 6cm dish, and drug concentrations were 0, 0.125, 0.25, 0.5, and 1μM.

An *in vivo* study was also conducted using NOD.SCID mice bearing SUM-159 orthotopic mammary fat pad xenografts. Experimental procedures in mice were done in accordance with protocols approved by The Ohio State University Institutional Animal Care and Use Committee. Mice were anesthetized with 4% isoflurane inhalant anesthesia. The left inguinal region was prepped using 70% ethanol and a sterile gauze swab. Mice were injected with $5x10^5$ cells in 0.1mL 50/50 PBS-Matrigel in the left fourth mammary fat pad. A 25ga needle was inserted subcutaneously at the level of the nipple and advanced craniolaterally, bevel up. Ear punching and initial body weights were recorded at the same time. Tumor incidence was monitored by twice weekly palpation. Tumors were measured by calipers and body weights were recorded once weekly. When the tumor volume reached approximately 50-75mm^3, mice were recruited to the study and randomized to either a vehicle control or Cpd25 treatment group. Vehicle consisted of 10% DMSO in methylcellulose/Tween. Cpd25 was prepared at 10mg/mL (100mg/kg) by dissolving the solid powered drug in DMSO (10% final solution volume) and sonicating in a water bath sonicator for 5 minutes, then adding the methylcellulose/Tween solution and sonicating for 1 hour three times with 5 minute intervals in between. The dissolved Cpd25 drug was prepared 48h in advance of its use in animal treatments and prepared fresh every 7 days. A total of 12 mice were recruited to the study in 3 cohorts separated by 1 week for a total of 6 per treatment group.

Following 21 days treatment, mice were euthanized using CO2 asphyxiation followed by cervical dislocation. Mice were submerged whole in 70% ethanol to sterilize, then

mammary fat pad tumors were dissected out using sterile instruments working in the biosafety hood. The tumors were rapidly immersed in 70% ethanol, then 1X PBS, then were dissected manually using scissors and a scalpel blade. Each mouse was subject to complete post-mortem examination, and a complete set of tissues was preserved in 10% NBF. Fixed organ weights were recorded and relative organ weights were compared between treatment groups. Tumor fragments were retained in liquid nitrogen for later protein or nucleic acid extraction as needed. Minced tumor was suspended in 1mL unsupplemented RPMI, then transferred to a sterile 15mL conical vial and kept on ice. In the cell culture hood, 100µL 10X collagenase/hyaluronase was added to each vial. Samples were periodically gently agitated and incubated in the 37 deg C water bath for 30 minutes. Cell suspensions were then strained into 50mL conical vials using a 40µm nylon mesh filter and grinding with a sterile Eppendorf tube. The filter was rinsed with an extra 1mL supplemented media. Cell suspensions were counted on the cell counter, diluting up to 4X as needed. Aliquots were separated out for FACS and sorting. $1x10^6$ cells were aliquoted for FACS, and $2x10^6$ were aliquoted for sorting. The samples were centrifuged at 5000rpm for 2 minutes, and the supernatants were decanted. Cells for analysis were resuspended in 1mL ALDH buffer plus 5µL ALDH substrate, then split into two conditions: one without DEAB and one with DEAB. These were incubated at 37 deg C for 45 minutes, protected from light. Cells for sorting were resuspended in 100µL sterile PBS plus 1µL anti-mouse MHC I antibody (H-2Kd) and incubated on ice for 30 minutes, protected from light. After first incubation, all tubes were then centrifuged at 5000rpm for 2 minutes and decanted. Analysis cells were resuspended in 500µL ALDH

buffer, and sorting cells were resuspended in 500μL PBS. 7-AAD staining (BD Biosciences) was performed by adding 5μL 7-AAD to each tube and incubating on ice, protected from light for 30 minutes. All samples were then processed in the FACS core facility. 50,000 events were collected from the sorting aliquots into 1mL supplemented RPMI in 15mL conical vials. Tubes were centrifuged at 1000rpm for 5 minutes then carefully decanted. Cells were resuspended in mammosphere media including the MammoCult growth supplement and 1% pen-strep, 1:1000 hydrocortisone, and 1:1000 heparin. Mammosphere assays were plated in 24-well ultra-low attachment culture plates. Cells were seeded in triplicate at 1,000 and 5,000 cells per well for the first cohort, then at 5,000 and 10,000 cells per well for the second and third cohorts. Mammosphere assays were cultured in the cell incubator for 7 days, then were counted and photographed.

Statistical analysis

In vitro experiments were performed at least three times and data are presented as means ± SD. Group means were compared using one-way ANOVA followed by Student's *t* tests. For the *in vivo* experiments, differences in tumor incidence and tumor volume were analyzed by log-rank test and Student's *t* test, respectively. Differences were considered significant at $p < 0.05$.

Results

Suppressive effect of HDAC inhibitors on BCSC is associated with Notch1 downregulation

The pan-HDAC inhibitors AR-42 and SAHA (vorinostat) downregulate BCSC biomarkers Notch1, activated Notch1 (NICD), nestin, Zeb-1, and BMI-1 concurrently with bulk histone hyperacetylation in the TNBC cell lines MDA-MB-231 (Fig. 3.2A) and SUM-159 (Fig. 3.2B). The class I selective HDAC inhibitor depsipeptide also downregulates Notch1. Mammosphere formation is also significantly reduced in a dose-dependent fashion by the three aforementioned HDAC inhibitors in both TNBC cell lines relative to controls ($p<0.05$). This suggests that one or more of the class I HDAC isoforms – HDAC1, 2, 3, or 8 – could be responsible for downregulation of CSC biomarkers and tumorsphere formation. The class I HDAC inhibitor MS-275, which lacks HDAC8 inhibitory activity, was effective in suppressing mammosphere formation in breast cancer cell lines (data not shown).

Evidence that HDAC8 is responsible for HDAC inhibitor-induced Notch1 downregulation

When MDA-MB-231 cells are treated with the HDAC8-selective pharmacologic inhibitor PCI-34051, dose-dependent downregulation of Notch1, nestin, and BMI-1 is observed, independent of bulk histone hyperacetylation (Fig. 3.3). Relative mammosphere formation is also significantly reduced in a dose-dependent manner upon treatment with PCI-34051 up to 40μM (Fig. 3.3). PCI-34051 has been shown to have over 290-fold selectivity for HDAC8 over the other class I HDAC isoforms as well as HDAC6 and HDAC10. Thus, we posit that HDAC8 alone is sufficient to achieve BCSC biomarker and tumorsphere downregulation in TNBC. To further investigate this

hypothesis, individual siRNA knockdown of HDAC1, 2, 3, and 6 was performed in TNBC cell lines MDA-MB-231 and SUM-159 (Fig. 3.4). Three siRNA clones per isoform were utilized. No other HDAC isoform induced Notch1 downregulation. When HDAC8 knockdown was performed in MDA-MB-231 and SUM-159 cells using shRNA, Notch1, nestin, and BMI-1 are downregulated and tumorsphere formation is significantly reduced ($p<0.001$). This response mirrors the effect of PCI-34051 used in the same cell lines. Thus, we conclude that HDAC8 blockade alone is sufficient to downregulate BCSC pathways including Notch1 and mammosphere formation. Concordantly, when HDAC8 is overexpressed in MDA-MB-231 and SUM-159 cells (Fig. 3.5), we observed upregulation of Notch1, activated Notch1, Jagged-1, nestin, and BMI-1 relative to sham-transfected cells, as well as a significant increase in relative tumorsphere formation ($p<0.001$). This suggests that HDAC8 is strongly correlated with a BCSC phenotype in TNBC cells.

HDAC8 inhibition downregulates Notch1 through Fbwx7-dependent protein degradation

Using stable-knockdown TNBC MDA-MB-231 and SUM-159 compared to the parental cell lines, we used the proteasome inhibitor MG132 to evaluate whether Notch1 downregulation following HDAC8 blockade could be rescued by MG132 (Fig. 3.6A). We found that in HDAC8 knockdown TNBC cell lines, proteasome inhibition reversed the suppressive effect of HDAC8 loss on Notch1. Using the same conditions of parental versus stable knockdown of HDAC8 in MDA-MB-231 cells with or without the proteasome inhibitor, we immunoprecipitated Notch1 to evaluate its ubiquitination status.

MG132 is expected to cause accumulation of proteins destined for degradation by the ubiquitin-proteasome system. In parental MDA-MB-231 cells treated with MG132, we observed Notch1 ubiquitination which increases in the HDAC8 knockdown condition (Fig. 3.6B). This suggests that in the absence of HDAC8, Notch1 is increasingly ubiquitinated and subject to proteasomal degradation. To investigate how HDAC8 could cause Notch1 ubiquitination, we focused on Fbwx7, the E3 ligase that ubiquitinates Notch1 to terminate its signaling activity. When Fbwx7 is suppressed by siRNA in parental MDA-MB-231 cells, we see an increase in Notch1 protein, attributed to its accumulation in the absence of ubiquitination and proteasomal degradation (Fig 3.7A). Similarly, when Fbwx7 is knocked down in MDA-MB-231 HDAC8^{KD} cells, Notch1 downregulation is reversed (Fig. 3.7B). This suggests that the effect of HDAC8 on Notch1 is indirect, and that HDAC8 inhibitor-driven Notch1 downregulation is mediated through Fbwx7. Taken together, we conclude that in the setting of HDAC8 inhibition, Notch1 undergoes polyubiquitination by Fbwx7 and subsequent proteasomal degradation. In other words, HDAC8 promotes Notch1 stability by protecting it from ubiquitin-mediated proteasomal degradation.

HDAC8 contributes to breast tumorigenicity *in vivo*

An *in vivo* study was undertaken to evaluate the tumorigenicity of HDAC8 knockdown TNBC compared to sham-transfected cells (Fig. 3.8). At 28 days post-injection, the tumor-free incidence of MDA-MB-231 HDAC8^{KD} was significantly greater than for MDA-MB-231 tumors ($p=0.0118$) (Fig. 3.9). This finding is consistent with data

generated in mammosphere assays using pharmacologic and siRNA mediated HDAC8 inhibition, and suggests that HDAC8, via Notch1, plays an integral role in tumorigenesis in TNBC cells.

Cpd25 has potent anti-tumor effects on TNBC *in vitro*

MTT assay found a dose- and time-dependent decrease in cell viability with an IC50 at 72h of approximately 0.5μM in MDA-MB-231 cells (Fig. 3.10A). At all doses tested, relative mammosphere formation was significantly reduced in a dose-dependent manner compared to control cells ($p<0.05$) (Fig. 3.10C). Concordantly, MDA-MB-231 cells treated with submicromolar concentrations of Cpd25 also demonstrate Notch1 protein downregulation (Fig. 3.10B).

Cpd25 downregulates CSC phenotype *in vivo* without evidence of limiting toxicity

Ex vivo analysis – mammospheres

Ex vivo BCSC populations were analyzed following an orthotopic xenograft study using Cpd25 in mice bearing SUM-159 tumors (Fig. 3.11). Tumor cells sorted in the ACSR were selected by using anti-mouse MHC antibody (H-2Kd) and 7-AAD to exclude mouse and non-viable cells, respectively. No growth was observed in either of the two conditions plated from the first cohort. In the second and third cohorts, cells plated at 10,000 per well were able to grow mammospheres. Mammospheres over 60μm diameter were quantified by light microscope in each well, then mean per mouse was calculated. Representative photomicrographs were taken for each sample. These data suggest that

there is reduced mammosphere formation in cells sorted from the Cpd25-treated mice compared to vehicle-treated mice (Fig. 3.12A). However, there were only n=3 mice in the vehicle-treated group and n=2 mice in the drug-treated group (cohorts 2 and 3).

Ex vivo analysis – ALDEFLUOR

Tumor cells processed for FACS were stained using anti-mouse MHC antibody (H-2Kd) and 7-AAD to exclude mouse and non-viable cells, respectively. In this gated population, ALDH positivity was analyzed, and percent ALDH positive was calculated. Concordant with the mammosphere assay data, mice in the vehicle treatment group demonstrated a generally higher percentage ALDH positivity compared to the Cpd25-treated mice (Fig. 3.12B). However, this observation is limited by the extremely small numbers of mice per treatment group, and the trend is not uniform among the 5 mice available for evaluation.

Mean adjusted body weights did not significantly differ between the vehicle and drug-treated mice, though both groups did show a similar overall decrease in body weight over the course of the three-week study (Fig. 3.13). Mice in the vehicle and drug-treated groups also showed similar tumor growth throughout the course of the study; by the end of the study, the drug treatment group had slightly larger tumors than the vehicle control group (data not shown). Relative organ weights of the heart, spleen, kidneys, and liver did not differ significantly between groups (Fig. 3.13).

Discussion

In this study, we report a novel non-epigenetic function of HDAC8 in regulating CSC-like properties in breast cancer cells by maintaining the protein stability of Notch1, which might underlie the reported activity of HDAC inhibitors to activate Notch1 signaling in cancer cells [168]. Although HDAC8 is the best structurally characterized HDAC isoform due to ease of purification, its biological function has yet not been fully defined, because its function might vary with its cellular locality in a cell type and/or cellular context-specific manner [169]. For example, although HDAC8 has been reported to catalyze the deacetylation of histone variants *in vitro* [170-174], it was also found to be associated with the actin cytoskeleton in the cytoplasm of human smooth muscle cells to regulate smooth muscle contractility [175-177]. Moreover, despite structural similarity to other class I HDACs, HDAC8 does not require additional protein cofactors to catalyze deacetylation. [169] In addition, HDAC8 has been shown to bind the transcription factor CREB and protein phosphatase 1 in the nucleus of HEK293 cells, leading to decreased CREB activation [180]. As high expression levels of HDAC8 have been associated with childhood neuroblastoma [182] and hepatocellular carcinoma [183], the potential tumorigenic role of HDAC8 warrants attention.

Mechanistically, HDAC8 could facilitate tumorigenesis through distinct mechanisms at the epigenetic and/or cellular level in different tumor cell types. For example, HDAC8 has been reported to form corepressor complexes with Stat3 to repress the proapoptotic target gene *BMF* in colon cancer cells [151], and to activate Jak2/Stat signaling through epigenetic repression of *SOCS1* and *SOCS3* gene in K562 and HEL erythroleukemia cells

[184]. Similar to our findings, other studies demonstrated a niche role of cytoplasmic HDAC8 in determining the fate of non-histone substrates. We demonstrated that HDAC8 protects Notch1 from Fbwx7-mediated protein degradation in breast cancer cells, which is reminiscent of the reported protective effect of HDAC8 on hEST1B protein stability in HeLa cells [146]. The protective effect on Notch1 we observed might be associated with the ability of HDAC8 to regulate Fbwx7 activity. In addition to HDAC8, HDAC3 has also been reported to regulate CSCs via histone modifications in the liver [185]. In addition to deacetylase activity on core histones, HDAC3 also shows biological functions beyond transcriptional repression [186]. The putative role of HDAC3 in regulating CSCs is supported by our finding that the class I HDAC inhibitor MS-275, which is deficient in HDAC8 inhibitory activity, was also effective in suppressing mammosphere formation in breast cancer cell lines (data not shown). HDAC3 targeting could also underlie some of the anti-CSC effect of AR-42. From a mechanistic perspective, the potential interplay between HDAC8 and HDAC3 in mediating the non-epigenetic versus epigenetic effects of HDAC inhibitors on CSCs warrants attention. In this study, we provide evidence of a novel role for HDAC8 in maintaining Notch1 protein stability in breast cancer cells by limiting Fbwx7-mediated proteasomal degradation, leading to promotion of CSC phenotype. These findings suggest that the inhibition of HDAC8 may represent a therapeutic approach for targeting the breast CSC subpopulation.

Our work in this chapter elucidates an effect of HDAC8 on Notch1 mediated by Fbwx7, where we concluded that HDAC8 maintains Notch1 stability by protecting it from

Fbwx7-mediated proteasomal degradation. Fbwx7 is an E3 ligase that promotes the ubiquitination and degradation of Notch1, among other substrates [187]. Dysregulation of Fbwx7 has been associated with cancer [187]. Fbwx7 activity depends on dimerization; in the absence of such an association, Fbwx7 is polyubiquitinated and degraded in the proteasome [187]. Pin1 promotes Fbwx7 degradation through disrupting its dimerization [187]. Pin1 is a peptidyl prolyl isomerase that catalyzes cis/trans isomerization of phosphorylated Ser/Thr-Pro residues. It has been reported that the relative abundance of Fbwx7 and Pin1 are inversely correlated in colon cancer [187]. Notch1 escapes proteasomal degradation by Fbwx7 upon its interaction with Pin1 [188]. In this way, it can be said that Pin1 promotes and perpetuates Notch1 signaling both by disrupting its normal Fbwx7-mediated degradation and by direct binding to and stabilization of NICD. Pin1 suppression is a potentially valuable therapeutic target for CSC depletion [188]. Pin1 overexpression is positively correlated with activated Notch, irrespective of functional Fbwx7 [188]. Pin1 sustains NICD by displacing Fbwx7 [188]. However, the incidence of Notch1 and Fbwx7 mutations in breast cancer is estimated at only 2-8% [188]. High NICD levels can persist in breast cancer in the face of wild type Fbwx7 due to high Pin1 expression. Isomerization of NICD by Pin1 blocks recognition by Fbwx7 [188]. Based on our data, it is plausible that HDAC8 could play a role in Fbwx7 dysregulation.

Limitations and Future Directions

Our studies in TNBC provide strong evidence for a non-epigenetic role of HDAC8 at the cell line level; however, patient data such as TMA are needed to establish correlational significance among HDAC8, Notch1, and survival, recurrence, and incidence of metastasis. It is also important to look beyond breast cancer to other tumor types in which Notch1 is overexpressed, mutated, or dysregulated, such as leukemias and lymphomas, to test whether Notch1 inhibition via HDAC8 blockade could be of any value in this population. From the comparative pathology perspective, thorough characterization of the human and murine acetylome, particularly with regard to non-histone targets of HDACs, will be important as these putative therapeutic targets move into animal models. The role of HDAC8 in other cancers must also be analyzed. At the proteomic level, more mechanistic studies are needed to determine the nature of the interaction among Notch1, Fbwx7, and HDAC8, including mass-spectrometry, matrix-assisted laser desorption ionization imaging mass-spectrometry (MALDI-IMS), crystallography, and advanced computer modeling.

As a potential therapeutic target, it would be worthwhile to evaluate the efficacy of HDAC8 inhibition, such as by Cpd25, concurrent with other antitumor therapies to assess endpoints such as tumor recurrence and metastasis, which are reportedly linked to cancer stem cells. There are few HDAC8 isoform-selective inhibitors available, and PCI-34051 has not proven efficacious in solid tumors such as mammary cancer. Further exploration of the effects of Cpd25 in *in vitro* and *in vivo* studies is warranted, given the extremely limited number of mice available for evaluation in our experiments. Additionally, *ex vivo*

analysis endpoints could be complemented by analysis of tumoral biomarkers by western blot and IHC. Though oncogenic Notch1 has been drugged by several other agents such as GSIs, it is a significant challenge to devise a therapy that selectively targets CSCs while sparing the non-neoplastic stem cell compartments, such as in the gut and bone marrow. It is important to note that a truly CSC-targeted therapeutic may not demonstrate drastic tumor volume reduction as is seen with cytotoxic agents, so *ex vivo* analysis through FACS, mammosphere assays, or limiting dilution and retransplantation assays are critical to understanding the BCSC response to a drug. Conditional HDAC8 knockdown in the mammary gland would also provide an interesting model to evaluate the function of HDAC8 in developmental biology among normal mammary stem cells.

A.

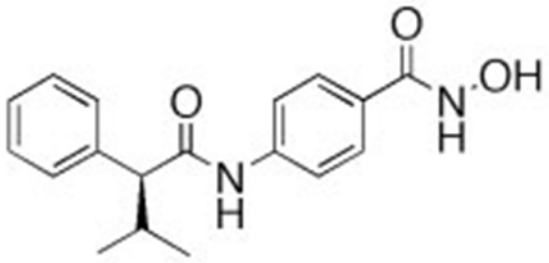

B.

Cell line	AR-42 72h IC50 (μM)
MDA-MB-231	0.71
SUM-159	0.69
PC3	0.48
LNCaP	0.30
DU-145	0.43
PLC5	0.72
Huh7	0.58
Hep3B	0.71

Figure 3.1 AR-42 and cancer.

A. Chemical structure of AR-42 ($C_{18}H_{20}N_2O_3$). B. The IC50 of AR-42 in multiple breast, prostatic, and hepatic cancer cell lines as reported in the literature and determined in our laboratory.

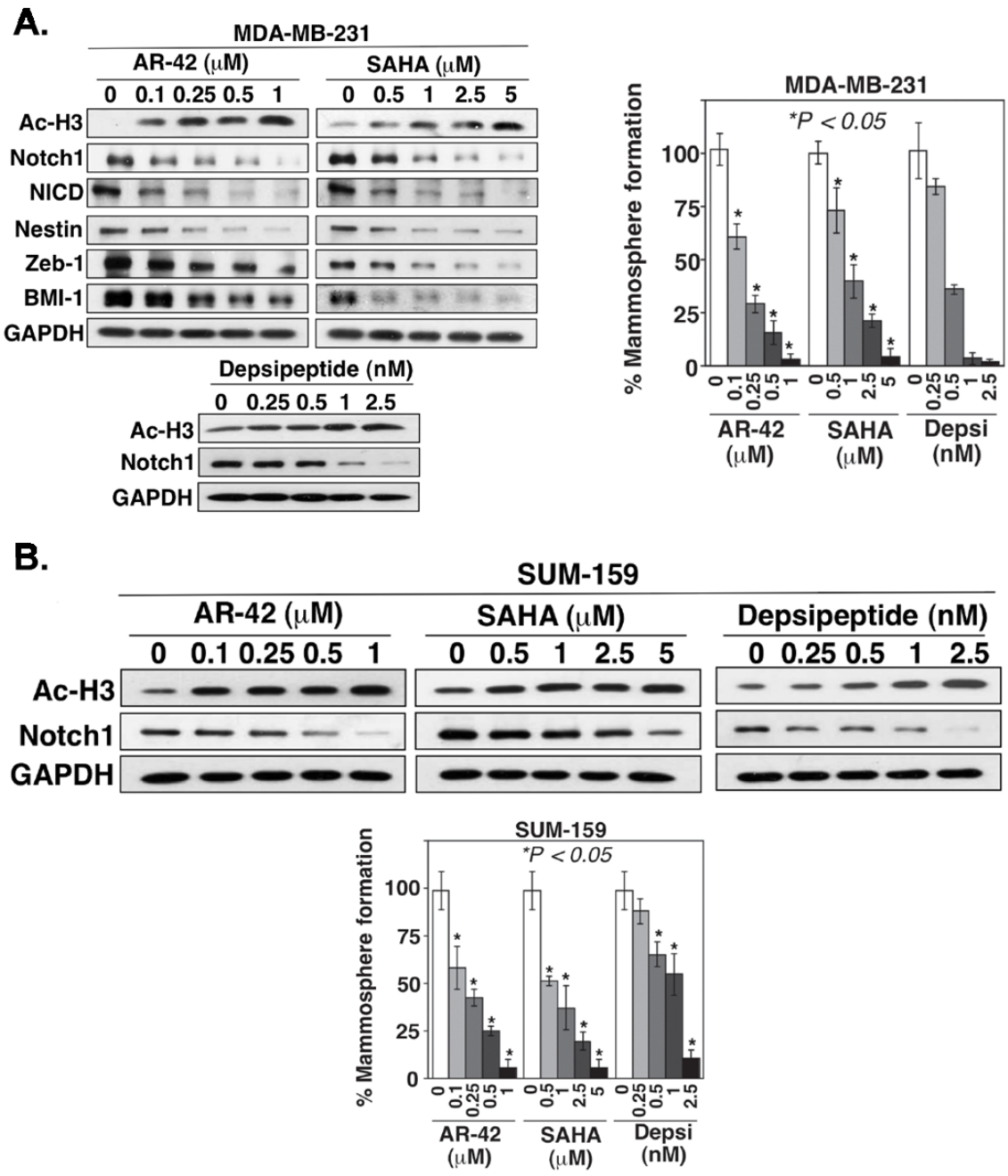

Figure 3.2 Evaluation of pharmacologic HDAC inhibitors in TNBC cell lines.

Increasing doses of AR-42, SAHA, and depsipeptide were applied to MDA-MB-231 (A) and SUM-159 (B) cells. HDACi downregulate Notch1 and other CSC biomarkers, as well as mammosphere formation in TNBC cells in a dose-dependent manner.

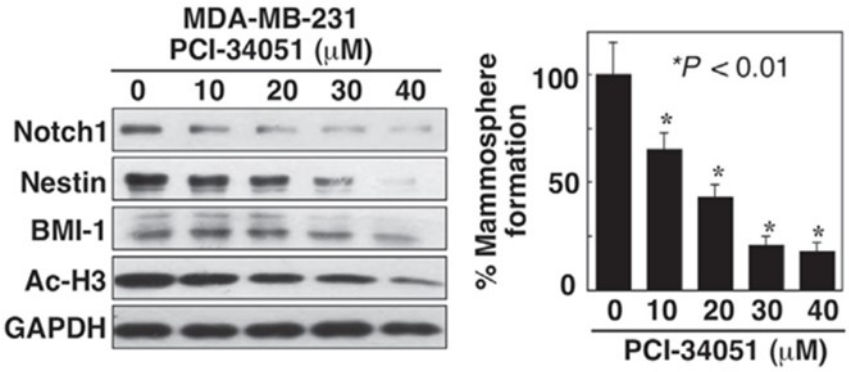

Figure 3.3 Use of the pharmacologic HDAC8-selective isoform inhibitor PCI-34051 in MDA-MB-231 cells.

Pharmacologic HDAC8 inhibition also reduces Notch1, CSC biomarkers, and mammosphere formation in a dose-dependent manner in TNBC, although at much higher micromolar concentrations than the class I and II inhibitors.

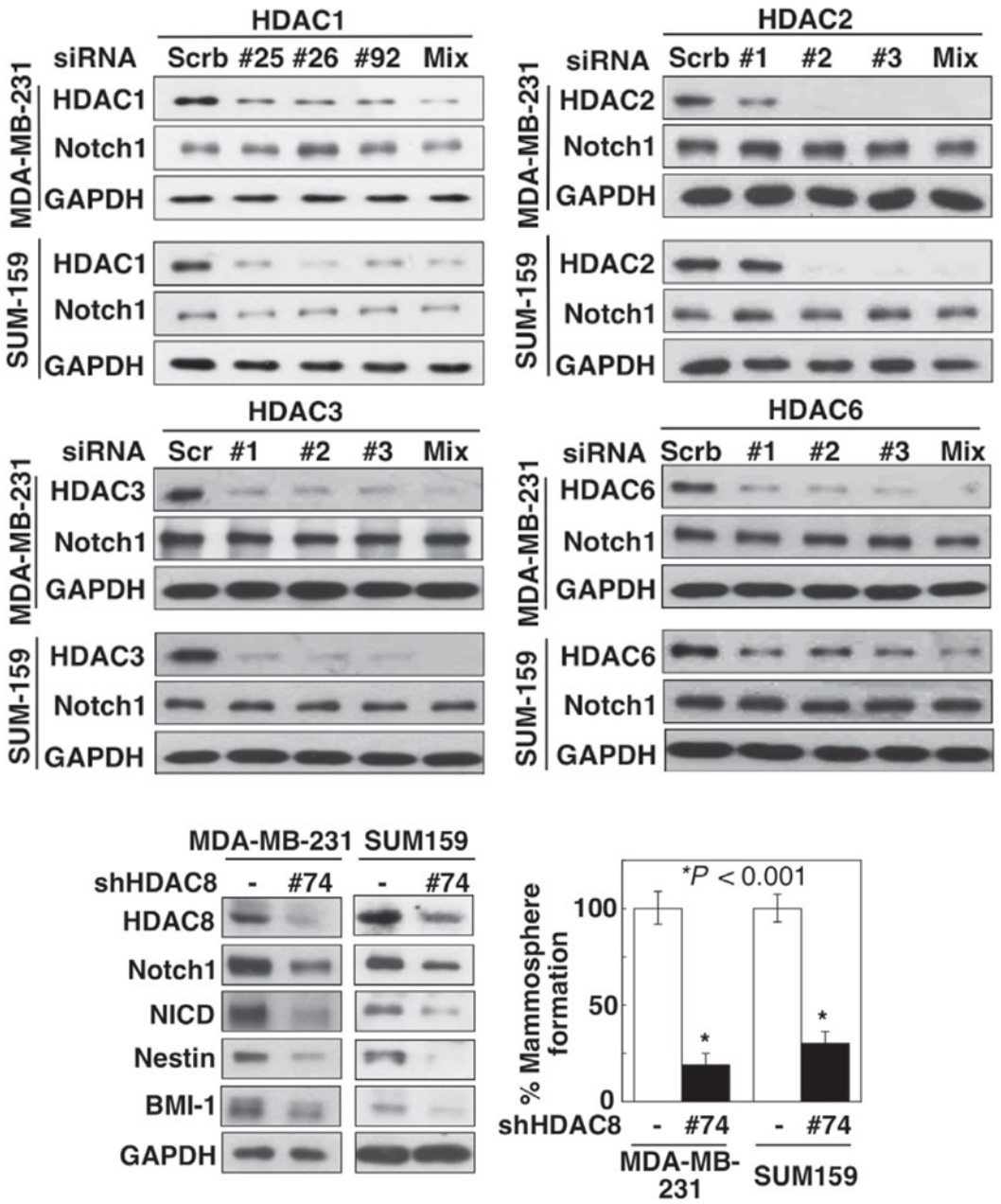

Figure 3.4 Class I isoform and HDAC6 knockdown in TNBC.

Three different siRNA clones were used for HDADC1, 2, 3, and 6 knockdown. Scrb indicates scrambled, nontargeting siRNA used as a negative control. Individual HDAC isoform knockdown in MDA-MB-231 and SUM-159 cells demonstrates that HDAC8 suppression alone by shRNA is able to induce Notch1 downregulation, as well as reduced mammosphere formation, in TNBC.

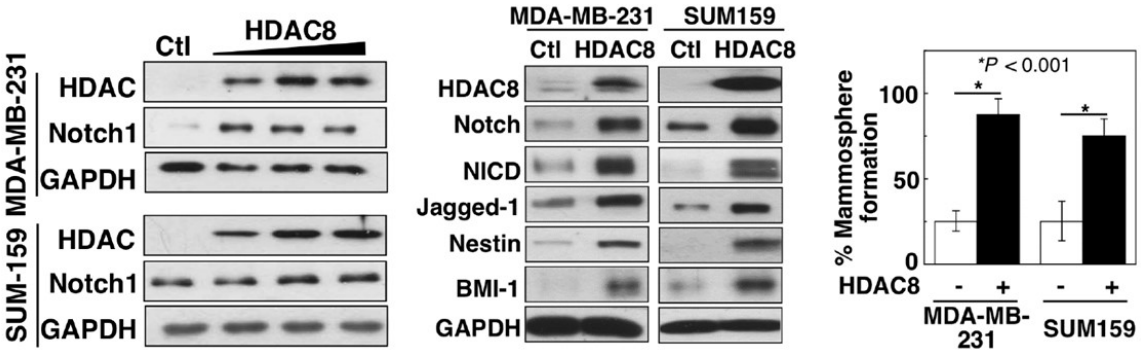

Figure 3.5 Overexpression of HDAC8 in TNBC.

Ectopic HDAC8 overexpression vectored by lentiviral transfection in TNBC leads to upregulation of Notch1 and CSC biomarkers, as well as significantly increased tumorsphere formation.

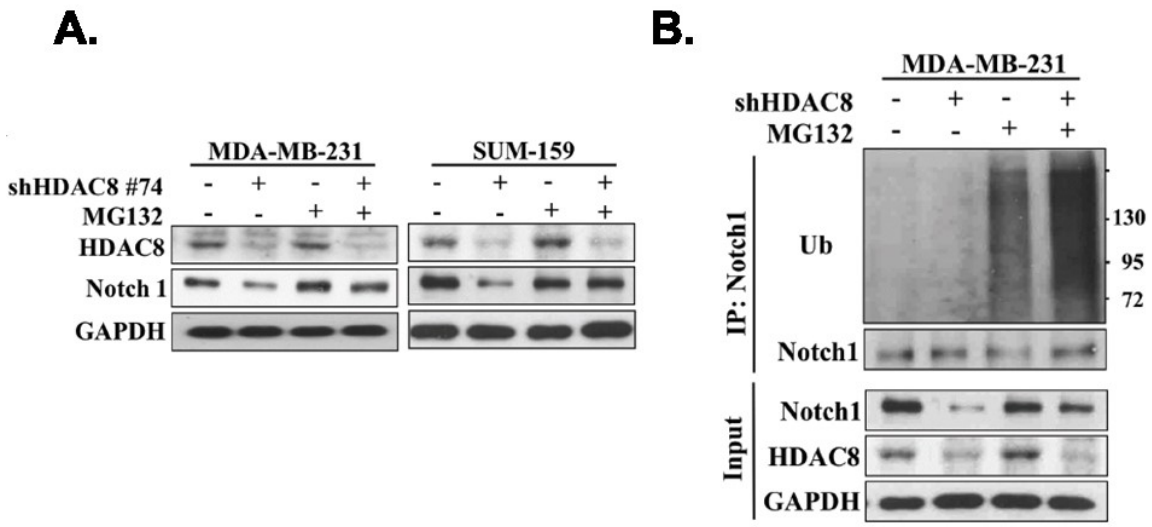

Figure 3.6 Proteasome inhibitor and IP experiments in HDAC8 knockdown TNBC.

A. HDAC8 knockdown-driven Notch1 downregulation is rescued by proteasomal inhibition in MDA-MB-231 and SUM-159 cells. B. Notch1 immunoprecipitation. Proteasomal inhibition in HDAC8 knockdown TNBC rescues Notch1 downregulation and shows that Notch1 is increasingly ubiquitinated.

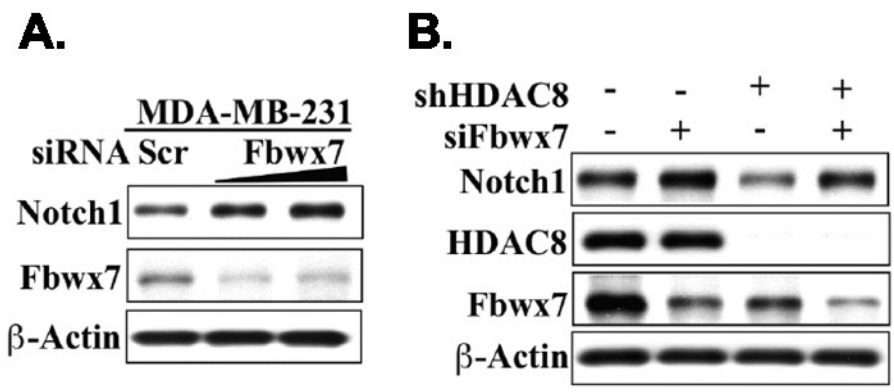

Figure 3.7 HDAC8 influences Notch1 indirectly through the E3 ligase Fbwx7.

A. Fbwx siRNA knockdown in MDA-MB-231 cells increases Notch1 protein level in MDA-MB-231 cells. B. Knockdown of Fbwx7 rescues effect of HDAC8 knockdown on Notch1 downregulation in TNBC. HDAC8 knockdown also decreased the Fbwx7 protein level.

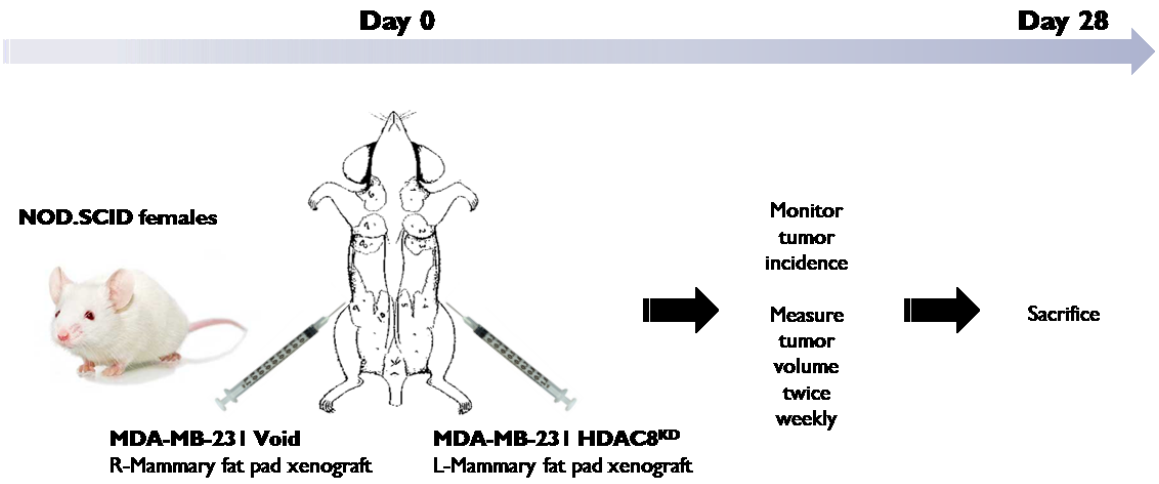

Figure 3.8 Schematic of TNBC orthotopic xenograft study of HDAC8 knockdown.

NOD.SCID mice were injected in the left fourth mammary fat pad with HDAC8 stable knockdown MDA-MB-231 cells and in the contralateral mammary fat pad with sham-transfected MDA-MB-231 cells. Tumor incidence and volume was monitored for 28d.

NOD scid spontaneous mutant mouse model ©Taconic, retrieved from: http://www.taconic.com/mouse-model/nod-scid
Mouse dissection ©J.M. Ward and Erin Parsoneault, retrieved from: http://www.k-state.edu/biology/pob/mouse_dissection.pdf

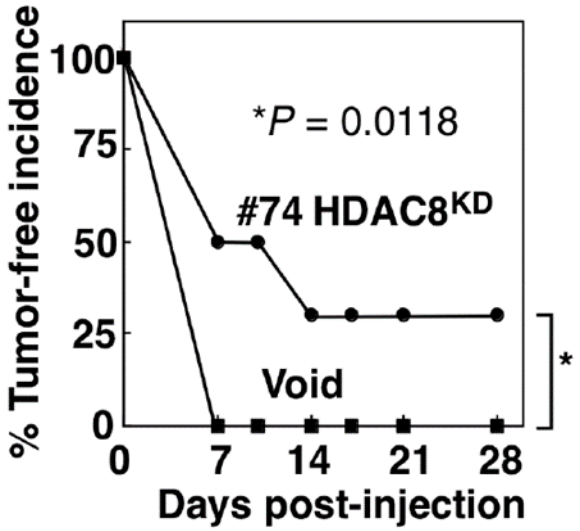

Figure 3.9 Percent tumor-free incidence in HDAC8^{KD} *in vivo* study.

Tumorigenicity is reduced by shRNA HDAC8 knockdown in a xenograft study of TNBC, as evidenced by a significantly higher tumor-free incidence in MDA-MB-231 HDAC8^{KD} compared to the parental cell line.

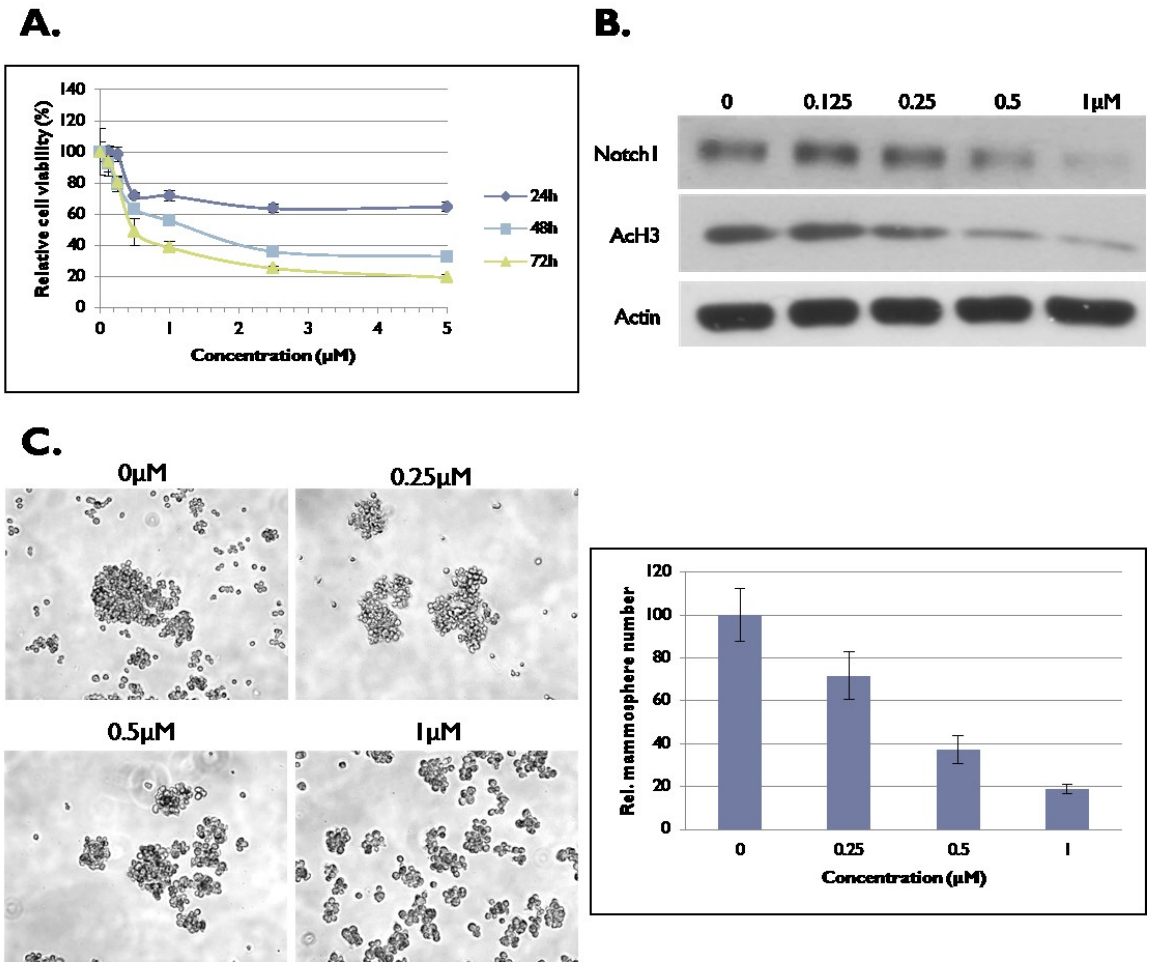

Figure 3.10 *In vitro* data demonstrating anti-CSC effects of the novel HDAC8 inhibitor Cpd25 in TNBC.

A. MTT assay evaluating relative cell viability in MDA-MB-231 cells at 24, 48, and 72 hour timepoints demonstrate a time- and dose-dependent reduction in cell viability under Cpd25 treatment with a 72h IC50 of approximately 0.5μM. B. Western blot shows downregulation of NICD without evidence of bulk histone 3 hyperacetylation. C. Mammosphere assays in MDA-MB-231 cells show significantly decreased relative mammosphere numbers at all concentrations of Cpd25 tested.

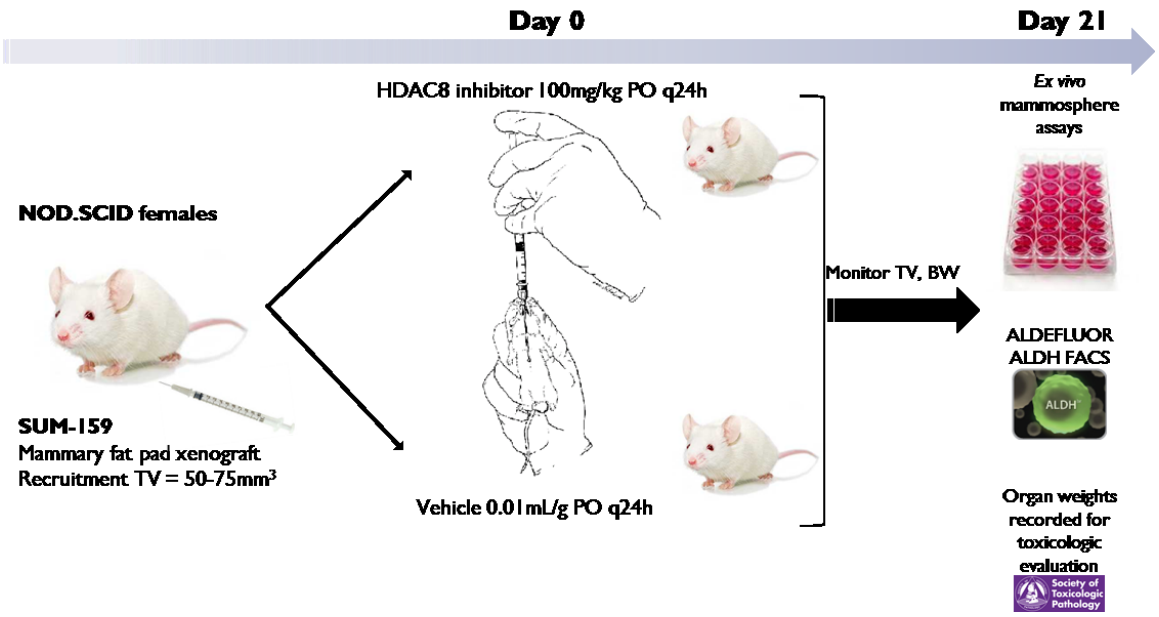

Figure 3.11 Schematic of TNBC orthotopic xenograft study of Cpd25.

NOD.SCID female mice were injected in the left fourth mammary fat pad with $5x10^5$ SUM-159 cells. Tumor growth was monitored until recruitment volume was reached, then mice were randomized to one of two treatment groups receiving either 100mg/kg Cpd25 orally once a day or an equal volume of vehicle. Body weight and tumor volume were monitored for 21d, then mice were sacrificed. Tumor cells were harvested for *ex vivo* analysis by mammosphere assays and flow cytometry, and group organ weights were compared for toxicologic evaluation.

NOD scid spontaneous mutant mouse model ©Taconic, retrieved from: http://www.taconic.com/mouse-model/nod-scid
Oral Gavage ©University of Illinois at Chicago Biologic Resources Laboratory, retrieved from: https://www.brl.uic.edu/node/37
Cell culture plates ©Lushpix Stock Images, retrieved from: http://www.fotosearch.com/ULY249/u18729508
ALDH ©STEMCELL Technologies, retrieved from: https://www.stemcell.com/tissue-and-cell-types/mammary.html
Logo ©Society of Toxicologic pathology, retrieved from: http://www.toxpath.org

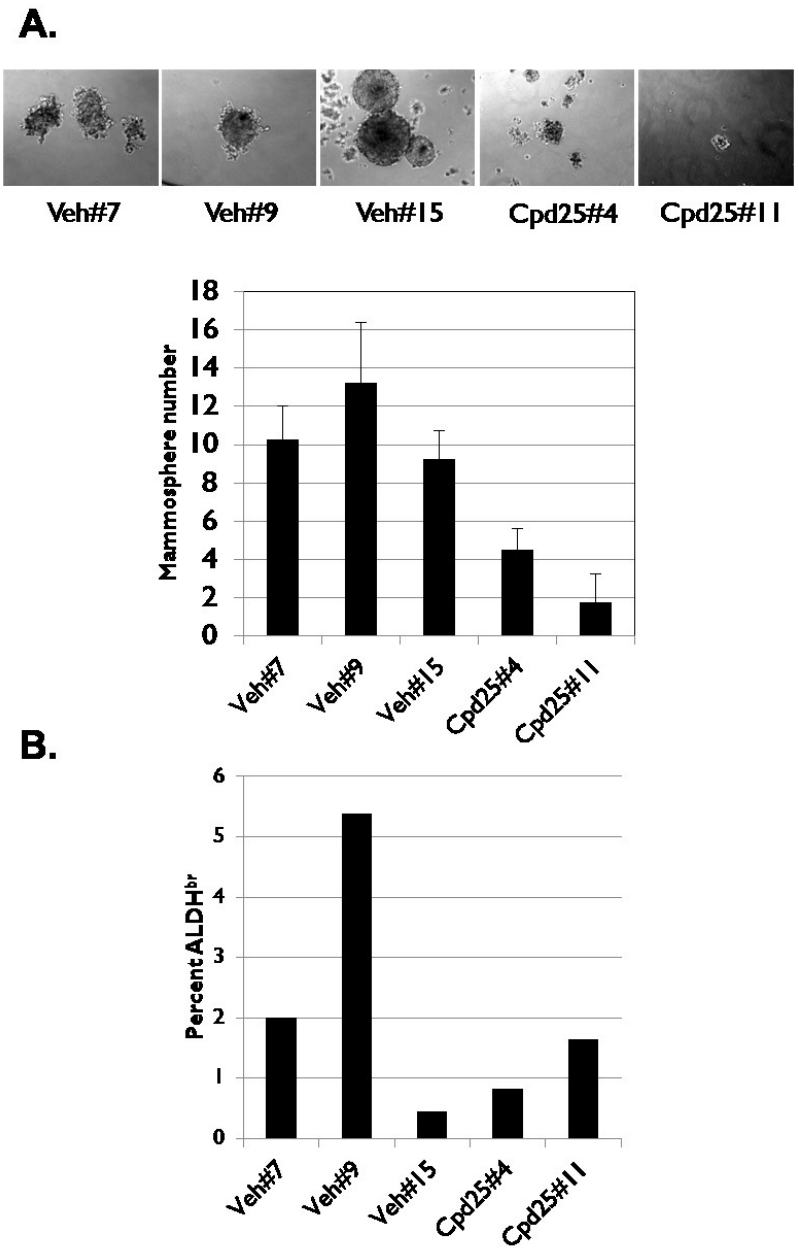

Figure 3.12 *Ex vivo* analysis of mammosphere formation and ALDH positivity in 5 mice.

A. Photomicrographs and quantification of *ex vivo* tumorsphere assays from SUM-159 orthotopic xeongrafts in vehicle- and Cpd25-treated mice. B. Percent $ALDH^{br}$ cells in *ex vivo* ALDEFLUOR assays from SUM-159 orthotopic xenografts in vehicle-and Cpd25-treated mice.

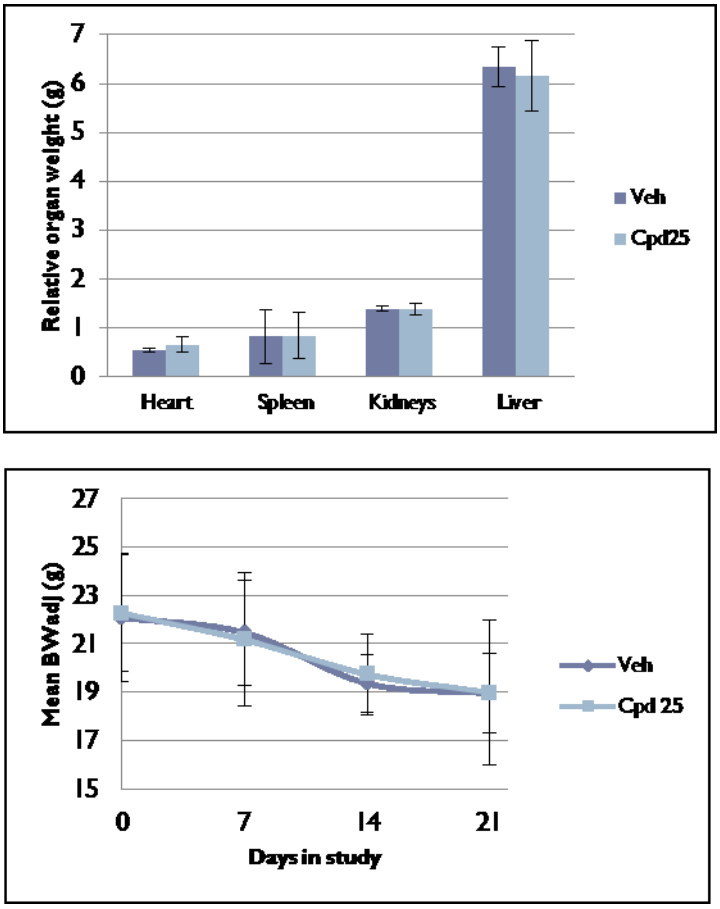

Figure 3.13 Toxicopathologic parameters for Cpd25 *in vivo* study.

Mean adjusted body weight and relative organ weights are shown for SUM-159 orthotopic xenograft-bearing mice treated with vehicle or Cpd25. Results do not differ significantly between vehicle- and Cpd25-treated groups.

Chapter 4 : Characterization of breast cancer stem cells in the MMTV-Her2/neu mouse model and mechanistic insights into response to HDAC inhibitors

Abstract

Thus far, there is a paucity of data validating a mouse model for the investigation of breast cancer stem cells (BCSC) in chemotherapeutic and chemopreventive studies. Mounting evidence suggests that a BCSC subpopulation exists in the MMTV-Her2/neu mouse. The MMTV-Her2/neu mouse model of human breast cancer is superior to xenograft or syngeneic models in that it is immunocompetent and that tumors arise in a stochastic manner. Our experiments in human triple-negative breast cancer cell lines have elucidated a mechanistic link between Notch1 and HDAC8 that may be important in regulating BCSC. Projects in chapter 4 build on this framework. We have utilized NT5 mammary tumor cells derived from the MMTV-Her2/neu mouse to predict the *in vivo* effects of HDAC inhibition on BCSC in this model. *In vitro* experiments using pan-HDAC inhibitors AR-42 and vorinostat and the HDAC8-selective inhibitor PCI-34051 demonstrated downregulation of stem cell biomarkers and decreased tumorsphere formation. NT5-allografted mice treated with dietary AR-42 showed marked tumor suppression. We have also optimized ALDH1 and Notch1 immunohistochemistry to demonstrate putative BCSC populations in mouse Her2/neu tumor sections. Our studies

elucidate a dual antitumor effect of AR-42 in its capacity to eliminate CSC by modulating the Notch1 signaling pathway and downregulate *neu*. Taken together, our data support the hypothesis that histone deacetylases are involved in regulating the BCSC population and have translational potential to give rise to new therapeutic approaches for breast cancer chemotherapy via non-epigenetic targeting of oncogenic pathways.

Introduction

Approximately 10-30% of breast cancers have amplification and overexpression of Her2/neu (ErbB2) oncogene, which encodes for a member of the family of EGFR tyrosine kinases and correlates with poor patient outcome [134, 139, 189]. Human Her2+ cancers have amplification of Her2 leading to dimerization, autophosphorylation of the tyrosine kinase, and signal transduction which drives proliferation [15]. Her2 overexpression in normal and malignant mammary epithelial cells has been reported to increase the proportion of progenitor cells [25, 114, 125, 134]. Notch1 has been characterized as a transcriptional activator of ErbB2 in differentiating glial cells of the brain [190]. Tumorsphere and limiting dilution cell transplantation experiments in the ErbB2 mouse model suggest that as many as half of the tumor cells have tumor-initiating capacity *in vitro* [137]. Cicalese et al. report that in the ErbB2 transgenic mouse model of breast cancer, there are increased numbers of CSCs, which undergo unlimited and asymmetric self-renewal that propagates their relative abundance in the tumor [123]. Use of an immunocompetent model is important in assessing CSC populations, as CSC populations may be shaped in part by EMT and the host immune response by CD8+ T

cells [119, 127]. This model is superior to other xenograft or syngeneic models in that it is immunocompetent and that tumors arise in a stochastic manner, similar to human cancers. However, to date, this model has not been used in a prospective study for therapies targeted at the CSC subset. Advantageously, this mouse has been well-characterized in the literature as a model of human breast cancer [191].

Lo et al. have characterized a tumor-initiating cell population in the MMTV-Her2/neu mouse by $CD49f^{high}/CD61^{high}$, $CD24^{+}$, and ESA^{+} [114, 125]. These cells demonstrate enhanced tumorsphere formation ability, greater tumorigenicity, and drug resistance to paclitaxel and doxorubicin [114, 125]. There is evidence that resistance to apoptosis by anticancer agents is mediated by Her2 signaling [139]. Other groups corroborate the use of $CD49f^{+}$, in addition to other markers, as indicative of a BCSC phenotype [192]. Furthermore, it has been reported that the gene signature of MMTV-Her2/neu mammary tumors is most congruent with that of human luminal progenitor cells [114, 125, 136]. Tumor-initiating cells identified in MMTV-Her2/neu model by Liu et al. 2012 – approximated at 2-4.6% frequency in tumors. TIC-enriched fraction has gene profile associated with dividing but not differentiating cells [193]. There is evidence that interplay between Her2/neu and Notch may maintain BCSC in Her2+ cancer [165]. Osipo et al. show that trastuzumab treatment drives Notch1 upregulation; in other words, as cells acquire trastuzumab resistance, they acquire a stem-like phenotype and are sensitized to GSI [194]. Inhibition of Notch signaling by the pharmacologic gamma secretase inhibitor MRK-003 has been experimentally shown to target tumor-initiating

cells in a mouse model of ErbB2 breast cancer and cause regression of large ErbB2+ xenograft tumors after a two-week treatment period [137]. Thus, we postulate that Notch1 inhibition by HDACi could achieve a similar result in this transgenic mouse model.

Interestingly, Pin1 has emerged as druggable target that affects both Notch1 and neu in breast cancer. Pin1 is a peptidyl prolyl isomerase that post-translationally modifies phosphoprotein structure by catalyzing cis/trans isomerization of phosphorylated Ser/Thr-Pro residues [195]. Multiple Pin1 isoforms with at least partial functional redundancy have been described in several animal species, and a functional Pin1 isoform has been identified in the mouse [195]. Elevated levels of Pin1 have been found in breast, ovarian, prostatic, and lung cancers and are thought to coincide with oncogenesis [195]. The Pin1 expression level is regulated by the transcription factor E2F, which activates the Pin1 promoter via E2 biding sites [196]. A strong correlation has been found between Pin1 and Notch1 activation in breast cancer [197]. A study by Girardini et al. found Pin1 overexpression in 68% of human primary breast carcinomas and proposed that the protein cooperates with mutant p53 for an aggressive transcriptional signature [198]. Pin1 is required for activation of p53 in the process of apoptosis or cell cycle arrest. p53 downregulates presenilin-1, part of the gamma secretase complex that is required for Notch1 cleavage and activation [199]. Pin1 potentiates Notch1 cleavage by gamma secretase [200]. Notch1 directly induces Pin1 transcription [200]. Pin1 binds directly to Notch1 and regulates its activity. Pin1 directly binds the Ser/Thr-Pro-rich region of

Notch1 in breast cancer cells in a phosphorylation-dependent manner [201]. Pin1 is also a direct transcriptional Notch1 target [200]. This hints at the positive feed-forward relationship between Pin1 and Notch1. Pin1 increases processing of Notch1 at the plasma membrane, and NICD can upregulate Pin1 gene expression in the nucleus [202]. Pin1 stabilizes NICD through direct interaction by blocking Fbw7-mediated polyubiquitination [197]. We have described a similar protective relationship between HDAC8 and NICD in human TNBC [168]. Pin1 binds directly to Notch1, enhancing its gamma secretase cleavage, and it enhances Notch1 transcriptional activity through stabilizing NICD [197]. Fulmer et al. thus conclude that there is an urgent need to design Pin1 inhibitors [202].

Pin1 has also been linked to oncogenic Neu. Pin1 enhances Her2 expression in breast cancer cells. Pin1 protein level is enhanced by oncogenic Neu signaling through activation of E2F [196]. Pin1 is highly expressed in 62% Her2+ breast cancers and enhances its protein stability. Pin1 was also found to be essential for Her2/neu promoter activity. Her2 is amplified in 25-30% of breast cancers. Pin1 overexpression is found in 54% of all breast cancers. Similar to its effect on Notch1, Pin1 regulates Her2 stability by interfering with its proteasomal degradation [203]. Neu overexpression has been linked to elevated Pin1 expression, and depletion of Pin1 in neu-overexpressing cells restored Fbw7-mediated degradation of its substrates [187]. Notch1, like most other Fbw7 substrates, has also been found to be a substrate of Pin1 [187]. Cyclin D1 is essential for neu-driven mammary tumorigenesis [204]. Pin1 and cyclin D1 levels are thought to be correlated: upregulation of Pin1 elevates cyclin D1 gene expression [204]. Pin1

transcription is enhanced by oncogenic Neu through E2F activation [204]. Pin1 is thought to be a Neu downstream target. Wulf et al. show that Pin1 ablation in MMTV-Neu transgenic mice abrogates induction of cyclin D1 and cancer incidence [204]. Pin1 deficiency blocks tumorigenesis in mice expressing oncogenic Her2 [205]. Pin1 simultaneously activates oncogenes and inactivates tumor suppressors [205]. Wulf et al. have proposed that a Pin1 inhibitor could be a useful component of an anticancer treatment regimen [204], and Pin1 has been therapeutically targeted by all-*trans* retinoic acid, which degrades and inhibits Pin1 in TNBC cells [205].

Materials and Methods

NT5 cell culture

NT5 cells are a murine mammary tumor cell line derived from the MMTV-Her2/neu mouse [206]. The NT5 cell line was graciously supplied by Dr. Lisa Yee. NT5 cells were cultured in IMDM supplemented with 10% FBS and 1% pen-strep in T75 flasks with passage at near-confluence. All cells were cultured at 37°C in a humidified incubator containing 5% CO2, and were used in fewer than 6 months of continuous passage. MTT assays were performed in 96 well plates with 2,000 cells per well. For western blot experiments, NT5 cells were seeded to 6cm dishes at $5x10^5$ cells per plate and allowed to attach for 24 hours. MTT results guided dose range selection. Drug-containing media was then added, and cells were collected after 48h treatment. For qPCR and IP experiments, NT5 cells were seeded to 10cm dishes at $8x10^5$ cells per plate and allowed to attach for 24 hours before drug treatments were added.

Western blotting

Western blotting was performed by lysing cells with sodium dodecyl sulfate (SDS) lysis buffer (1% SDS, 50mmol/L Tris-HCl pH 8.0, 10mmol/L EDTA) plus protease inhibitor cocktail (Sigma-Aldrich) and PhoSTOP phosphatase inhibitor (Roche) and sonication. Protein concentrations were standardized with a Micro BCA Protein Assay kit (Pierce Chemical), and each sample was homogenized in SDS sample buffer. SDS-PAGE gels were prepared at 1mm thickness immediately prior to sample loading and according to techniques modified from Harlow and Lane (Appendix A; Sambrook et al., 1989). The standard resolving gel percentage prepared was 10% with 8% used for proteins over 130kDa and 12% used for proteins under 20kDa. A 5% stacking gel was prepared in all cases. Samples were loaded and stacked in 1X running buffer at 130V for 15 minutes, then run at 100V for 60 minutes. Wet transfer to NC membrane was performed in 1X transfer buffer at 100V for 75-90 minutes. This was followed by blocking with 5% non-fat milk in TBS-T (TBS, 0.1% Tween-20) for 30-60 minutes. Incubation with primary antibodies was performed at a 1:500 dilution overnight at 4°C. Membranes were washed with TBS-T and incubated with horseradish peroxidase-conjugated secondary antibodies at a 1:5000 dilution at room temperature for 60-90 minutes. Signal detection was performed on x-ray film using a chemiluminescence system (Amersham).

Mammosphere formation assay

Five thousand NT5 cells/well were seeded onto ultra-low attachment 24-well flat bottom plates in serum-free culture medium (MammoCult™, STEMCELL Technologies; Vancouver, BC, Canada). Cells were then treated with the indicated compounds for 7 days, after which the numbers of mammospheres were counted at 100X magnification. In *ex vivo* experiments, 20,000 cells were seeded per well plus FBS supplementation. Mammospheres were counted after 14 days culture. Using the MammoCult mammosphere kit, including mammosphere basic media, growth supplement, 1% pen-strep, 1:1000 hydrocortisone, and 1:1000 heparin, NT5 cells in passage were seeded in 24 well ultra-low attachment plates with media containing increasing drug concentrations of AR-42, SAHA, or PCI-34051. Each treatment condition was plated in triplicate. Mammosphere growth was evaluated after 7 days in culture. Tumorspheres over 60μm were quantified by a microscope outfitted with a grid. Representative photomicrographs were taken. Means per treatment condition were calculated, and data are represented as relative values normalized to the untreated control group.

Proteasome inhibition

NT5 cells were cultured in 6cm dishes with media containing concentrations of HDACi at or below the IC50 as described previously. After 42h treatment (6h prior to collection), the proteasome inhibitor MG132 was added. Cells were then collected at 48h, and protein lysates were quantified and prepared per the previously described protocol.

Immunoprecipitation

Cells were harvested, incubated in IP lysis buffer (20 mM Tris-HCl pH 7.5, 150 mM NaCl, 1% Triton X-100) for 30 min on ice, and then sonicated (3 times for 10 sec each). After centrifugation, the supernatants were collected from each sample and then pre-cleared by incubation with 10 µl protein A/G agarose beads at 4°C for 1 h with rocking. After removal of the protein A/G beads by centrifugation, protein content in each sample was measured and aliquots containing 1,000-1,500 µg of protein were incubated with primary antibodies overnight at 4°C with rocking, followed by 20 µl protein A/G agarose beads for 2 h at 4°C. Samples were prepared from the whole cell lysate in parallel. The immunoprecipitates were washed with IP lysis buffer, collected by centrifugation, and resuspended in 2X sample buffer for analysis by immunoblotting. Loading volume of the IP samples was determined by normalizing to the IP protein of interest.

qPCR analysis

Total RNA was isolated from cells with TRIzol (Thermo Fisher Scientific) according to the manufacturer's protocol. One µg RNA from each sample was reversetranscribed into cDNA using the iScript™ cDNA Synthesis Kit (Bio-Rad; Hercules, CA), which was then mixed with buffer, dNTP, polymerase (Bio-Rad; Hercules, CA), ddH_2O and primers. qPCR was performed using the SYBR green kit (Thermo Fisher) and a BioRad CFX connect real-time system. Transcript levels were normalized to GAPDH. Primer sequences are tabulated in Appendix H.

GFP transfection

To lay the groundwork for a chemopreventive study utilizing MMTV-Her2/neu transgenic mice, an NT5 allograft study was planned to predict the effect of AR-42 in the transgenic mouse tumor model. NT5 cells were made to express GFP so that they could be sorted from resident mammary epithelial cells in an orthotopic model. Santa Cruz copGFP lentiviral particles were purchased. MOI 1 and 2 transfection was performed in 6-well plates with $1x10^5$ NT5 cells per well in IMDM supplemented with 10% FBS plus 1% pen-strep. Successful transfection was confirmed by checking the plates on a confocal fluorescent microscope. Selection used 0.4μg/mL puromycin with media changed every 48h for 10 days. Cells were then collected for sorting in the ACSR. The GFP bright population was selected, representing 19.1% of the scatter gate. This was followed by a period of expansion in cell culture, then a second sorting in the ACSR with selection of GFP bright cells, representing 58-66.2% of the scatter gate. The parental NT5 cell line was used as a control for size gating. A final expansion prior to culture was evaluated by confocal microscopy to be approximately 80-90% GFP+.

NT5-GFP allograft study

NOD.SCID mice (n=22) were procured for an allograft study. Experimental procedures in mice were done in accordance with protocols approved by The Ohio State University Institutional Animal Care and Use Committee. Genotype information is tabulated in Appendix B. NT5-GFP cells were grown to 80% confluence and collected for injection. 30 million cells were suspended in 3mL total volume of 50/50 PBS and Matrigel. Cells were kept on ice until injection. NOD.SCID female mice were anesthetized under 4%

inhalant isoflurane. The left inguinal region was prepped using 70% ethanol and a sterile gauze pad. A 1mL syringe and 25ga needle were used to inject 0.1mL in the left fourth mammary fat pad. The needle was inserted at the level of the nipple and advanced craniolaterally, bevel up. $1x10^6$ cells were injected per mammary fat pad. While anesthetized, mice were ear punched and weighed. Mice were monitored for tumor incidence twice weekly by palpation. When tumor volume reached approximately $100mm^3$, mice were recruited to the study and randomized to either a vehicle control group or an AR-42 treatment group. A total of 4 cohorts were recruited over the course of 2 weeks, giving a total of 21 mice in the study and group sizes of 10 and 11 for the vehicle and drug-treatment, respectively.

Treatments consisted of 50mg/kg (5mg/mL) AR-42 in 10% DMSO plus methylcellulose/Tween every other day for 10 days for a total of 5 treatments, or an equal volume (0.01mL/g) 10% DMSO plus methylcellulose/Tween (vehicle) administered at the same frequency. Vehicle or drug was administered by oral gavage to mice anesthetized under 3% inhalant isoflurane. Tumor volume and body weight were recorded weekly. Following 10 days treatment, mice were euthanized using CO2 asphyxiation followed by cervical dislocation. Mice were submerged whole in 70% ethanol to sterilize, then mammary fat pad tumors were dissected out using sterile instruments working in the biosafety hood. The tumors were rapidly immersed in 70% ethanol, then 1X PBS, then were dissected manually using scissors and a scalpel blade. Each mouse was subject to complete post-mortem examination, and a complete set of

tissues was preserved in 10% NBF. Tumor fragments were retained in liquid nitrogen for later protein or nucleic acid extraction as needed. Minced tumor was suspended in 1mL unsupplemented IMDM, then transferred to a sterile 15mL conical vial and kept on ice. In the cell culture hood, 100µL 10X collagenase/hyaluronase was added to each vial. Samples were periodically gently agitated and incubated in the 37 deg C water bath for 30-45 minutes. Cell suspensions were then strained into 50mL conical vials using a 40µm nylon mesh filter and grinding with a sterile Eppendorf tube. The filter was rinsed with an extra 1mL supplemented media. Cell suspensions were counted on the cell counter. Aliquots were separated out for analysis and sorting: $1x10^6$ cells were aliquoted for analysis, and $2x10^6$ were aliquoted for sorting. The samples were centrifuged at 5,000 rpm for 2 minutes, and the supernatants were decanted. Cells for sorting were resuspended in 495µL PBS plus 5µL 7-AAD (BD Biosciences) and incubated on ice, protected from light for 30 minutes. These samples were then taken to the ACSR for sorting. Cells for analysis were resuspended in 95.5µL PBS plus 1µL 7-AAD, 1µL CD49f antibody (BD Biosciences, prediluted in PBS at 1:1), and 2.5µL CD61 antibody (BD Biosciences). After approximately 60 minutes incubation on ice, protected from light, 1mL PBS was added to each analysis tube. Samples were centrifuged at 5,000 rpm for 2 minutes then decanted and resuspended in 300µL PBS and taken to the ACSR for analysis. Single-positive controls were prepared using the parental NT5 cell line and unstained NT5-GFP cells collected from remaining tumor extracts.

In the ACSR, the population of interest was identified as GFP positive and 7-AAD negative to select for allografted, viable cells, respectively using the BD FACSAria III sorter. 50,000-125,000 events were collected from the sorting aliquots into 1mL supplemented IMDM in 15mL conical vials. Tubes were centrifuged at 1000rpm for 5 minutes then carefully decanted. Cells were resuspended in mammosphere media including the MammoCult growth supplement and 1% pen-strep, 1:1000 hydrocortisone, and 1:1000 heparin. Mammosphere assays were plated in 24-well ultra-low attachment culture plates. Cells were seeded in triplicate at 5,000 and 10,000 cells per well for the first cohort, then at 10,000 and 20,000 cells per well for the second through fourth cohorts. Mammosphere assays were cultured in the cell incubator for 14 days, then were counted and photographed.

FACS – $CD49f^{+}/CD61^{+}$

Ex vivo NT5-GFP tumor cells were analyzed for percentage double-positive for CD49f and CD61 in the ACSR using the BD LSR II. For each mouse, approximately 0.5-1.5 million events were captured. The relative percent difference between double-positivity in the AR-42 treatment group compared to the mean of the vehicle-treated group was calculated for each cohort to make comparison across cohorts possible. There were 9 mice per treatment group analyzed. An F-test was performed to determine variance, followed by Student's t-test. Significance was set *a priori* at $p<0.05$.

Immunohistochemistry

Tumor sections from previously-conducted studies using MMTV-Her2/neu transgenic mice (n=20) and NT5-allgorafted mice (n=11) in the Yee Lab were utilized to optimize novel immunohistochemical stains for putative breast cancer stem cell markers. Biomarkers of interest included ALDH, Notch1, and Neu. All IHC staining was performed in the CPMPSR. Manufacturer protocols were followed for each antibody, and relevant concentrations are shown in Appendix D. Positive control blocks were selected for each antibody based on known or anticipated expression levels in respective tissues. For ALDH, this included liver, kidney, lung, spleen, and bone marrow. For Notch1, this included mammary gland and epidermis. For Neu, transgenic MMTV-Her2/neu tumors were used. Following primary antibody incubation, specimens were incubated with biotinylated secondary antibody and DAB chromagen, then counterstained with hematoxylin. Slides were evaluated and photographed on a light microscope outfitted with a camera, and representative photomicrographs were captured.

Results

Mouse mammary tumor cells are sensitive to HDAC inhibitors

MTT assays were performed using NT5 cells seeded in 96 well plates at 2,000 cells per well. Cells were allowed to attach for 24 hours, then drug-containing media was added to 6 wells per condition. Timepoints were developed at 24 and 48 hours after treatment. For AR-42, SAHA, and PCI-34051, a time-dependent and dose-dependent decrease in cell viability was observed with 48 hour IC50 values of approximately 0.4, 1, and 18μM, respectively, comparable to values measured in human breast cancer cell lines (Fig. 4.1).

Cancer stem cell biomarkers and mammosphere formation are downregulated by HDAC inhibitors

Treatment of NT5 cells with AR-42 and SAHA (vorinostat) shows a dose-dependent decrease in stem cell markers Notch1 and Jagged1 with downregulation of the oncoprotein c-myc, (Fig. 4.2). Tumorsphere assays using the same cell line demonstrate that both AR-42 and vorinostat can achieve greater than 50% reduction in tumorspheres at 0.25μM drug treatment (Fig. 4.3). Significant reduction in relative tumorsphere formation was observed at all HDAC inhibitor doses tested ($p<0.05$). Taken together, downregulation of stemness biomarkers and decreased tumorsphere formation by HDACi strongly support our hypothesis that HDAC inhibition modulates stemness in this murine mammary cancer cell line.

Proteasome inhibition partially rescues HDAC inhibitor-driven Notch1 downregulation

Notch1 downregulation is apparent upon treatment of NT5 cells with the pan-HDAC inhibitor AR-42 (0.5μM) and with the HDAC8-selective inhibitor PCI-34051 (20μM), and this effect is partially rescued by proteasome inhibition by MG132 (Fig. 4.4). As in previous experiments, bulk histone hyperacetylation is not evident upon PCI-34051 treatment, indicative of its isoform-specificity. Neu protein downregulation is uniquely observed under AR-42 treatment, and this effect is partially rescued by proteasome inhibition, suggesting some degree of post-translational effect of pan-HDAC inhibition on neu. Protein levels of HDAC8 are also affected differentially by the HDAC inhibitors.

AR-42 treatment downregulates the HDAC8 protein level irrespective of proteasomal inhibition, while HDAC8 protein is more dramatically downregulated by PCI-34051 and this effect is partially rescued by proteasome inhibition.

Notch1 and Neu mRNA are downregulated by AR-42 and PCI-34051 in NT5 cells

Both Notch1 and Neu mRNA levels are downregulated by sub-IC50 concentrations of AR-42 and PCI-34051 in NT5 cells in a dose-dependent manner (Fig. 4.5). Taken together, we have seen that AR-42 downregulates Notch1 and Neu at both the mRNA and protein levels. Similarly, PCI-34051 downregulates Notch1 at both the mRNA and protein levels. However, although no effect on Neu protein level was observed in the previous experiment (Fig. 4.4), Neu mRNA was downregulated by PCI-34051.

4T1 mouse mammary cancer model

To test the hypothesis that the HDAC8-Notch1 relationship is an important mediator of breast cancer stem cells in mouse models irrespective of transgene status or molecular phenotype, the 4T1 murine mammary cancer cell line was used. 4T1 cells have been reported to have stem-like features, including high Oct4 expression and capacity for mammosphere formation [207] and have been used in anticancer drug studies targeting CSCs [208, 209]. 4T1 cells obtained from the Chen Lab were cultured in RPMI supplemented with 10% FBS and 1% pen-strep. Cells in passage treated with the HDAC8 inhibitor PCI-34051 were subject to MTT assay, western blot, and qPCR to analyze the effect on Notch1 protein and mRNA levels. MTT assay established a dosing range for the

4T1 line and demonstrated that these cells are slightly more sensitive to the drug than NT5 cells, with an IC50 of approximately 15μM. 4T1 cells were also treated with AR-42 for comparison, and MTT results indicate that this line is less sensitive than NT5 cells, with an IC50 of approximately 1μM. Drug treatment with the HDAC8 inhibitor causes a decrease in Notch1 mRNA and protein levels (Fig. 4.6). However, the Notch1 protein level appears to increase in 4T1 cells under AR-42 treatment (data not shown).

Evaluation of Notch1 regulators

Transcription factors with documented binding sites at the Notch1 promoter were identified through literature search and GeneCards online gene database. Other Notch1 post-transcriptional interacting proteins were also identified. Western blot was performed to determine whether these factors are decreased in response to HDAC inhibitor treatment at the levels at which Notch1 mRNA was observed to decrease. Of the candidate proteins identified, none were found to demonstrate dose-dependent downregulation, particularly at the concentrations at which Notch1 mRNA depletion was attained (Fig. 4.7). Thus, we conclude that downregulation of Notch1 at the transcriptional level is caused by a yet-unidentified transcription factor, a distant transcriptional coactivator that interacts with the Notch1 promoter through conformational changes, or possibly through upregulation of a miR that targets and degrades Notch1 mRNA.

Assessment of HSP90 in role of HDACi-driven Neu downregulation; Neu is also downregulated by AR-42, and this effect is minimally abrogated by proteasome inhibition

HSP90 clients were evaluated as a possible mechanistic explanation for post-translational Neu downregulation by AR-42. Hyperacetylation of HSP90 leads to decrease in its chaperone function and subsequent loss or degradation of its client proteins. Neu is a client protein of HSP90. We hypothesize that treatment with pan-HDAC inhibitors could lead to hyperacetylation of HSP90 and thereby post-translational loss of Neu through protein degradation. To test this hypothesis, we identified several other strong HSP90 client proteins that have both similar and different subcellular functions (i.e. tyrosine kinase or non-tyrosine kinase) as Neu. Protein levels were analyzed by western blot in NT5 cells treated with HDAC inhibitors AR-42, SAHA, and PCI-34051. HSP90 clients cAbl and EGFR are also downregulated by AR-42, but not by SAHA or PCI-34051. HSP90, a chaperone protein, is often overexpressed in cancer and correlates with poor prognosis and chemotherapeutic resistance. HSP90 is deacetylated by HDAC6, and HDACi that affect this isoform can induce hyperacetylation of HSP90, abrogating its function and causing proteasomal degradation of its client proteins, which include Her2/neu, ERBB1, ERBB2, Akt, c-Raf, BCR-ABL, and FLT3 [148].

Under AR-42 treatment, in which Neu downregulation was observed, experiments were performed in which either Neu or HSP90 was immunoprecipitated (Fig. 4.8). In both blots, we found evidence of HSP90-Neu coimmunoprecipitation which, in IP-HSP90,

appears to decrease under drug treatment, suggesting that AR-42 could interrupt the HSP90-Neu interaction. Blotting for acetylated lysine in the HSP90 immunoprecipitate also suggests that a 90kDa band may become increasingly acetylated under AR-42 treatment, although this was not corroborated by use of an acetyl-HSP90 antibody in either the immunoprecipitate or whole cell lysate. Concordantly with previous data, both HSP90 and Neu are downregulated in the whole cell lysate under AR-42 treatment, and bulk histone hyperacetylation was observed.

HDAC8 co-immunoprecipitates with Notch1, which becomes increasingly ubiquitinated under HDAC inhibitor treatment

Notch1 was immunoprecipitated in NT5 cells treated with either AR-42 or PCI-34051 to assess whether HDAC8 physically associates with Notch1, and whether Notch1 is acetylated or ubiquitinated following drug treatment. Interestingly, HDAC8 and Notch1 did co-immunoprecipitate, but this association appears to be disrupted by drug treatment, as HDAC8 levels in the Notch1 immunoprecipitate decrease while the Notch1 level remains steady (Fig. 4.9). Blotting for ubiquitin in the Notch1 immunoprecipitate showed Notch1 ubiquitination which appears to increase slightly following drug treatment. Notch1 ubiquitination status may be better assessed by examining the same drug treatment conditions concurrently with proteasomal inhibition by MG132, to capture any polyubiquitinated proteins before degradation. As in previous experiments, Notch1 was markedly downregulated by both AR-42 and PCI-34051 at doses below the IC50 in the whole cell lysate.

Pin1 as a master regulator of Notch1 and Neu in the NT5 model

The observation that both Notch1 and Neu mRNA levels are decreased upon HDAC inhibitor treatment, including by the isoform-specific inhibitor PCI-34051, prompted the search for a candidate protein that can explain concurrent downregulation of Notch1 and Neu at the protein level. Pin1 has been reported to interact with and enhance signaling through both Notch1 and Neu post-translationally through direct binding and protein stabilization, as well as by protection from protein degradation by the ubiquitin-proteasome system. Treatment of NT5 cells with AR-42 or PCI-34051 found downregulation of Pin1 by the HDAC8 inhibitor at the protein, but not mRNA level (Fig. 4.10). A similar effect was not observed under AR-42 treatment. Thus, we suggest that the post-translational effect of HDAC8 on Notch1 could be mediated through Pin1, whereby HDAC8 could function as a Pin1 agonist, blocking its effect on Fbwx7 dimerization and subsequent Notch1 ubiquitination, or whereby HDAC8 could function as a Pin1 agonist, cooperating in its direct binding to and stabilization of Notch1.

AR-42 demonstrates proven antitumor efficacy in MMTV-Her2/neu transgenic model in a NT5 allograft experiment

Following extensive *in vitro* descriptive investigation of the effect of HDACi in the MMTV-Her2/neu model, we turned to *in vivo* analysis of the efficacy of HDACi in this model. In the laboratory of Dr. Lisa Yee, athymic nude mice bearing NT5 allografts were fed AR-42-containing diet for 4 weeks, and tumor volume was monitored. Dietary

composition of 208ppm AR-42 is equivalent to 25mg/kg/d by oral gavage. At the end of the study, tumor volume and mass were compared between mice fed control diet versus dietary AR-42. A striking tumor suppressive effect of AR-42 was observed as early as 1 week after beginning treatment and persisting for the duration of the study (Fig. 4.11).

Optimization of ALDH1, Notch1, and Neu immunohistochemical stains

For ALDH1A1, specific, granular cytoplasmic staining was observed multifocally throughout the tumor sections in 8 of 20 unique MMTV-Her2/neu tumors evaluated. A small total proportion of cells (under 10%) was assessed as positive (Fig. 4.12). For Notch1, diffuse positive cytoplasmic staining was observed throughout all tumor sections in varying degrees of intensity in all NT5 allograft sections evaluated (n=11) (Fig. 4.12). This corresponds with high Notch1 expression levels observed in *in vitro* experiments using the NT5 cell line. For Neu, specific plasma membrane staining was observed in the MMTV-Her2/neu tumor sections, consistent with the known localization of Neu (Fig. 4.12). Each of these markers may be useful in allograft or transgenic studies analyzing BCSC endpoints by IHC in the Her2 mouse model.

AR-42 treatment downregulates breast cancer stem cells in an allograft orthotopic model

NT5 cells were stably transfected to express GFP. A brightfield photomicrograph and the corresponding fluorescent image are shown in Fig. 4.13. NT5 cells were highly sensitive to puromycin at concentrations required for selection, so selection was performed with a combination of puromycin followed by sequential enrichment in the GFP+ fraction by

FACS sorting. Final GFP expression at the time of injection was estimated at 80-90%. Our experimental design for the NT5 allograft study with CSC endpoints is illustrated in Fig. 4.14. A statistically significant, 25.3% decrease in proportion of double-positive cells was identified in the AR-42 treated tumor cells compared to vehicle controls (p=0.0002) (Fig. 4.15A). Mammosphere assays presented a technical challenge, as NT5 cells were poorly viable following processing and sorting. Conditions were optimized as the experiment progressed, and for recruitment cohorts 3 and 4, it was found that addition of FBS to the mammosphere media and an increased seeding density of 20,000 cells per well was necessary. Mammosphere assays from the first two cohorts plated at 5,000, 10,000, and 20,000 cells per well without FBS had no growth at 21 days. For cohorts 3 and 4, the three-well total for each mouse was counted after 14 days of growth, then relative mammosphere number normalized to vehicle-treated mice was calsulcated. Analysis of *ex vivo* tumorsphere formation found reduced tumorsphere formation in AR-42 treated mice relative to controls (Fig. 4.15B); however, this finding is purely observational and is limited by the total number of animals available for evaluation (n=3 vehicle, n=5 AR-42) and low statistical power.

Discussion

Our studies elucidate a unique inhibitory effect of HDACi on BCSC populations in the MMTV-Her2/neu model through acting on non-histone targets. The pan-HDAC inhibitor AR-42 showed potent *in vitro* and *in vivo* antitumor and anti-CSC effects, driven by downregulation of Notch1 and Neu at the mRNA and protein levels. We found that AR-

42-driven Notch1 downregulation was partially rescued by proteasomal inhibition, suggesting a post-translational effect, and demonstrated that Notch1 is increasingly ubiquitinated following AR-42 treatment. We also observed that HDAC8 and Notch1 coimmunoprecipitate in NT5 cells, but that their association appears to be disrupted by AR-42. Neu downregulation was also partially rescued by proteasomal inhibition. We found that Neu and its chaperone HSP90 coimmunoprecipitate, and that their association is disrupted by AR-42, possibly due to HSP90 hyperacetylation. Though we evaluated several transcription factors that could be affected by AR-42 to explain the Notch1 and Neu mRNA downregulation, none was found. Nonetheless, the post-translational links between Notch1-HDAC8 and Neu-HSP90 warrant further investigation, and the capability of AR-42 to dually downregulate Notch1 and Neu mRNA may be an attractive therapeutic benefit. Complete elucidation of the effects of AR-42 is difficult, as it is a promiscuous drug and functions more broadly as a deacetylase inhibitor, rather than an HDAC inhibitor, potentially affecting a multitude of enzymatic targets and their substrates. We were able to demonstrate an anti-CSC effect of AR-42 in our *in vivo* NT5 allograft study, evidenced by a statistically significant 25.3% decrease in proportion of $CD49f^{+}/CD61^{+}$ cells in AR-42-treated mice compared to vehicle controls. Other endpoints that might complement the *ex vivo* data in this study include analysis of intratumoral biomarkers, with particular attention to Notch1 at the protein and mRNA levels by western blot, PCR, IHC, and/or ISH.

The HDAC8-selective inhibitor PCI-34051 achieved Notch1 downregulation at the mRNA and protein levels, as well as Neu downregulation at the mRNA level and Pin1 downregulation at the protein level. We found that PCI-34051-driven Notch1 downregulation was also partially rescued by proteasomal inhibition, as in the AR-42 treated cells, suggesting that HDAC8 may be primarily responsible for Notch1 protein modulation in this cell line. We also found that HDAC8 coimmunoprecipitated with Notch1 in NT5 cells, an interaction which was decreased upon HDAC8 inhibition. Pin1 protein, but not mRNA, was uniquely downregulated by this HDAC inhibitor, but not the pan-HDAC inhibitor AR-42. Loss of Notch1 protein could be mediated in part through Pin1, which normally stabilizes cleaved Notch1 and protects it from degradation, perpetuating Notch1 signaling and thereby the CSC phenotype. This would hypothetically implicate HDAC8 in the Pin1-Fbwx7-Notch1 axis, by which HDAC8 would play an integral role in protecting Notch1 from Fbwx7-mediated degradation directly, inhibiting Fbwx7 dimerization and subsequent Notch1 degradation, or by facilitating Pin1 binding to and stabilizing Notch1. As in the AR-42 treatment conditions, we were unable to identify transcription factors which could explain Notch1 and Neu mRNA downregulation. HDAC8 has been recently shown to associate with corepressor complexes, and other HDACs such as HDAC1 and 3 are also known to associate with multiprotein transcription complexes. It is possible that the effects of AR-42 and PCI-34051 at the transcriptional level are mediated through similar non-histone functions of HDACs.

Limitations and Future Directions

It would be interesting to investigate, through *in vitro* studies, the relative contribution of Notch1 and Neu downregulation to tumorigenicity and the BCSC phenotype in time-course studies comparing AR-42 to other pharmacologic agents such as trastuzumab and gamma secretase inhibitors in the MMTV-Her2/neu model. We have built evidence that HDAC8 inhibition alone has a potent antitumor effect in NT5 cells, apparently through its effect on Notch1 mRNA and protein levels. This could prove to be a useful therapeutic target, as pharmacologic Her2 inhibitors in human Her2+ cancer drive cancer cells towards a CSC phenotype, making them potentially susceptible to Notch1 inhibition, which could be achieved through HDAC8 blockade. Another way to evaluate the relative contribution of Notch1 and Neu to tumorigenicity and stemness would be to ectopically overexpress each protein (shRNA) in the setting of pharmacologic inhibition, for example by AR-42. Similarly, the role of Pin1 in the setting of HDAC8 inhibition in the NT5 model could be dissected by concurrent siRNA HDAC8 blockade and plasmid-vectored Pin1 overexpression in an *in vitro* model.

Our allograft experiments provide the basis for further study of the effects of HDACi in the MMTV-Her2/neu mouse. It is important to highlight that the antitumor effect observed with dietary AR-42 in a long-term (4 week) study may differ mechanistically from the anti-CSC effect appreciated in our 10-day study. Prolonged treatment with any anticancer agent provokes evolution within a tumor and emergence of resistant subclones, reminding us that it is extremely unlikely that any one antitumor drug is likely to succeed

as a monotherapy, but rather that an optimal cocktail or sequence of drug treatments should be identified for eradication of bulk tumor cells and CSC. The next logical step is to undertake a prospective study using transgenic mice. The following questions can be ascertained: does HDACi intervention prevent pre-neoplasia? If so, when? Does HDACi chemoprevention affect normal mammary development? Can HDACi prevent progression of pre-neoplasia to carcinoma? Can HDACi reverse pre-neoplasia after its onset? Does long-term HDACi reduce the total tumor incidence, burden, and/or metastasis? A proposal for such endpoints has been formulated below.

These experiments will be conducted using female MMTV-Her2/neu mice from Jackson Laboratory. Mice will be randomized to four treatment groups receiving early-intervention AR-42 (n=30), early-intervention AR-42 with early removal (n=30), late-intervention AR-42 (n=30), or control diet (n=30). Because ErbB2 expression in mammary epithelium of mice begins at approximately 6 weeks of age, dietary AR-42 will be administered beginning at this time in the early-intervention groups. AR-42 will be administered orally via a specially formulated diet (Research Diets, Inc., New Brunswick, NJ). Dietary drug delivery is favored for a study of this duration to minimize handling stress, anesthetic events, and untoward side-effects of chronic oral gavage. Dietary administration of 208ppm AR-42 diet for 18 weeks has been reported in the transgenic adenocarcinoma of the mouse prostate (TRAMP) model to be equally efficacious as 25mg/kg/d oral gavage dosing and without significant or irreversible adverse effects [141]. Mice will be palpated twice weekly to monitor for tumor incidence, then two-

dimensional tumor measurements will be recorded and the volume will be calculated. Body weights will be recorded once weekly. Mice are expected to begin developing mammary neoplasms around 24 weeks of age. The early-intervention AR-42 with early removal treatment group will be sacrificed at 24 weeks of age to evaluate hyperplastic and pre-neoplastic changes of the mammary gland. The study will terminate when mice in the early-intervention AR-42 and control groups reach 36 weeks of age, at which time animals will be humanely sacrificed and subject to complete post-mortem examination. For all treatment groups, relevant organ weights will be recorded and examined histologically for evidence of toxicity according to the Best Practices established by the Society of Toxicologic Pathology. Study endpoints include tumor latency, multiplicity, incidence, and tumor weight, as well as biomarker modulation. Tumor tissue will be collected to analyze CSC populations using FACS (ALDH, CD49f, CD61), western blot, RT-PCR, tumorsphere assays, and immunohistochemistry with digital quantitative analysis.

Female MMTV-Her2/neu mice characterized as the late-intervention AR-42 group will not begin receiving dietary AR-42 until 24 weeks of age, at which point most animals are expected to begin developing pre-neoplastic mammary lesions. The purpose of including this group is to evaluate the effect of HDACi on CSC following the initiation of proliferative changes and assess its capacity to halt or reverse tumor progression. Mice will be humanely euthanized at 36 weeks of age and subject to complete post-mortem examination. Study endpoints include tumor multiplicity, incidence, and tumor weight, as

well as biomarker modulation. Tumor tissue will be collected to analyze CSC populations using FACS (ALDH, CD49f, CD61), western blot, RT-PCR, tumorsphere assays, and immunohistochemistry with digital quantitative analysis.

In light of the data obtained in our NT5 allograft study, we hypothesize that dietary AR-42 will reduce CSC populations, leading to delayed onset of pre-neoplastic lesions (atypical hyperplasia, carcinoma *in situ*) and malignant neoplasia (adenocarcinoma), reduced tumor incidence, and decreased tumor volume. Furthermore, we predict that tumor regression can be induced with dietary AR-42 administration via CSC depletion. *Ex vivo* analysis of tumor composition from AR-42-treated mice is expected to show reduced tumorsphere formation, smaller proportions of $ALDH^+$ and $CD49f^+/CD61^+$ cells by flow cytometry, and decreased protein biomarkers associated with stemness compared to mice receiving control diet. In addition, we predict that immunohistochemistry on tumors from AR-42-treated animals will reveal smaller proportions of cells expressing ALDH and activated Notch1.

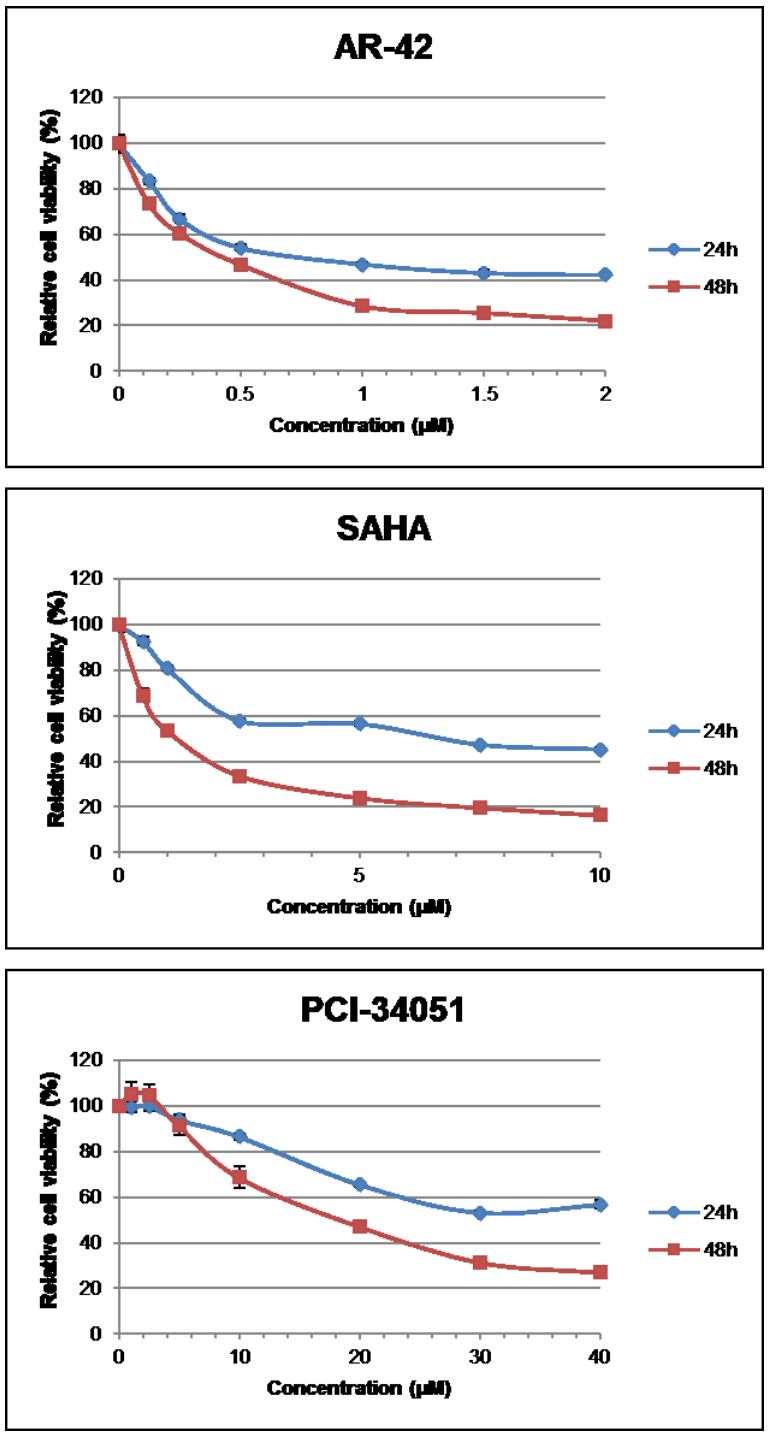

Figure 4.1 MTT assays using pharmacologic HDAC inhibitors in NT5 cells.

HDAC inhibitors AR-42, SAHA, and PCI-34051 reduce cell viability in NT5 cells in a dose- and time-dependent manner. All HDACi have similar potency in this murine mammary carcinoma cell line as in human breast cancer cell lines.

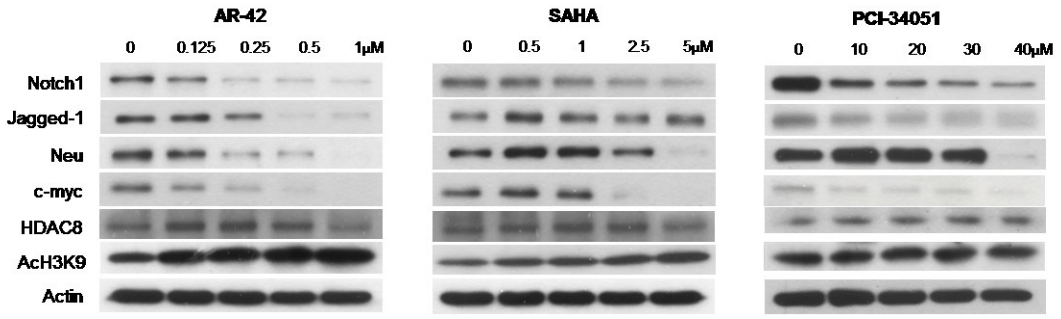

Figure 4.2 Western blot analysis of Notch1 and other biomarkers in NT5 cells treated with pharmacologic HDAC inhibitors.

NT5 cells were treated with HDACi for 48 hours, then protein lysates were collected. HDAC inhibitors, including the HDAC8-selective inhibitor PCI-34051, downregulate Notch1 in NT5 cells. Jagged1, a Notch1 ligand, and Neu are also downregulated by AR-42 at doses below the IC50. There is prominent H3 hyperacetylation under AR-42 treatment, a hallmark of class I HDAC inhibition.

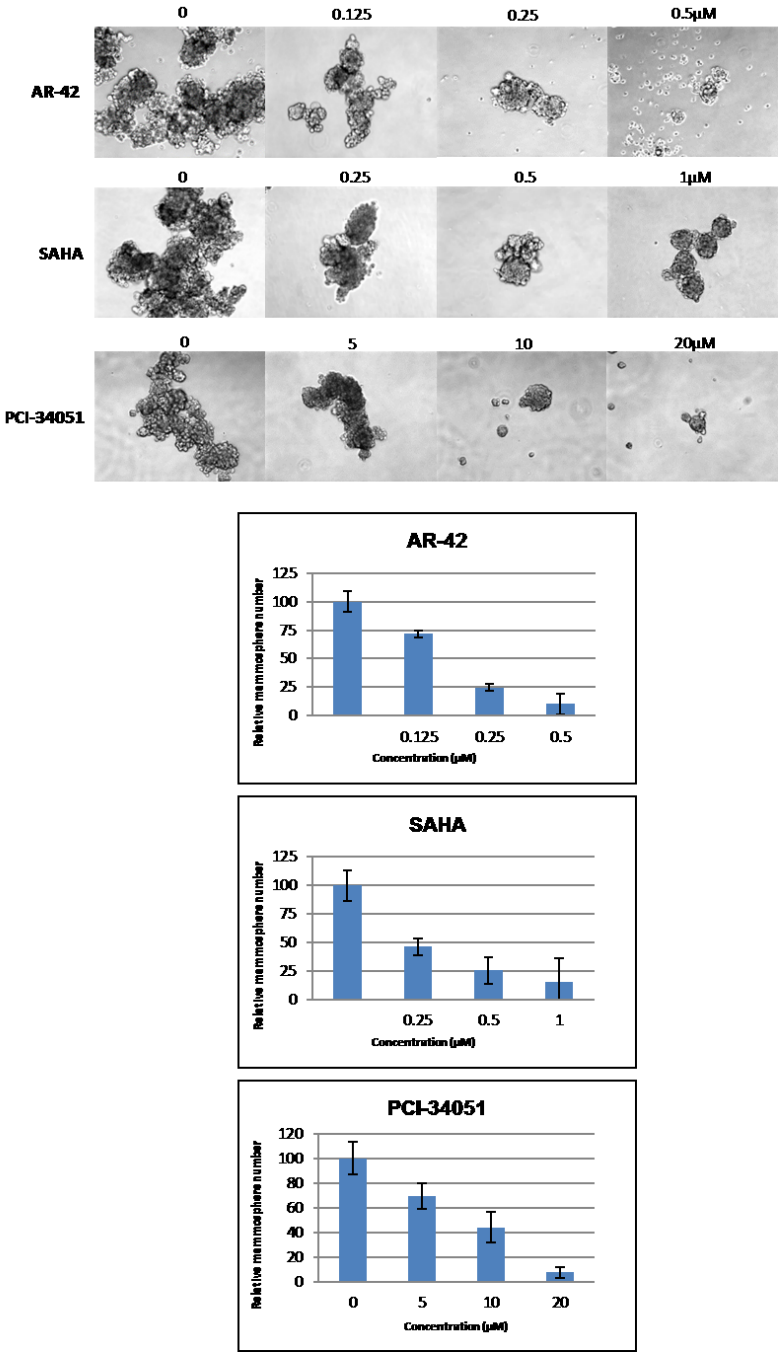

Figure 4.3 Mammosphere assays using pharmacologic HDAC inhibitors in NT5 cells.

Mammosphere assays were performed in triplicate and interpreted at 14d. Mammosphere formation is reduced by pan-HDAC inhibitors and PCI-34051 in NT5 cells.

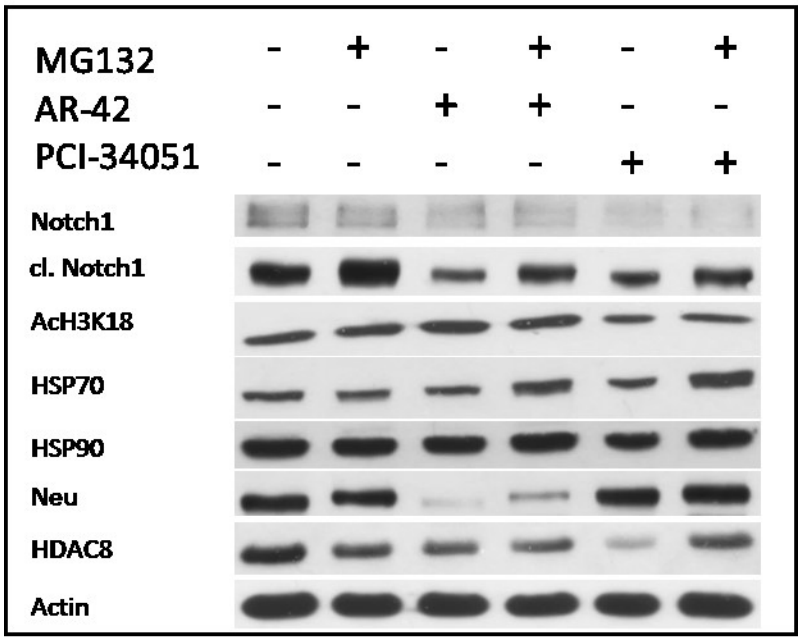

Figure 4.4 Proteasome inhibition in NT5 cells treated with AR-42 or PCI-34051.

NT5 cells were treated with AR-42 or PCI-34051 with or without MG132 for a total of 48h. HDAC inhibitor-driven Notch1 downregulation is partially rescued by proteasome inhibition. Histone 3 hyperacetylation is induced by AR-42. HSP70 is induced under MG132 treatment. Neu is downregulated by AR-42 but not PCI-34051, and this effect is also partially rescued by MG132. HDAC8 appears to be slightly downregulated by both HDAC inhibitors; more strikingly but reversibly under PCI-34051 treatment.

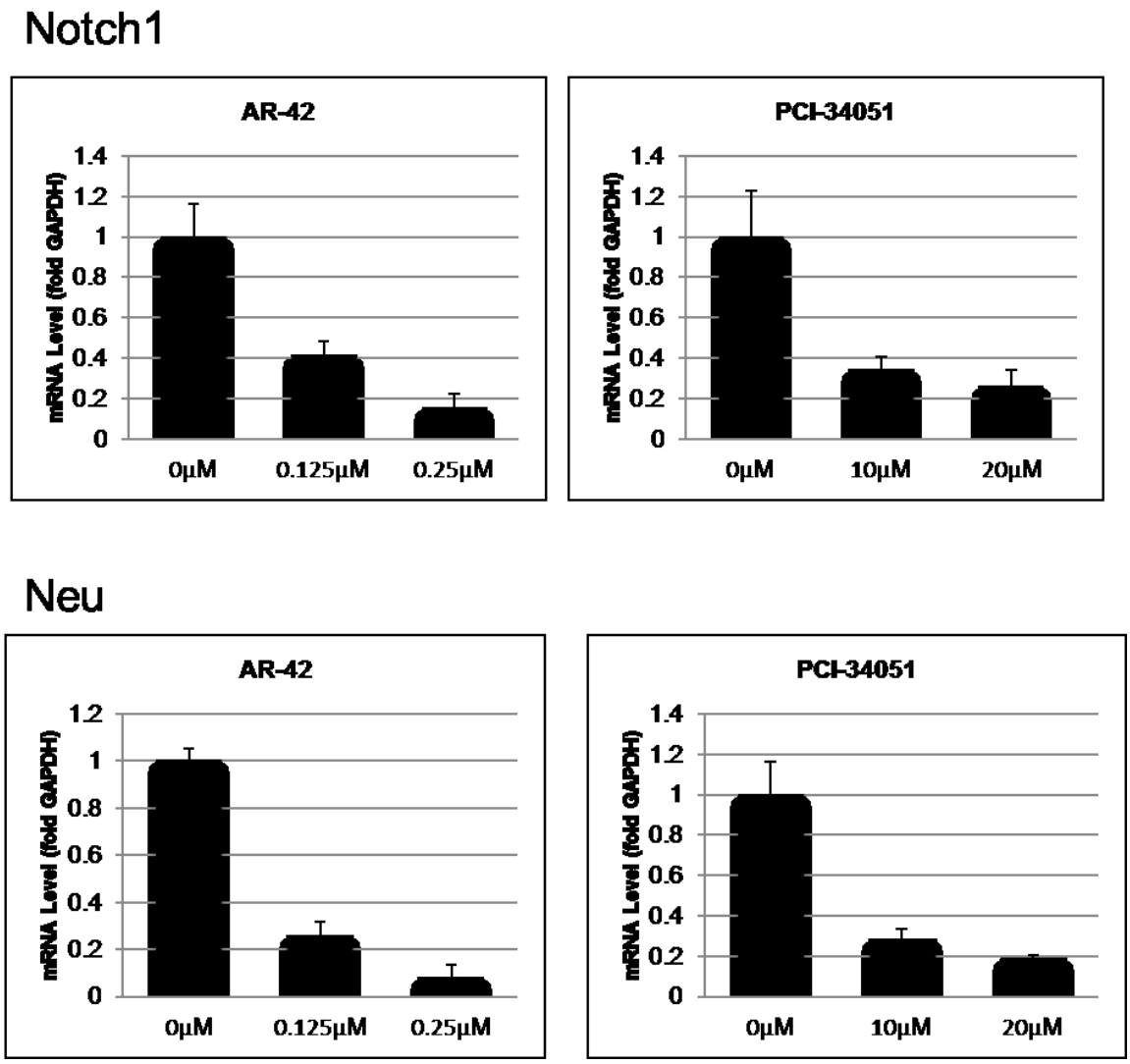

Figure 4.5 qPCR analysis of NT5 cells treated with AR-42 or PCI-34051.

Both Notch1 and Neu are significantly downregulated by AR-42 and PCI-34051 at the mRNA level at concentrations below the IC50. Experiments were performed in triplicate.

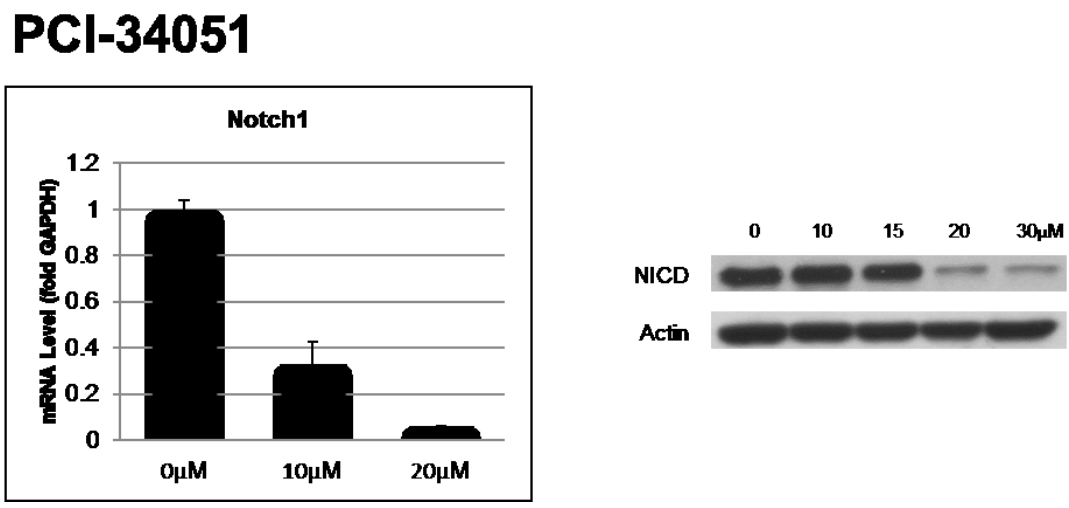

Figure 4.6 4T1 cells treated with PCI-34051.

Notch1 mRNA and protein are downregulated by PCI-34051 in the 4T1 model. Notch1 mRNA downregulation appears at a lower drug dose than protein-level downregulation.

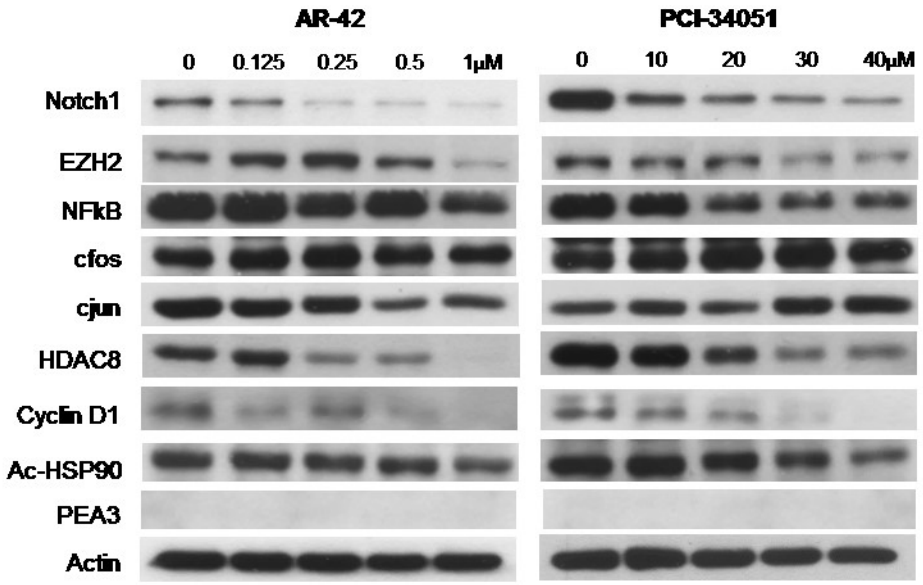

Figure 4.7 Western blot analysis of Notch1 transcription factors in NT5 cells treated with AR-42 or PCI-34051.

Screening for a Notch1 transcription factor influenced by HDAC inhibitors. We were unable to identify downregulation of a Notch agonist at drug doses where Notch1 is downregulated by AR-42 and PCI-34051 in NT5 cells. Additionally, cyclin D1 was downregulated by both HDACi, acetylation of HSP90 was not found, and we identified no PEA3 expression in NT5 cells.

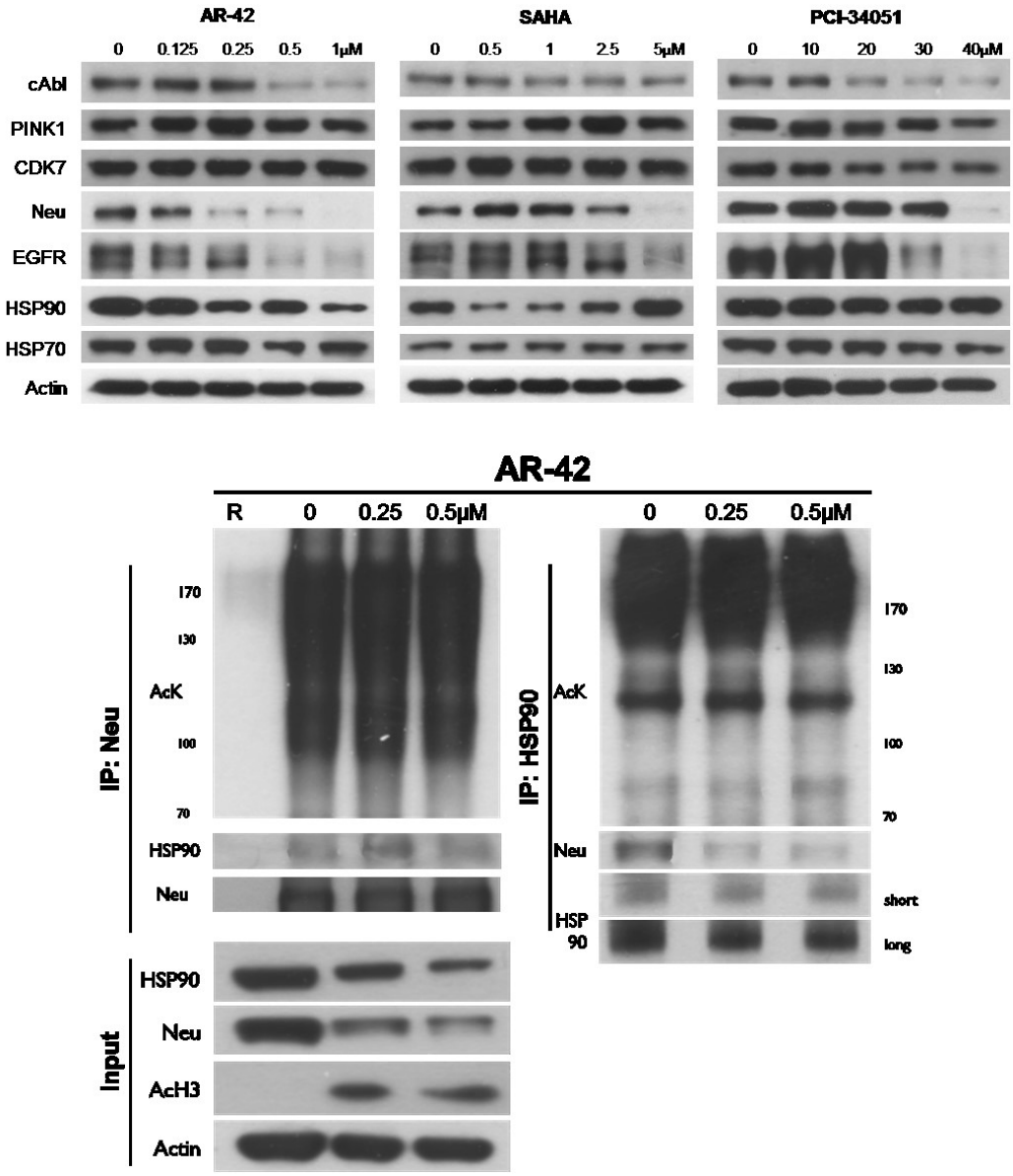

Figure 4.8 Western blot and IP analysis of HSP90 clients in NT5 cells treated with HDAC inhibitors.

Neu, and HSP90 client protein, is downregulated by AR-42 but not other HDACi. Other HSP90 clients cAbl, PINK1, CDK7, and EGFR were evaluated for similar downregulation after 48h treatment. IP of Neu and HSP90 in NT5 cells treated with AR-42. Neu and HSP90 co-immunoprecipitate, and both are downregulated by AR-42. IP HSP90 demonstrated slight drug-induced acetylation and dissociation from Neu.

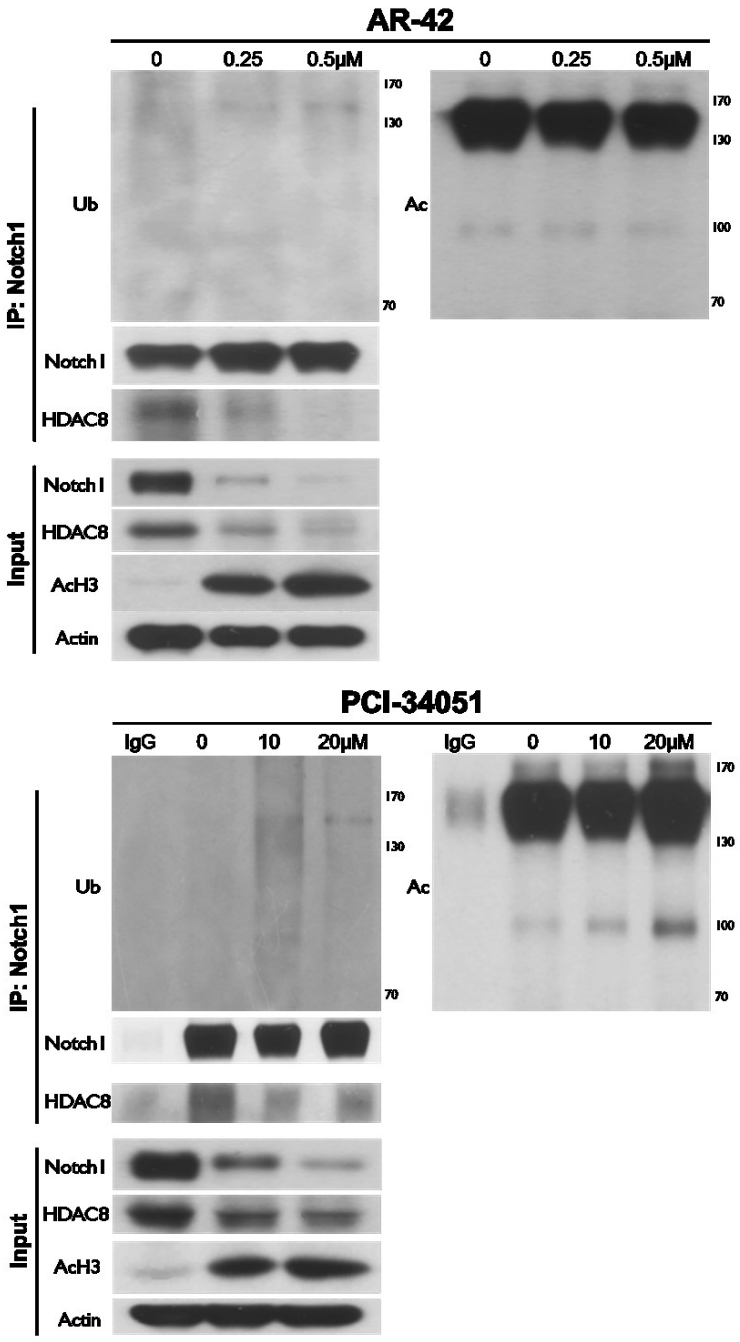

Figure 4.9 IP analysis of Notch1 in NT5 cells treated with AR-42 or PCI-34051.

Notch1 IP in NT5 cells shows that HDAC8 coimmunoprecipitates with Notch1, but its association is decreased by HDAC inhibitors. Notch1 also becomes ubiquitinated following HDACi treatment.

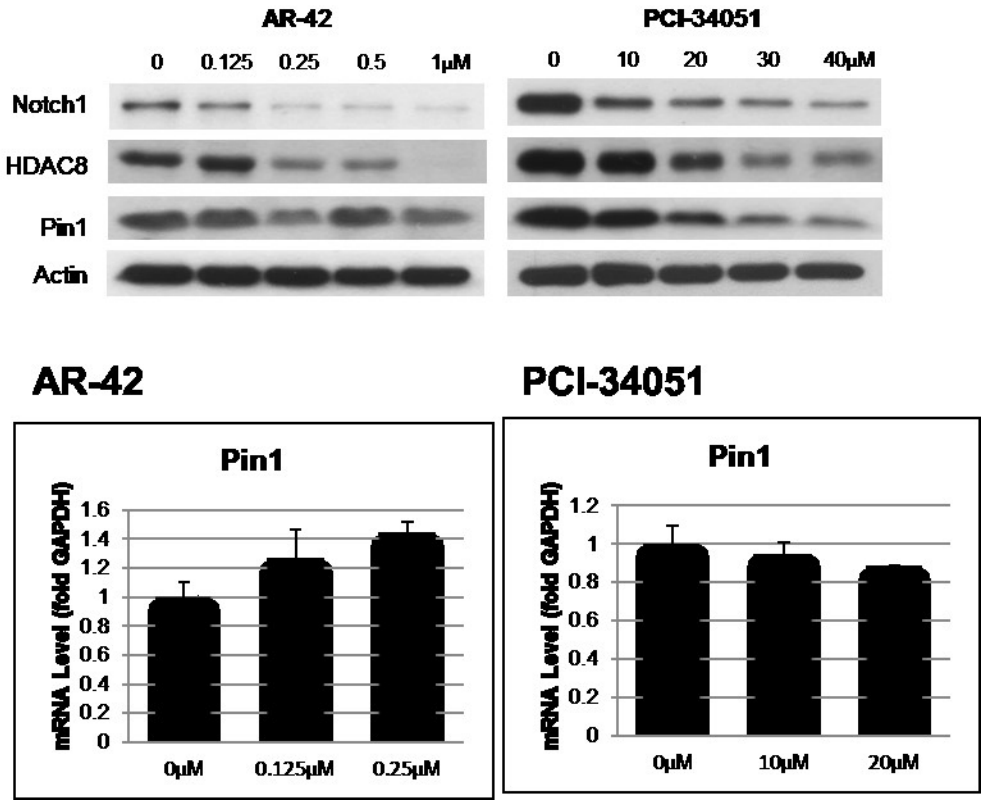

Figure 4.10 Western blot and qPCR analysis of Pin1 in NT5 cells treated with AR-42 or PCI-34051.

Pin1 is downregulated by HDAC8-selective inhibition at the post-transcriptional level, but a significant change was not found in Pin1 mRNA.

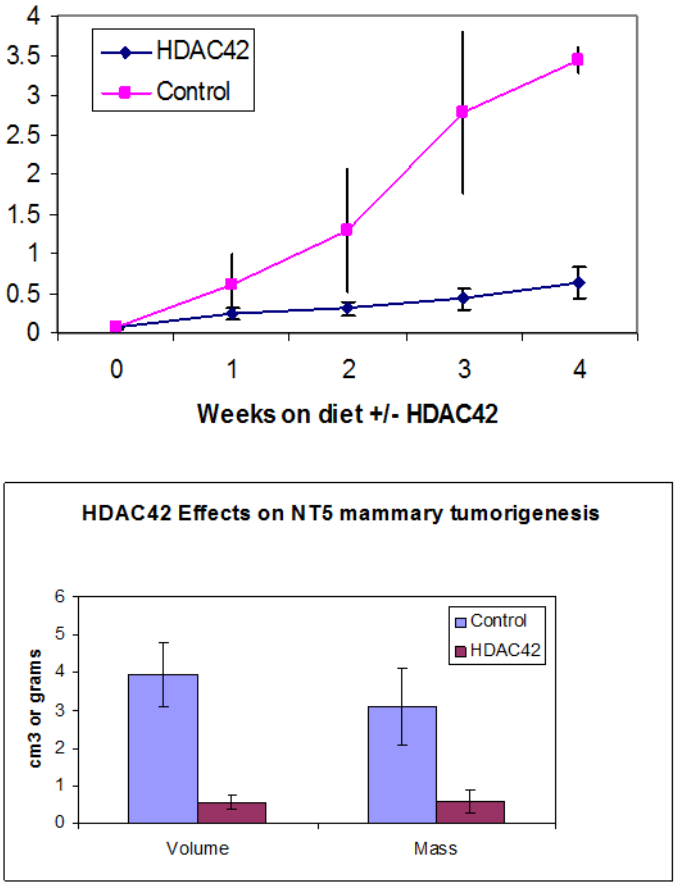

Figure 4.11 *In vivo* orthotopic allograft study using dietary AR-42 in an NT5 model.

AR-42 has potent anti-tumor effects in the NT5 Her2 model, as significant reductions in final tumor volume and mass were observed compared to mice fed a control diet.

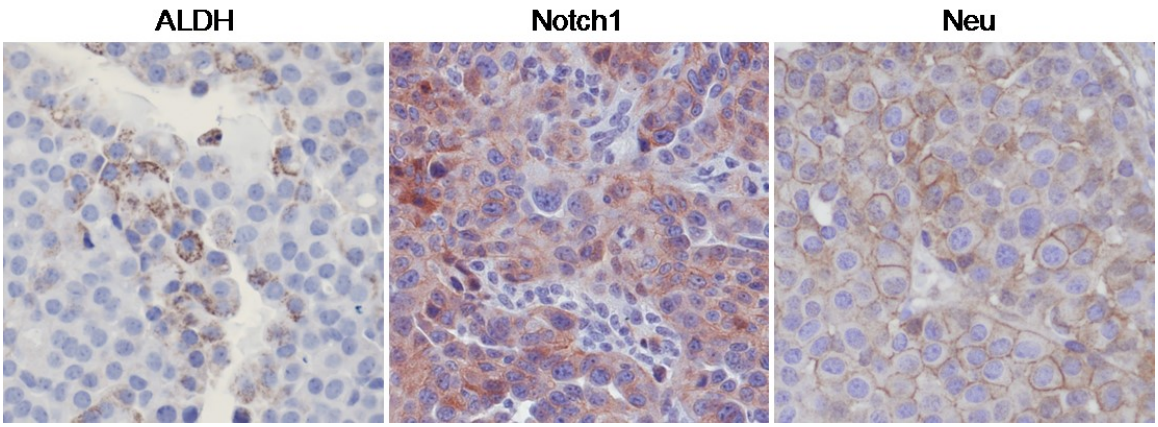

Figure 4.12 Immunohistochemical analysis of three novel protein targets in the MMTV-Her2/neu murine model.

Optimization of three novel antibodies for IHC identification of ALDH1, Notch1, and Neu in a murine model of mammary cancer (Appendix D).

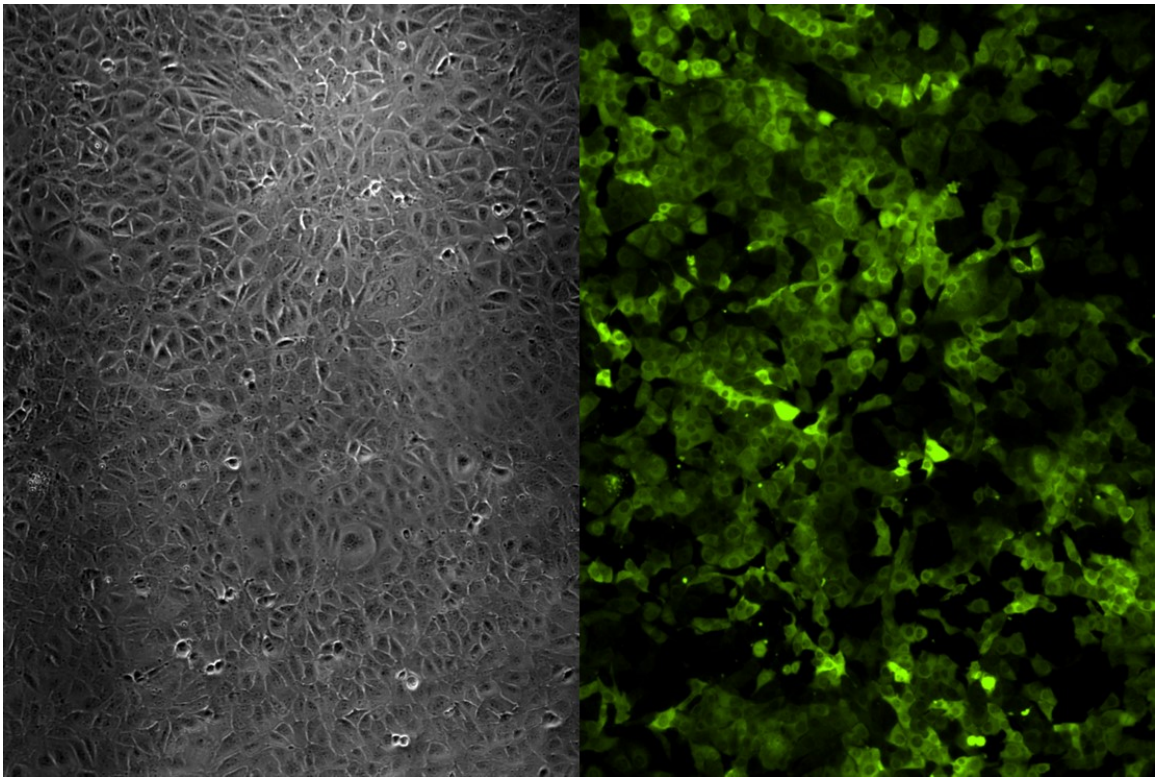

Figure 4.13 NT5-GFP transfection.

Photomicrographs demonstrating GFP fluorescence of NT5 cells following lentiviral transfection, selection, and sorting. A brightfield image of NT5 cells at confluence is shown on the left, and the same field showing GFP+ is on the right.

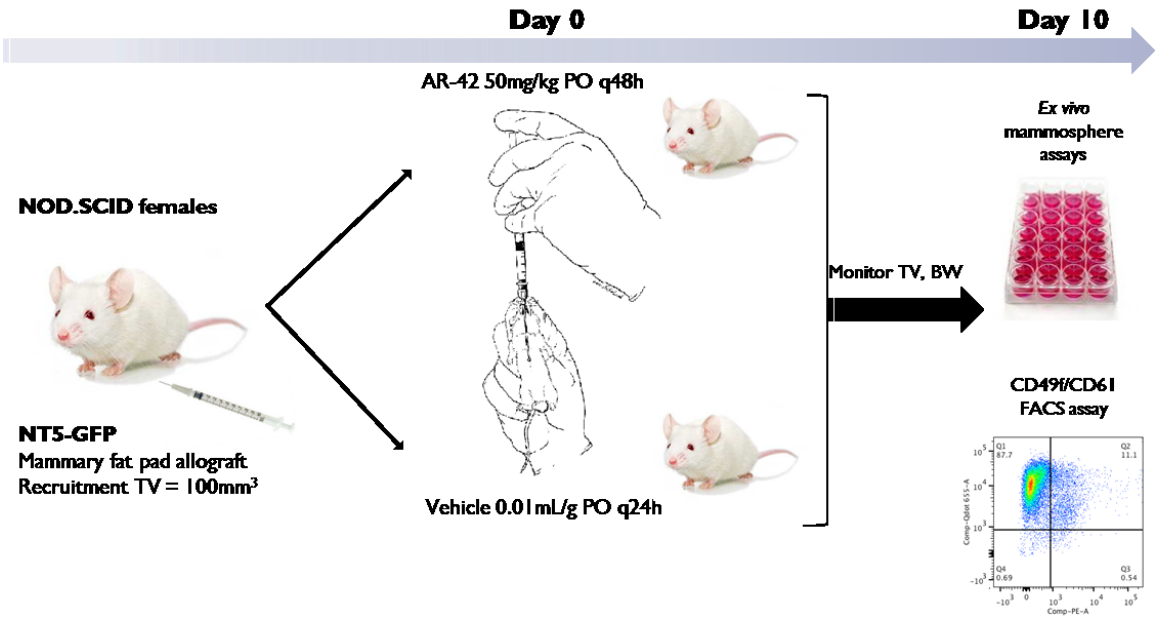

Figure 4.14 Schematic of NT5-GFP orthotopic allograft study using AR-42.

NOD.SCID female mice were injected in the left fourth mammary fat pad with $1x10^6$ NT5-GFP cells. Tumor growth was monitored until recruitment volume was reached, then mice were randomized to one of two treatment groups. Mice received either 50mg/kg AR-42 orally every 48h or an equal volume of vehicle. Mice were treated for a total of 10d, then were sacrificed for *ex vivo* analysis by mammosphere assay and flow cytometry.

NOD scid spontaneous mutant mouse model ©Taconic, retrieved from: http://www.taconic.com/mouse-model/nod-scid
Oral Gavage ©University of Illinois at Chicago Biologic Resources Laboratory, retrieved from: https://www.brl.uic.edu/node/37
Cell culture plates ©Lushpix Stock Images, retrieved from: http://www.fotosearch.com/ULY249/u18729508

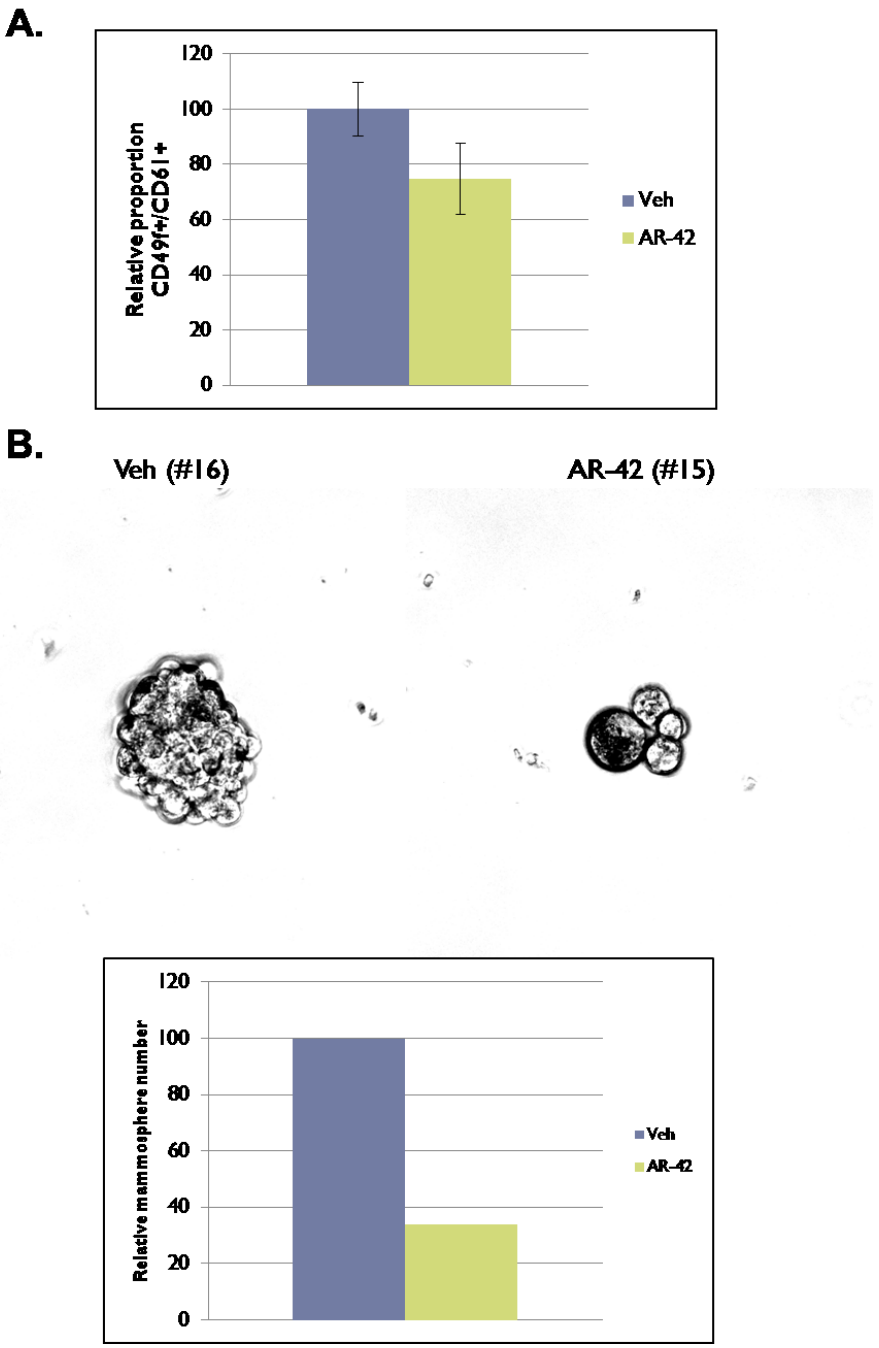

Figure 4.15 *Ex vivo* analysis by flow cytometry and mammosphere assay.

A. We observed significant downregulation of double-positivity in BCSC markers CD49f/CD61 (n=9/group; p=0.0002). B. There was also decreased mammosphere formation in cells from mice treated with AR-42 (n=3 vehicle, n=5 AR-42).

Appendices

Appendix A: Western Blotting Preparations

TABLE 18.3 Solutions for Preparing Resolving Gels for Tris-glycine SDS-Polyacrylamide Gel Electrophoresis

Solution components	Component volumes (ml) per gel mold volume of							
	5 ml	10 ml	15 ml	20 ml	25 ml	30 ml	40 ml	50 ml
6%								
H_2O	2.6	5.3	7.9	10.6	13.2	15.9	21.2	26.5
30% acrylamide mix	1.0	2.0	3.0	4.0	5.0	6.0	8.0	10.0
1.5 M Tris (pH 8.8)	1.3	2.5	3.8	5.0	6.3	7.5	10.0	12.5
10% SDS	0.05	0.1	0.15	0.2	0.25	0.3	0.4	0.5
10% ammonium persulfate	0.05	0.1	0.15	0.2	0.25	0.3	0.4	0.5
TEMED	0.004	0.008	0.012	0.016	0.02	0.024	0.032	0.04
8%								
H_2O	2.3	4.6	6.9	9.3	11.5	13.9	18.5	23.2
30% acrylamide mix	1.3	2.7	4.0	5.3	6.7	8.0	10.7	13.3
1.5 M Tris (pH 8.8)	1.3	2.5	3.8	5.0	6.3	7.5	10.0	12.5
10% SDS	0.05	0.1	0.15	0.2	0.25	0.3	0.4	0.5
10% ammonium persulfate	0.05	0.1	0.15	0.2	0.25	0.3	0.4	0.5
TEMED	0.003	0.006	0.009	0.012	0.015	0.018	0.024	0.03
10%								
H_2O	1.9	4.0	5.9	7.9	9.9	11.9	15.9	19.8
30% acrylamide mix	1.7	3.3	5.0	6.7	8.3	10.0	13.3	16.7
1.5 M Tris (pH 8.8)	1.3	2.5	3.8	5.0	6.3	7.5	10.0	12.5
10% SDS	0.05	0.1	0.15	0.2	0.25	0.3	0.4	0.5
10% ammonium persulfate	0.05	0.1	0.15	0.2	0.25	0.3	0.4	0.5
TEMED	0.002	0.004	0.006	0.008	0.01	0.012	0.016	0.02
12%								
H_2O	1.6	3.3	4.9	6.6	8.2	9.9	13.2	16.5
30% acrylamide mix	2.0	4.0	6.0	8.0	10.0	12.0	16.0	20.0
1.5 M Tris (pH 8.8)	1.3	2.5	3.8	5.0	6.3	7.5	10.0	12.5
10% SDS	0.05	0.1	0.15	0.2	0.25	0.3	0.4	0.5
10% ammonium persulfate	0.05	0.1	0.15	0.2	0.25	0.3	0.4	0.5
TEMED	0.002	0.004	0.006	0.008	0.01	0.012	0.016	0.02
15%								
H_2O	1.1	2.3	3.4	4.6	5.7	6.9	9.2	11.5
30% acrylamide mix	2.5	5.0	7.5	10.0	12.5	15.0	20.0	25.0
1.5 M Tris (pH 8.8)	1.3	2.5	3.8	5.0	6.3	7.5	10.0	12.5
10% SDS	0.05	0.1	0.15	0.2	0.25	0.3	0.4	0.5
10% ammonium persulfate	0.05	0.1	0.15	0.2	0.25	0.3	0.4	0.5
TEMED	0.002	0.004	0.006	0.008	0.01	0.012	0.016	0.02

TABLE 18.4 Solutions for Preparing 5% Stacking Gels for Tris-glycine SDS-Polyacrylamide Gel Electrophoresis

Solution components	Component volumes (ml) per gel mold volume of							
	1 ml	2 ml	3 ml	4 ml	5 ml	6 ml	8 ml	10 ml
H_2O	0.68	1.4	2.1	2.7	3.4	4.1	5.5	6.8
30% acrylamide mix	0.17	0.33	0.5	0.67	0.83	1.0	1.3	1.7
1.0 M Tris (pH 6.8)	0.13	0.25	0.38	0.5	0.63	0.75	1.0	1.25
10% SDS	0.01	0.02	0.03	0.04	0.05	0.06	0.08	0.1
10% ammonium persulfate	0.01	0.02	0.03	0.04	0.05	0.06	0.08	0.1
TEMED	0.001	0.002	0.003	0.004	0.005	0.006	0.008	0.01

Tables 18.3 and 18.4 are modified from Harlow and Lane (1988).

Appendix B: Mouse Strains

Strain	Common name	Vendor	Gender
NCr-nu/nu, strain 01B74	Athymic nude	NIH Animal Procurement Program	female
NOD.CB17-*Prkdcscid*/ NCrHsd	NOD.SCID	Harlan	female
FVB/N-Tg(MMTVneu)202Mul/J	MMTV-Her2/neu	Jackson Laboratories	female

Appendix C: IHC Antibodies, Chapter 3

Primary antibody	Manufacturer	Working concentration
Cleaved caspase 3	Cell Signaling	1:180
Doublecortin	Abcam	1:500
GFAP	Dako	1:5000
Iba1	Abcam	1:800
Ki67	Abcam	1:200

Appendix D: IHC Antibodies, Chapter 4

Primary antibody	Manufacturer	Species derivation	Clonality	Working concentration
ALDH1A1	Abcam	Rabbit	mono	1:200
Neu	Santa Cruz	Rabbit	poly	1:500
Notch1	Cell Signaling	Rabbit	mono	1:400

Appendix E: Cleaved Caspase 3 Quantitative Algorithm

Algorithm	Positive Pixel Count v9
*** Algorithm Inputs ***	*** Algorithm Inputs ***
Version	9.1
View Width	1000
View Height	1000
Overlap Size	0
Image Zoom	1.
Classifier	None
Class List	
Classifier Neighborhood	0
Pixel Area (millimeter-squared)	5.9536e-008
Hue Value (Center)	0.1
Hue Width	0.5
Color Saturation Threshold	4.e-002
Intensity Threshold WEAK (Upper Limit)	200
Intensity Threshold WEAK (Lower Limit)	150
Intensity Threshold MEDIUM (Upper Limit)	150
Intensity Threshold MEDIUM (Lower Limit)	200
Intensity Threshold STRONG (Upper Limit)	200
Intensity Threshold STRONG (Lower Limit)	0
Intensity Threshold Negative Pixels	-1

Appendix F: Ki67 Quantitative Algorithm

Algorithm	Nuclear v9.1
*** Algorithm Inputs ***	*** Algorithm Inputs ***
View Width	1000
View Height	1000
Overlap Size	100
Image Zoom	1.
Classifier	None
Class List	
Classifier Neighborhood	0
Pixel Size (µm)	0.244
Averaging Radius (µm)	1.
Averaging Radius (Pixels)	4
Curvature Threshold	2.5
Segmentation Type	2
Threshold Type	1
Lower Intensity Threshold	0
Upper Intensity Threshold	230
Min Nuclear Size (µm^2)	20.
Min Nuclear Size (Pixels)	336
Max Nuclear Size (µm^2)	1.e+006
Max Nuclear Size (Pixels)	1.67966e+007
Min Roundness	0.1
Min Compactness	0.
Min Elongation	0.1
Remove Light Objects	0.
Weak(1+) Threshold	210
Moderate(2+) Threshold	188
Strong(3+) Threshold	162
Black Threshold	0
Edge Trim	Weighted
Markup Image Type	Analysis
Nuclear Red OD	0.696858
Nuclear Green OD	0.643073
Nuclear Blue OD	0.317563
Positive Red OD	0.244583
Positive Green OD	0.509334
Positive Blue OD	0.825081
Color(3) Red OD	0.
Color(3) Green OD	0.
Color(3) Blue OD	0.
Clear Area Intensity	240
Classifier Type	IHCNuclear

Appendix G: Doublecortin Quantitative Algorithm

*** Algorithm Inputs ***	*** Algorithm Inputs ***
Algorithm	Positive Pixel Count v9
Version	9.1
View Width	1000
View Height	1000
Overlap Size	0
Image Zoom	1
Classifier	None
Class List	
Classifier Neighborhood	0
Pixel Area (millimeter-squared)	5.95E-08
Hue Value (Center)	0.1
Hue Width	0.5
Color Saturation Threshold	4.00E-02
Intensity Threshold WEAK (Upper Limit)	180
Intensity Threshold WEAK (Lower Limit)	137
Intensity Threshold MEDIUM (Upper Limit)	137
Intensity Threshold MEDIUM (Lower Limit)	123
Intensity Threshold STRONG (Upper Limit)	123
Intensity Threshold STRONG (Lower Limit)	0
Intensity Threshold Negative Pixels	-1

Appendix H: PCR Primers

Gene	Species	Forward sequence	Reverse sequence
GAPDH	Mouse	CATGGCCTTCCGTGTTCCTA	GCGGCACGTCAGATCCA
Pin1[a]	Mouse	ACAGTTCAGTGATTGCAG	TCCGTAGAGCAAACGACG
Neu[b]	Rat	CGGAACCCACATCAGGCC	TTTCCTGCAGCAGCCTACGC
Notch1[c]	Mouse	CTGACGCCCTTGCTCTGCCTAA	AGTGCCACCATGGTCCACAACG

[a]Kap YS et al. *Neurogenetics* September 2006 vol. 8 no. 1 21-27.
[b]Siegel PM et al. *Mol. Cell. Biol.* November 1994 vol. 14 no. 11 7068-7077.
[c]Somekawa S et al. *PNAS* July 2012 vol. 109 no. 30 12064–12069.

References

Chapter 1

1. Dieci, M. V., E. Orvieto, M. Dominici, P. Conte and V. Guarneri (2014). "Rare breast cancer subtypes: histological, molecular, and clinical peculiarities." Oncologist **19**(8): 805-813.

2. Saunus JM, et al. “Chapter 5: Breast cancer heterogeneity in primary and metastatic disease” in *Breast cancer metastasis and drug resistance: Progress and prospects*. Ahmad, A, ed. (2013). New York, NY: Springer.

3. Swart R, et al. (2015). “Breast cancer histology.” Accessed 12 April 2016. Web http://emedicine.medscape.com/article/1954658-overview

4. Burstein, M. D., A. Tsimelzon, G. M. Poage, K. R. Covington, A. Contreras, S. A. Fuqua, M. I. Savage, C. K. Osborne, S. G. Hilsenbeck, J. C. Chang, G. B. Mills, C. C. Lau and P. H. Brown (2015). "Comprehensive genomic analysis identifies novel subtypes and targets of triple-negative breast cancer." Clin Cancer Res **21**(7): 1688-1698.

5. Weigelt, B., L. Pusztai, A. Ashworth and J. S. Reis-Filho (2012). "Challenges translating breast cancer gene signatures into the clinic." Nat Rev Clin Oncol **9**(1): 58-64.

6. Kittaneh, M., A. J. Montero and S. Gluck (2013). "Molecular profiling for breast cancer: a comprehensive review." Biomark Cancer **5**: 61-70.

7. Lam, S. W., C. R. Jimenez and E. Boven (2014). "Breast cancer classification by proteomic technologies: current state of knowledge." Cancer Treat Rev **40**(1): 129-138.

8. Piva, R., D. A. Spandidos and R. Gambari (2013). "From microRNA functions to microRNA therapeutics: novel targets and novel drugs in breast cancer research and treatment (Review)." Int J Oncol **43**(4): 985-994.

9. DeSantis, C., J. Ma, L. Bryan and A. Jemal (2014). "Breast cancer statistics, 2013." CA Cancer J Clin **64**(1): 52-62.

10. Jonkers, J. and P. W. Derksen (2007). "Modeling metastatic breast cancer in mice." J Mammary Gland Biol Neoplasia **12**(2-3): 191-203.

11. Burstein, H. J., S. Temin, H. Anderson, T. A. Buchholz, N. E. Davidson, K. E. Gelmon, S. H. Giordano, C. A. Hudis, D. Rowden, A. J. Solky, V. Stearns, E. P. Winer and J. J. Griggs (2014). "Adjuvant endocrine therapy for women with hormone receptor-positive breast cancer: american society of clinical oncology clinical practice guideline focused update." J Clin Oncol **32**(21): 2255-2269.

12. Nelson HD, et al. (2013) Use of medications to reduce risk for primary breast cancer: a systematic review for the U.S. Preventive Services Task Force. Ann Intern Med **158**:604-614.

13. Rasotto, R., D. Caliari, M. Castagnaro, R. Zanetti and V. Zappulli (2011). "An Immunohistochemical study of HER-2 expression in feline mammary tumours." J Comp Pathol **144**(2-3): 170-179.

14. Peña, L., A. Gama, M. H. Goldschmidt, J. Abadie, C. Benazzi, M. Castagnaro, L. Diez, F. Gartner, E. Hellmen, M. Kiupel, Y. Millan, M. A. Miller, F. Nguyen, A. Poli, G. Sarli, V. Zappulli and J. M. de las Mulas (2014). "Canine mammary tumors: a review and consensus of standard guidelines on epithelial and myoepithelial phenotype markers, HER2, and hormone receptor assessment using immunohistochemistry." Vet Pathol **51**(1): 127-145.

15. Li, S. G. and L. Li (2013). "Targeted therapy in HER2-positive breast cancer." Biomed Rep **1**(4): 499-505.

16. Griffiths, C. L. and J. L. Olin (2012). "Triple negative breast cancer: a brief review of its characteristics and treatment options." J Pharm Pract **25**(3): 319-323.

17. Sikov, W. M., D. A. Berry, C. M. Perou, B. Singh, C. T. Cirrincione, S. M. Tolaney, C. S. Kuzma, T. J. Pluard, G. Somlo, E. R. Port, M. Golshan, J. R. Bellon, D. Collyar, O. M. Hahn, L. A. Carey, C. A. Hudis and E. P. Winer (2015). "Impact of the addition of carboplatin and/or bevacizumab to neoadjuvant once-per-week paclitaxel followed by dose-dense doxorubicin and cyclophosphamide on pathologic complete response rates in stage II to III triple-negative breast cancer: CALGB 40603 (Alliance)." J Clin Oncol **33**(1): 13-21.

18. Goldschmidt, M., L. Pena, R. Rasotto and V. Zappulli (2011). "Classification and grading of canine mammary tumors." Vet Pathol **48**(1): 117-131.

19. Liu, D., H. Xiong, A. E. Ellis, N. C. Northrup, C. O. Rodriguez, Jr., R. M. O'Regan, S. Dalton and S. Zhao (2014). "Molecular homology and difference between spontaneous canine mammary cancer and human breast cancer." Cancer Res **74**(18): 5045-5056.

20. Seixas, F., C. Palmeira, M. A. Pires, M. J. Bento and C. Lopes (2011). "Grade is an independent prognostic factor for feline mammary carcinomas: a clinicopathological and survival analysis." Vet J **187**(1): 65-71.

21. Zappulli, V., R. Rasotto, D. Caliari, M. Mainenti, L. Pena, M. H. Goldschmidt and M. Kiupel (2015). "Prognostic evaluation of feline mammary carcinomas: a review of the literature." Vet Pathol **52**(1): 46-60.

22. Wiese DA et al. (2013) Feline mammary basal-like adenocarcinomas: a potential model for human triple-negative breast cancer (TNBC) with basal-like subtype. BMC Cancer **13**:403.

23. Hughes, K. and J. M. Dobson (2012). "Prognostic histopathological and molecular markers in feline mammary neoplasia." Vet J **194**(1): 19-26.

24. Soares, M., J. Correia, P. Rodrigues, M. Simoes, A. de Matos and F. Ferreira (2013). "Feline HER2 protein expression levels and gene status in feline mammary carcinoma: optimization of immunohistochemistry (IHC) and *in situ* hybridization (ISH) techniques." Microsc Microanal **19**(4): 876-882.

25. Klonisch, T., E. Wiechec, S. Hombach-Klonisch, S. R. Ande, S. Wesselborg, K. Schulze-Osthoff and M. Los (2008). "Cancer stem cell markers in common cancers - therapeutic implications." Trends Mol Med **14**(10): 450-460.

Chapter 2

26. Domercq M, Matute C. Neuroprotection by tetracyclines. *Trends Pharmacol Sci* 2004;25(12): 609-612.

27. Kim HS, Suh YH. Minocycline and neurodegenerative diseases. *Behav Brain Res* 2009;196(2):168-179.

28. Plane JM, Shen Y, Pleasure DE, Deng W. Prospects for minocycline neuroprotection. *Arch Neurol* 2010;67(12):1442-1448.

29. Garrido-Mesa N, Zarzuelo A, Galvez J. Minocycline: far beyond an antibiotic. *Br J Pharmacol*, 2013;169(2):337-352.

30. Yrjänheikki J, Keinänen R, Pellikka M, Hökfelt T, Koistinaho J. Tetracyclines inhibit microglial activation and are neuroprotective in global brain ischemia. *PNAS* 1998;95:15769-15774.

31. Popovic N, Schubart A, Goetz BD, Zhang SC, Linington C, Duncan ID. Inhibition of autoimmune encephalomyelitis by a tetracycline. *Ann Neurol* 2002;51(2):215-223.

32. Wang J, Wei Q, Wang CY, Hill WD, Hess DC, Dong Z. Minocycline up-regulates Bcl-2 and protects against cell death in mitochondria. *J Biol Chem* 2004;279(19):19948-19954.

33. Switzer JA, Hess DC, Ergul A, Waller JL, Machado LS, Portik-Dobos V, et al. Matrix metalloproteinase-9 in an exploratory trial of intravenous minocycline for acute ischemic stroke. *Stroke* 2011;42(9):2633-2635.

34. Won SJ, Kim JH, Yoo BY, Sohn M, Kauppinen TM, Park M-S, et al. Prevention of hypoglycemia-induced neuronal death by minocycline. *J Neuroinflammation* 2012;9:225.

35. Lee C-K, Shin J-I, Cho Y-S. Protective effect of minocycline against cisplatin-induced ototoxicity. *Clin Exp Otorhinolaryngol* 2011;4(2):77-82.

36. Du Y, Ma Z, Lin S, Dodel RC, Gao F, Bales KR, et al. Minocycline prevents nigrostriatal dopaminergic neurodegeneration in the MPTP model of Parkinson's disease. *PNAS* 2001;98(25):14669-14674.

37. Casha S, Zygun D, McGowan MD, Bains I, Yong VW, Hurlbert RJ. Results of a phase II placebo-controlled randomized trial of minocycline in acute spinal cord injury. *Brain* 2012;135:1224-1236.

38. Christie LA, Acharya MM, Parihar VK, Nguyen A, Martirosian V, Limoli CL. Impaired cognitive function and hippocampal neurogenesis following cancer chemotherapy. *Clin Cancer Res* 2012;18(7):1954-1965.

39. Winocur G, Henkelman M, Wojtowicz JM, Zhang H, Binns MA, Tannock IF. The effects of chemotherapy on cognitive function in a mouse model: a prospective study. *Clin Cancer Res* 2012;18(11):3112-3121.

40. Johnston IN. Chemotherapy-induced cognitive deficits, white matter pathologies and cytokines. *Brain Behav Immun* 2014;35:21-22.

41. Seigers R, Fardell JE. Neurobiological basis of chemotherapy-induced cognitive impairment: a review of rodent research. *Neurosci Biobehav Rev* 2011;35(3):729-741.

42. Raffa RB. A proposed mechanism for chemotherapy-related cognitive impairment ('chemo-fog'). *J Clin Pharm Ther* 2011;36(3):257-259.

43. Cheng H, Yang Z, Dong B, Chen C, Zhang M, Huang Z, et al. Chemotherapy-induced prospective memory impairment in patients with breast cancer. *Psycho-Oncology* 2013. Epub DOI: 10.1002/pon.3291

44. Gandal MJ, Ehrlichman RS, Rudnick ND, Siegel SJ. A novel electrophysiological model of chemotherapy-induced cognitive impairments in mice. *Neuroscience* 2008;157(1):95-104.

45. Jim HS, Phillips KM, Chait S, Faul LA, Popa MA, Lee YH, et al. Meta-analysis of cognitive functioning in breast cancer survivors previously treated with standard-dose chemotherapy. *J Clin Oncol*, 2012;30(29):3578-3587.

46. Foulkes WD, Smith IE, Reis-Filho JS. Current concepts: triple-negative breast cancer. *N Eng J Med* 2010;363(20):1938-1948.

47. Holliday DL, Speirs V. Choosing the right cell line for breast cancer research. *Breast Cancer Res* 2011;13: 215.

48. Chuang, H. C., N. Kapuriya, S. K. Kulp, C. S. Chen and C. L. Shapiro (2012). "Differential anti-proliferative activities of poly(ADP-ribose) polymerase (PARP) inhibitors in triple-negative breast cancer cells." Breast Cancer Res Treat **134**(2): 649-659.

49. O'Toole SA, Beith JM, Millar EK, West R, McLean A, Cazet A, et al. Therapeutic targets in triple negative breast cancer. *J Clin Pathol* 2013;66(6):530-542.

50. Block KI, Koch AC, Mead MN, Tothy PK, Newman RA, Gyllenhaal C. Impact of antioxidant supplementation on chemotherapeutic toxicity: a systematic review of the evidence from randomized controlled trials. *Int J Cancer* 2008;123(6):1227-1239.

51. Simone CB, Simone NL, Simone V, Simone CB. Antioxidants and other nutrients do not interfere with chemotherapy or radiation therapy and can increase kill and increase survival, part 2. *Altern Ther Health Med* 2007;13(2):40-47.

52. Lawenda BD, Kelly KM, Ladas EJ, Sagar SM, Vickers A, Blumberg JB. Should supplemental antioxidant administration be avoided during chemotherapy and radiation therapy? *J Natl Cancer Inst* 2008;100(11):733-783.

53. Yasueda A, Urushima H, Ito T. Efficacy and interaction of antioxidant supplements as adjuvant therapy in cancer treatment: A systematic review. *Integr Cancer Ther* 2016;15(1):17-39.

54. Konat GW, Kraszpulski M, James I, Zhang HT, Abraham J. Cognitive dysfunction induced by chronic administration of common cancer chemotherapeutics in rats. *Metab Brain Dis* 2008;23(3):325-333.

55. Pourgholami MH, Mekkawy AH, Badar S, Morris DL. Minocycline inhibits growth of epithelial ovarian cancer. *Gynecol Oncol* 2012;125(2):433-440.

56. Parangi S, O'Reilly M, Christofori G, Holmgren L, Grosfeld J, Golkman J, et al. Antiangiogenic therapy of transgenic mice impairs *de novo* tumor growth. *PNAS* 1996;93:2002-2007.

57. Haber M, et. Al. (2013) Minocycline plus N-acetylcysteine synergize to modulate inflammation and prevent cognitive and memory deficits in a rat model of mild traumatic brain injury. Experimental Neurology **249**:169-177.

58. Cai Z, Yan Y, Wang Y. (2013) Minocycline alleviates beta-amyloid protein and tau pathology via restraining neuroinflammation induced by diabetic metabolic disorder. Clinical Interventions in Aging **8**:1089-1095.

59. Tikka TM and Koistinaho JE. (2001) Minocycline provides neuroprotection against *N*-Methyl-d-aspartate neurotoxicity by inhibiting microglia. J Immunol **166**:7527-7533.

60. Mizumatsu S et al. 2003 Extreme sensitivity of adult neurogenesis to low doses of x-irradiation Cancer Res 63:4021-4027

61. Dumont, E. A., S. P. Lutgens, C. P. Reutelingsperger, G. M. Bos and L. Hofstra (2010). "Minocycline inhibits apoptotic cell death in a murine model of partial flap loss." J Reconstr Microsurg **26**(8): 523-528.

62. van Dam FSAM, Schagen SB, Muller MJ, Boogerd W, vd Wall E, Droogleever Fortuyn ME, et al. Impairment of cognitive function in women receiving adjuvant treatment for high-risk breast cancer: high-dose versus standard-dose therapy. *J Natl Cancer Inst* 1998;90(3):210-218.

63. Villanueva MT. (2012) Breast cancer: chemo fog becomes clearer. Nat Rev Clin Oncol **9**(11):609.

64. Germain E, et al. (1998) Enhancement of doxorubicin cytotoxicity by polyunsaturated fatty acids in the human breast tumor cell line MDA-MB-231: relationship to lipid peroxidation. Int J Cancer **75**:578-583.

65. Greenlee, H., D. L. Hershman and J. S. Jacobson (2009). "Use of antioxidant supplements during breast cancer treatment: a comprehensive review." Breast Cancer Res Treat **115**(3): 437-452.

66. Simões-Wüst AP, et al. (2002). Bcl-2/bcl-xL bispecific antisense treatment sensitizes breast cancer cells to doxorubicin, paclitaxel, and cyclophosphamide. Breast Cancer Res Treat **76**: 157-166.

67. Vardy J, Rourke S, Tannock IF. (2007) Evaluation of cognitive function associated with chemotherapy: a review of published studies and recommendations for future research. J Clin Oncol **25**:2455-2463.

68. Monje M, Dietrich J. Cognitive side effects of cancer therapy demonstrate a functional role for adult neurogenesis. *Behav Brain Res* 2012;227(2):376-379.

69. Craig CD, et al. (2014) Cognitive impairment in gynecologic cancers: a systematic review of current approaches to diagnosis and treatment. Supportive Care in Cancer **22**(1):279-287.

70. Evenden J. 2013 Cognitive impairments and cancer chemotherapy: translational research at a crossroads. Life Sciences 93: 589-595.

71. Reuter-Lorenz PA, Cimprich B. Cognitive function and breast cancer: promise and potential insights from functional brain imaging. *Breast Cancer Res Treat* 2013;137(1):33-43.

72. Collins B, et al. (2014) Persistent cognitive changes in breast cancer patients 1 year following completion of chemotherapy. J Int Neuropsychol Soc **20**(4):370-379.

73. Shilling V, Jenkins V, Trapala IS. The (mis)classification of chemo-fog--methodological inconsistencies in the investigation of cognitive impairment after chemotherapy. *Breast Cancer Res Treat* 2006;95(2):125-129.

74. Schagen SB, Muller MJ, Boogerd W, Mellenbergh GJ, van Dam FS. Change in cognitive function after chemotherapy: a prospective longitudinal study in breast cancer patients. *J Natl Cancer Inst* 2006;98(23):1742-1745.

75. Ahles TA, Saykin AJ. Candidate mechanisms for chemotherapy-induced cognitive changes. *Nat Rev Cancer* 2007;7(3):192-201.

76. Pomykala KL, Ganz PA, Bower JE, Kwan L, Castellon SA, Mallam S, et al. The association between pro-inflammatory cytokines, regional cerebral metabolism, and cognitive complaints following adjuvant therapy for breast cancer. *Brain Imaging Behav* 2013;7:511-523.

77. Andreotti C, Root JC, Schagen SB, McDonald BC, Saykin AJ, Atkinson TM, et al. Reliable change in neuropsychological assessment of breast cancer survivors. *Psycho-Oncology* 2016;25(1):43-50.

78. Bruno, J., S. M. Hosseini and S. Kesler (2012). "Altered resting state functional brain network topology in chemotherapy-treated breast cancer survivors." Neurobiol Dis **48**(3): 329-338.

79. O'Shaughnessy J. (2003). Chemotherapy-related cognitive dysfunction in breast cancer. Seminars in Oncology Nursing **19**(4): S2, 17-24

80. Kaiser J, Dietrich J. Challenges in research on the neural basis of chemobrain. *Transl Neurosci* 2014;5(3):222-225.

81. Piccolini VM et al 2013 Platinum drugs and neurotoxicity: effects on intracellular calcium homeostasis. Cell Biol Toxicol 29:339-353

82. Yang M, Kim JS, Song MS, Kim SH, Kang SS, Bae CS, et al. Cyclophosphamide impairs hippocampus-dependent learning and memory in adult mice: Possible involvement of hippocampal neurogenesis in chemotherapy-induced memory deficits. *Neurobiol Learn Mem* 2010;93(4):487-494.

83. Kim J-S, Lee H-J, Kim JC, Kang SS, Bae C-S, Shin T, et al. Transient Impairment of Hippocampus-dependent Learning and Memory in Relatively Low-Dose of Acute Radiation Syndrome is Associated with Inhibition of Hippocampal Neurogenesis. *J Radiat Res* 2008;49(5):517-526.

84. Mandelblatt JS, et al. (2014) Cognitive impairment in older patients with breast cancer before systemic therapy: is there an interaction between cancer and comorbidity? J Clin Oncol **32**(18):1909-1918

85. Sambrook J, Fritsch EF, Maniatis T. Molecular Cloning: a Laboratory Manual, 2nd ed. Vol. 3. Cold Spring Harbor Laboratory Press. 1989.

86. Crissman JW, Goodman DG, Hildebrandt PK, Maronpot RR, Prater DA, Riley JH, et al. Best Practices Guideline: Toxicologic Histopathology. *Toxicol Pathol* 2004;32(1):126-131.

87. Bolon B, Garman RH, Pardo ID, Jensen K, Sills RC, Roulois A, et al. STP position paper: Recommended practices for sampling and processing the nervous system (brain, spinal cord, nerve, and eye) during nonclinical general toxicity studies. *Toxicol Pathol* 2013;41(7):1028-1048.

88. Agwuh KN, MacGowan A. Pharmacokinetics and pharmacodynamics of the tetracyclines including glycylcyclines. *J Antimicrob Chemother* 2006;58:256-265.

89. Araujo MVF, Ifa DR, Ribeiro W, Moraes ME, Moraes MO, de Nucci G. Determination of minocycline in human plasma by high-performance liquid chromatography coupled to tandem mass spectrometry: application to bioequivalence study. *J Chromatogr B* 2001;755:1-7.

90. Setiawati E, Purnomo A, Deniati SH, Yunaidi DA, Handayani LR, Harinato G, et al. Bioequivalence study of two minocycline capsule formulations in healthy volunteers. *Arzneimittelforschung* 2009;59(10):532-536.

91. Abramowicz M (editor). Extended-release minocycline (Solodyn) for acne. *Med Letter Drugs Ther* 2006;48(1248):95-96.

92. Gupta AK, Gover MD, Abramovits W, Perlmutter A. Solodyn (Minocycline HCl, USP) extended release tablets. *SKINmed* 2006;5:291-292.

93. Gewirtz DA. A critical evaluation of the mechanisms of action proposed for the antitumor effects of the anthracycline antibiotics adriamycin and daunorubicin. *Biochem Pharmacol* 1999;57:727-741.

94. Engel D, Peshock R, Armstrong RC, Sivasubramanian N, Mann DL. Cardiac myocyte apoptosis provokes adverse cardiac remodeling in transgenic mice with targeted TNF overexpression. *Am J Physiol Heart Circ Physiol* 2004;287:H1303-H1311.

95. Franci C, Zhou J, Jiang Z, Modrusan Z, Good Z, Jackson E, et al. Biomarkers of residual disease, disseminated tumor cells, and metastases in the MMTV-PyMT breast cancer model. *PLoS One* 2013;8(3):e58183.

96. Dubois M, Lapinte N, Villier V, Lecointre C, Roy V, Tonon M-C, et al. Chemotherapy-induced long-term alteration of executive functions and hippocampal cell proliferation: role of glucose as adjuvant. *Neuropharmacology* 2014;79:234-248.

97. Zhao C, Teng EM, Summers Jr RG, Ming G-L, Gage FH. Distinct morphological stages of dentate granule neuron maturation in the adult mouse hippocampus. *J Neurosci* 2006;26(1):3-11.

98. Acharya MM, Martirosian V, Chmielewski NN, Hanna N, Tran KK, Liao AC, et al. Stem cell transplantation reverses chemotherapy-induced cognitive dysfunction. *Cancer Res* 2015;75(4):676-686.

99. Borniger JC, Gaudier-Diaz MM, Zhang N, Nelson RJ, DeVries AC. Cytotoxic chemotherapy increases sleep and sleep fragmentation in non-tumor-bearing mice. *Brain, Behavior, and Immunity* 2015;47:218-227.

100. Churchill NW, Cimprich B, Askren MK, Reuter-Lorenz PA, Jung MS, Peltier S, et al. Scale-free brain dynamics under physical and psychological distress: pre-treatment effects in women diagnosed with breast cancer. *Hum Brain Mapp* 2015;36:1077-1092.

101. Bernstein LJ, Catton PA, Tannock IF. Intra-individual variability in women with breast cancer. *J Int Neuropsychol Soc* 2014;20:380-390.

102. Sleight A. Coping with cancer-related cognitive dysfunction: a scoping review of the literature. *Disabil Rehabil* 2016;38(4):400-408.

103. Fallowfield L, Jenkins V. Psychosocial/survivorship issues in breast cancer: are we doing better? *J Natl Cancer Inst* 2015;107(1):dju335.

Chapter 3

104. Al-Hajj, M., et al. (2003). "Prospective identification of tumorigenic breast cancer cells." PNAS **100**(7): 3983-3988.

105. Cheng, L., et al. (2010). "Mouse models for cancer stem cell research." Toxicol Pathol **38**(1): 62-71.

106. Clevers, H. (2011). "The cancer stem cell: premises, promises and challenges." Nat Med **17**(3): 313-319.

107. Takebe, N., et al. (2011). "Targeting cancer stem cells by inhibiting Wnt, Notch, and Hedgehog pathways." Nat Rev Clin Oncol **8**(2): 97-106.

108. Scheel, C. and R. A. Weinberg (2012). "Cancer stem cells and epithelial-mesenchymal transition: concepts and molecular links." Semin Cancer Biol **22**(5-6): 396-403.

109. Nigam, A. (2013). "Breast cancer stem cells, pathways, and therapeutic perspectives 2011." Indian J Surg **75**(3): 170-180.

110. Li, X., et al. (2008). "Intrinsic resistance of tumorigenic breast cancer cells to chemotherapy." J Natl Cancer Inst **100**(9): 672-679.

111. Tanei, T., et al. (2009). "Association of breast cancer stem cells identified by aldehyde dehydrogenase 1 expression with resistance to sequential Paclitaxel and epirubicin-based chemotherapy for breast cancers." Clin Cancer Res **15**(12): 4234-4241.

112. Alison, M. R., et al. (2010). "Finding cancer stem cells: are aldehyde dehydrogenases fit for purpose?" J Pathol **222**(4): 335-344.

113. Gong, C., et al. (2010). "Markers of tumor-initiating cells predict chemoresistance in breast cancer." PLoS One **5**(12): e15630.

114. Lo, P. K., et al. (2012). "CD49f and CD61 identify Her2/neu-induced mammary tumor-initiating cells that are potentially derived from luminal progenitors and maintained by the integrin-TGFbeta signaling." Oncogene **31**(21): 2614-2626

115. Chen, D., et al. (2013). "ANTXR1, a stem cell-enriched functional biomarker, connects collagen signaling to cancer stem-like cells and metastasis in breast cancer." Cancer Res **73**(18): 5821-5833.

116. Ropero, S. and M. Esteller (2007). "The role of histone deacetylases (HDACs) in human cancer." Mol Oncol **1**(1): 19-25.

117. Atadja, P. W. (2010). HDAC Inhibitors and Cancer Therapy. In *Epigenetics and Disease: Pharmaceutical Opportunities* (pp. 175-195). Basel: Springer.

118. West, A. C. and R. W. Johnstone (2014). "New and emerging HDAC inhibitors for cancer treatment." J Clin Invest **124**(1): 30-39.

119. Owens, T. W. and M. J. Naylor (2013). "Breast cancer stem cells." Front Physiol **4**: 225.

120. Furth, J., et al. (1937). "The transmission of leukemia of mice with a single cell." Cancer Res **31**: 276-282.

121. Pierce, G. B. and W. C. Speers (1988). "Tumors as caricatures of the process of tissue renewal: prospects for therapy by directing differentiation." Cancer Res **48**: 1996-2004.

122. Bonnet, D. and J. E. Dick (1997). "Human acute myeloid leukemia is organized as a hierarchy that originates from a primitive hematopoietic cell." Nature Medicine **3**(7): 730-737.

123. Cicalese, A., et al. (2009). "The tumor suppressor p53 regulates polarity of self-renewing divisions in mammary stem cells." Cell **138**(6): 1083-1095.

124. Hallett, R. M., et al. (2012). "Small molecule antagonists of the Wnt/beta-catenin signaling pathway target breast tumor-initiating cells in a Her2/Neu mouse model of breast cancer." PLoS One **7**(3): e33976.

125. Lo, P. K. and H. Chen (2013). "Cancer stem cells and cells of origin in MMTV-Her2/neu-induced mammary tumorigenesis." Oncogene **32**(10): 1338-1340.

126. Dou, J., & Gu, N. (2012). Biomarkers of Cancer Stem Cells. In *Advances in Cancer Stem Cell Biology* (pp. 45-67). New York: Springer.

127. Singh, A. and J. Settleman (2010). "EMT, cancer stem cells and drug resistance: an emerging axis of evil in the war on cancer." Oncogene **29**(34): 4741-4751.

128. Fessler, E., F. E. Dijkgraaf, E. M. F. De Sousa and J. P. Medema (2013). "Cancer stem cell dynamics in tumor progression and metastasis: is the microenvironment to blame?" Cancer Lett **341**(1): 97-104.

129. Ponti D et al. (2005) Isolation and *in vitro* propagation of tumorigenic breast cancer cells with stem/progenitor properties. Cancer Res **65**(13):5506-5511.

130. Izrailit, J. and M. Reedijk (2012). "Developmental pathways in breast cancer and breast tumor-initiating cells: therapeutic implications." Cancer Lett **317**(2): 115-126.

131. Farnie, G., et al. (2007). "Novel cell culture technique for primary ductal carcinoma *in situ*: role of Notch and epidermal growth factor receptor signaling pathways." J Natl Cancer Inst **99**(8): 616-627.

132. Ginestier, C., et al. (2007). "ALDH1 is a marker of normal and malignant human mammary stem cells and a predictor of poor clinical outcome." Cell Stem Cell **1**(5): 555-567.

133. Jung, G. A., et al. (2008). "Valproic acid induces differentiation and inhibition of proliferation in neural progenitor cells via the beta-catenin-Ras-ERK-p21Cip/WAF1 pathway." BMC Cell Biol **9**: 66.

134. Korkaya, H., et al. (2008). "HER2 regulates the mammary stem/progenitor cell population driving tumorigenesis and invasion." Oncogene **27**(47): 6120-6130.

135. Schmalhofer, O., et al. (2009). "E-cadherin, beta-catenin, and ZEB1 in malignant progression of cancer." Cancer Metastasis Rev **28**(1-2): 151-166.

136. Lim, E., et al. (2010). "Transcriptome analyses of mouse and human mammary cell subpopulations reveal multiple conserved genes and pathways." Breast Cancer Res **12**(2): R21.

137. Kondratyev, M., et al. (2012). "Gamma-secretase inhibitors target tumor-initiating cells in a mouse model of ERBB2 breast cancer." Oncogene **31**(1): 93-103.

138. Chen, S., et al. (2011). "Histone deacetylase (HDAC) activity is critical for embryonic kidney gene expression, growth, and differentiation." J Biol Chem **286**(37): 32775-32789.

139. Fuino, L., et al. (2003). "Histone deacetylase inhibitor LAQ824 down-regulates Her-2 and sensitizes human breast cancer cells to trastuzumab, taxotere, gemcitabine, and epothilone B." Mol Cancer Ther **2**: 971-984.

140. Miller T. A., et al. (2003). "Histone deacetylase inhibitors." J Med Chem **46**(24): 5097-5116.

141. Sargeant, A. M., et al. (2008). "OSU-HDAC42, a histone deacetylase inhibitor, blocks prostate tumor progression in the transgenic adenocarcinoma of the mouse prostate model." Cancer Res **68**(10): 3999-4009.

142. Bush, M. L., et al. (2011). "AR-42, a novel histone deacetylase inhibitor, as a potential therapy for vestibular schwannomas and meningiomas." Neuro-Oncology **13**(9): 983-999.

143. Keller, K. and M. Jung (2014). "Histone Deacetylase (HDAC) Inhibitors in Recent Clinical Trials for Cancer Therapy." 227-255.

144. Bai, L. Y., et al. (2011). "Antitumor activity of a novel histone deacetylase inhibitor (S)-HDAC42 in oral squamous cell carcinoma." Oral Oncol **47**(12): 1127-1133.

145. Ravillah, D., et al. (2014). "Chemopreventive effects of an HDAC2-selective inhibitor on rat colon carcinogenesis and APCmin/+ mouse intestinal tumorigenesis." J Pharmacol Exp Ther **348**(1): 59-68.

146. Lee, H., et al. (2006). "Histone deacetylase 8 safeguards the human ever-shorter telomeres 1B (hEST1B) protein from ubiquitin-mediated degradation." Mol Cell Biol **26**(14): 5259-5269.

147. Khan, O. and N. B. La Thangue (2012). "HDAC inhibitors in cancer biology: emerging mechanisms and clinical applications." Immunol Cell Biol **90**(1): 85-94.

148. Bolden, J. E., M. J. Peart and R. W. Johnstone (2006). "Anticancer activities of histone deacetylase inhibitors." Nat Rev Drug Discov **5**(9): 769-784.

149. Barneda-Zahonero, B. and M. Parra (2012). "Histone deacetylases and cancer." Mol Oncol **6**(6): 579-589.

150. Witt, O., et al. (2009). "HDAC family: What are the cancer relevant targets?" Cancer Lett **277**(1): 8-21.

151. Kang, Y., H. Nian, P. Rajendran, E. Kim, W. M. Dashwood, J. T. Pinto, L. A. Boardman, S. N. Thibodeau, P. J. Limburg, C. V. Lohr, W. H. Bisson, D. E. Williams, E. Ho and R. H. Dashwood (2014). "HDAC8 and STAT3 repress BMF gene activity in colon cancer cells." Cell Death Dis **5**: e1476.

152. Chakrabarti, A., I. Oehme, O. Witt, G. Oliveira, W. Sippl, C. Romier, R. J. Pierce and M. Jung (2015). "HDAC8: a multifaceted target for therapeutic interventions." Trends Pharmacol Sci **36**(7): 481-492.

153. Vannini, A., C. Volpari, P. Gallinari, P. Jones, M. Mattu, A. Carfi, R. De Francesco, C. Steinkuhler and S. Di Marco (2007). "Substrate binding to histone deacetylases as

shown by the crystal structure of the HDAC8-substrate complex." EMBO Rep **8**(9): 879-884.

154. Salvador, M. A., et al. (2013). "The histone deacetylase inhibitor abexinostat induces cancer stem cells differentiation in breast cancer with low Xist expression." Clin Cancer Res **19**(23): 6520-6531.

155. Leder, A. and P. Leder (1975). "Butyric acid, a potent inducer of erythroid differentiation in cultured erythroleukemic cells." Cell **5**: 319-322.

156. Wang, S., et al. (2008). "Control of endothelial cell proliferation and migration by VEGF signaling to histone deacetylase 7." Proc Natl Acad Sci U S A **105**(22): 7738-7743.

157. Marks, P. A., et al. (2001). "Histone deacetylases and cancer: causes and therapies." Nature Reviews Cancer **1**: 194-202.

158. Kulp, S. K., et al. (2006). "Antitumor effects of a novel phenylbutyrate-based histone deacetylase inhibitor, (S)-HDAC-42, in prostate cancer." Clin Cancer Res **12**(17): 5199-5206.

159. Lu, Y. S., et al. (2007). "Efficacy of a novel histone deacetylase inhibitor in murine models of hepatocellular carcinoma." Hepatology **46**(4): 1119-1130.

160. Zimmerman, B., et al. (2011). "Efficacy of novel histone deacetylase inhibitor, AR-42, in a mouse model of, human T-lymphotropic virus type 1 adult T cell lymphoma." Leuk Res **35**(11): 1491-1497.

161. Lu, Q., et al. (2005). "Structure-based optimization of phenylbutyrate-derived histone deacetylase inhibitors." J Med Chem **48**(17): 5530-5535.

162. Chen, C. S., et al. (2007). "Histone deacetylase inhibitors sensitize prostate cancer cells to agents that produce DNA double-strand breaks by targeting Ku70 acetylation." Cancer Res **67**(11): 5318-5327.

163. Lucas, D. M., et al. (2010). "The novel deacetylase inhibitor AR-42 demonstrates pre-clinical activity in B-cell malignancies *in vitro* and *in vivo*." PLoS One **5**(6): e10941

164. Andersson, E. R., R. Sandberg and U. Lendahl (2011). "Notch signaling: simplicity in design, versatility in function." Development **138**(17): 3593-3612.

165. Pannuti, A., K. Foreman, P. Rizzo, C. Osipo, T. Golde, B. Osborne and L. Miele (2010). "Targeting Notch to target cancer stem cells." Clin Cancer Res **16**(12): 3141-3152.

166. Wang, K., Q. Zhang, D. Li, K. Ching, C. Zhang, X. Zheng, M. Ozeck, S. Shi, X. Li, H. Wang, P. Rejto, J. Christensen and P. Olson (2015). "PEST domain mutations in Notch receptors comprise an oncogenic driver segment in triple-negative breast cancer sensitive to a gamma-secretase inhibitor." Clin Cancer Res **21**(6): 1487-1496.

167. Gu, J. W., P. Rizzo, A. Pannuti, T. Golde, B. Osborne and L. Miele (2012). "Notch signals in the endothelium and cancer "stem-like" cells: opportunities for cancer therapy." Vasc Cell **4**: 7.

168. Chao M-W et al. (2015) Non-epigenetic function of HDAC8 in regulating breast cancer stem cells by maintaining Notch1 protein stability. Oncotarget 7(2) 1796-1807

169. Wolfson NA, Pitcairn CA, Fierke CA. HDAC8 substrates: Histones and beyond. Biopolymers. 2013; 99: 112-126.

170. Buggy JJ, Sideris ML, Mak P, Lorimer DD, McIntosh B, Clark JM. Cloning and characterization of a novel human histone deacetylase, HDAC8. Biochem J. 2000; 350 Pt 1: 199-205.

171. Hu E, Chen Z, Fredrickson T, Zhu Y, Kirkpatrick R, Zhang GF, Johanson K, Sung CM, Liu R, Winkler J. Cloning and characterization of a novel human class I histone deacetylase that functions as a transcription repressor. J Biol Chem. 2000; 275: 15254-15264.

172. Van den Wyngaert I, de Vries W, Kremer A, Neefs J, Verhasselt P, Luyten WH, Kass SU. Cloning and characterization of human histone deacetylase 8. FEBS Lett. 2000; 478: 77-83.

173. Riester D, Hildmann C, Grunewald S, Beckers T, Schwienhorst A. Factors affecting the substrate specificity of histone deacetylases. Biochem Biophys Res Commun. 2007; 357: 439-445.

174. Gurard-Levin ZA, Mrksich M. The activity of HDAC8 depends on local and distal sequences of its peptide substrates. Biochemistry. 2008; 47: 6242-6250.

175. Waltregny D, De Leval L, Glenisson W, Ly Tran S, North BJ, Bellahcène A, Weidle U, Verdin E, Castronovo V. Expression of histone deacetylase 8, a class I histone deacetylase, is restricted to cells showing smooth muscle differentiation in normal human tissues. Am J Pathol. 2004; 165: 553-564.

176. Waltregny D, Glenisson W, Tran SL, North BJ, Verdin E, Colige A, Castronovo V. Histone deacetylase HDAC8 associates with smooth muscle alpha-actin and is essential for smooth muscle cell contractility. FASEB J. 2005; 19: 966-968.

177. de Leval L, Waltregny D, Boniver J, Young RH, Castronovo V, Oliva E. Use of histone deacetylase 8 (HDAC8), a new marker of smooth muscle differentiation, in the classification of mesenchymal tumors of the uterus. Am J Surg Pathol. 2006; 30: 319-327.

178. Karolczak-Bayatti M, Sweeney M, Cheng J, Edey L, Robson SC, Ulrich SM, Treumann A, Taggart MJ, Europe-Finner GN. Acetylation of heat shock protein 20 (Hsp20) regulates human myometrial activity. J Biol Chem. 2011; 286: 34346-34355.

179. Wilson BJ, Tremblay AM, Deblois G, Sylvain-Drolet G, Giguère V. An acetylation switch modulates the transcriptional activity of estrogen-related receptor alpha. Mol Endocrinol. 2010; 24: 1349-1358.

180. Deardorff MA, Bando M, Nakato R, Watrin E, Itoh T, Minamino M, Saitoh K, Komata M, Katou Y, Clark D, Cole KE, De Baere E, Decroos C et al. HDAC8 mutations in Cornelia de Lange syndrome affect the cohesin acetylation cycle. Nature. 2012; 489: 313-317.

181. Gao J, Siddoway B, Huang Q, Xia H. Inactivation of CREB mediated gene transcription by HDAC8 bound protein phosphatase. Biochem Biophys Res Commun. 2009; 379: 1-5.

182. Oehme I, Deubzer HE, Wegener D, Pickert D, Linke JP, Hero B, Kopp-Schneider A, Westermann F, Ulrich SM, von Deimling A, Fischer M, Witt O. Histone deacetylase 8 in neuroblastoma tumorigenesis. Clin Cancer Res. 2009; 15: 91-99.

183. Wu J, Du C, Lv Z, Ding C, Cheng J, Xie H, Zhou L, Zheng S. The up-regulation of histone deacetylase 8 promotes proliferation and inhibits apoptosis in hepatocellular carcinoma. Dig Dis Sci. 2013; 58: 3545-3553.

184. Gao SM, Chen CQ, Wang LY, Hong LL, Wu JB, Dong PH, Yu FJ. Histone deacetylases inhibitor sodium butyrate inhibits JAK2/STAT signaling through upregulation of SOCS1 and SOCS3 mediated by HDAC8 inhibition in myeloproliferative neoplasms. Exp Hematol. 2013; 41: 261-270 e264.

185. Liu C, Liu L, Shan J, Shen J, Xu Y, Zhang Q, Yang Z, Wu L, Xia F, Bie P, Cui Y, Zhang X, Bian X et al. Histone deacetylase 3 participates in self-renewal of liver cancer stem cells through histone modification. Cancer Lett. 2013; 339: 60-69.

186. Karagianni P, Wong J. HDAC3: taking the SMRT-N-CoRrect road to repression. Oncogene. 2007; 26: 5439-5449.

187. Min, S. H., A. W. Lau, T. H. Lee, H. Inuzuka, S. Wei, P. Huang, S. Shaik, D. Y. Lee, G. Finn, M. Balastik, C. H. Chen, M. Luo, A. E. Tron, J. A. Decaprio, X. Z.

Zhou, W. Wei and K. P. Lu (2012). "Negative regulation of the stability and tumor suppressor function of Fbw7 by the Pin1 prolyl isomerase." Mol Cell **46**(6): 771-783.

188. Rustighi, A., A. Zannini, L. Tiberi, R. Sommaggio, S. Piazza, G. Sorrentino, S. Nuzzo, A. Tuscano, V. Eterno, F. Benvenuti, L. Santarpia, I. Aifantis, A. Rosato, S. Bicciato, A. Zambelli and G. Del Sal (2014). "Prolyl-isomerase Pin1 controls normal and cancer stem cells of the breast." EMBO Mol Med **6**(1): 99-119.

Chapter 4

189. Ursini-Siegel, J., et al. (2007). "Insights from transgenic mouse models of ERBB2-induced breast cancer." Nature Reviews Cancer **7**: 389-397.

190. Patten, B. A., et al. (2006). “Notch1 signaling regulates radial glia differentiation through multiple transcriptional mechanisms.” J Neurosci **26**(12): 3102-3108.

191. Guy, C. T., et al. (1992). "Expression of the *neu* protooncogene in the mammary epithelium of transgenic mice induces metastatic disease." PNAS **89**: 10578-10582.

192. Saenz, F. R., V. Ory, M. AlOtaiby, S. Rosenfield, M. Furlong, L. R. Cavalli, M. D. Johnson, X. Liu, R. Schlegel, A. Wellstein and A. T. Riegel (2014). "Conditionally reprogrammed normal and transformed mouse mammary epithelial cells display a progenitor-cell-like phenotype." PLoS One **9**(5): e97666.

193. Liu JC et al. Seventeen-gene signature from enriched Her2/neu mammary tumor-initiating cells predicts clinical outcome for human Her2+:ERα- breast cancer 109(15):5832-5837.

194. Osipo, C., P. Patel, P. Rizzo, A. G. Clementz, L. Hao, T. E. Golde and L. Miele (2008). "ErbB-2 inhibition activates Notch-1 and sensitizes breast cancer cells to a gamma-secretase inhibitor." Oncogene **27**(37): 5019-5032.

195. Zhu, J. X., E. Dagostino, P. A. Rejto, B. Mroczkowski and B. Murray (2007). "Identification and characterization of a novel and functional murine Pin1 isoform." Biochem Biophys Res Commun **359**(3): 529-535.

196. Liou, Y. C., X. Z. Zhou and K. P. Lu (2011). "Prolyl isomerase Pin1 as a molecular switch to determine the fate of phosphoproteins." Trends Biochem Sci **36**(10): 501-514.

197. Baik, S. H., M. Fane, J. H. Park, Y. L. Cheng, D. Yang-Wei Fann, U. J. Yun, Y. Choi, J. S. Park, B. H. Chai, J. S. Park, S. H. Back, J. I. Jeong, Y. J. Jang, G. Bahn, J. Y. Lee, Y. I. Li, C. G. Sobey, T. Uchida, J. H. Park, H. T. Kim, S. C. Tang, T. V.

Arumugam and D. G. Jo (2015). "Pin1 promotes neuronal death in stroke by stabilizing Notch intracellular domain." Ann Neurol **77**(3): 504-516.

198. Girardini, J. E., M. Napoli, S. Piazza, A. Rustighi, C. Marotta, E. Radaelli, V. Capaci, L. Jordan, P. Quinlan, A. Thompson, M. Mano, A. Rosato, T. Crook, E. Scanziani, A. R. Means, G. Lozano, C. Schneider and G. Del Sal (2011). "A Pin1/mutant p53 axis promotes aggressiveness in breast cancer." Cancer Cell **20**(1): 79-91.

199. Takahashi, K., H. Akiyama, K. Shimazaki, C. Uchida, H. Akiyama-Okunuki, M. Tomita, M. Fukumoto and T. Uchida (2007). "Ablation of a peptidyl prolyl isomerase Pin1 from p53-null mice accelerated thymic hyperplasia by increasing the level of the intracellular form of Notch1." Oncogene **26**(26): 3835-3845.

200. Rustighi, A., L. Tiberi, A. Soldano, M. Napoli, P. Nuciforo, A. Rosato, F. Kaplan, A. Capobianco, S. Pece, P. P. Di Fiore and G. Del Sal (2009). "The prolyl-isomerase Pin1 is a Notch1 target that enhances Notch1 activation in cancer." Nat Cell Biol **11**(2): 133-142.

201. Swami M (2009). “Signalling: pinning down Notch activation.” Nat Rev Cancer 9:151.

202. Fulmer T 2009 Science-Business eXchange: targets and mechanisms. “Another notch on cancer’s belt” copyright Nature Publishing Group

203. Khanal, P., G. M. Namgoong, B. S. Kang, E. R. Woo and H. S. Choi (2010). "The prolyl isomerase Pin1 enhances HER-2 expression and cellular transformation via its interaction with mitogen-activated protein kinase/extracellular signal-regulated kinase kinase 1." Mol Cancer Ther **9**(3): 606-616.

204. Wulf G et al. (2004) Modeling breast cancer *in vivo* and *ex vivo* reveals an essential fole of Pin1 in tumorigenesis. The EMBO Journal **23**: 3397-3407.

205. Wei, S., S. Kozono, L. Kats, M. Nechama, W. Li, J. Guarnerio, M. Luo, M. H. You, Y. Yao, A. Kondo, H. Hu, G. Bozkurt, N. J. Moerke, S. Cao, M. Reschke, C. H. Chen, E. M. Rego, F. Lo-Coco, L. C. Cantley, T. H. Lee, H. Wu, Y. Zhang, P. P. Pandolfi, X. Z. Zhou and K. P. Lu (2015). "Active Pin1 is a key target of all-trans retinoic acid in acute promyelocytic leukemia and breast cancer." Nat Med **21**(5): 457-466.

206. Reilly, R. T., et al. (2000). “HER-2/neu is a tumor rejection target in tolerized HER-2/neu transgenic mice.” Cancer Res **60**: 3569-3576.

207. Kim RJ et al. 2011 OCT4 expression enhances features of cancer stem cells in a mouse model of breast cancer. Lab Anim Res 2011 **27**(2) 147-152.

208. Prud'homme GJ, Glinka Y, Toulina A, Ace O, Subramaniam V, et al. (2010) Breast Cancer Stem-Like Cells Are Inhibited by a Non-Toxic Aryl Hydrocarbon Receptor Agonist. PLoS ONE **5**(11): e13831. doi: 10.1371/journal.pone.0013831

209. Zhou, M., J. Zhao, M. Tian, S. Song, R. Zhang, S. Gupta, D. Tan, H. Shen, M. Ferrari and C. Li (2015). "Radio-photothermal therapy mediated by a single compartment nanoplatform depletes tumor initiating cells and reduces lung metastasis in the orthotopic 4T1 breast tumor model." Nanoscale **7**(46): 19438-19447.